Population Estimation of U.S. Atlantic Red Snapper

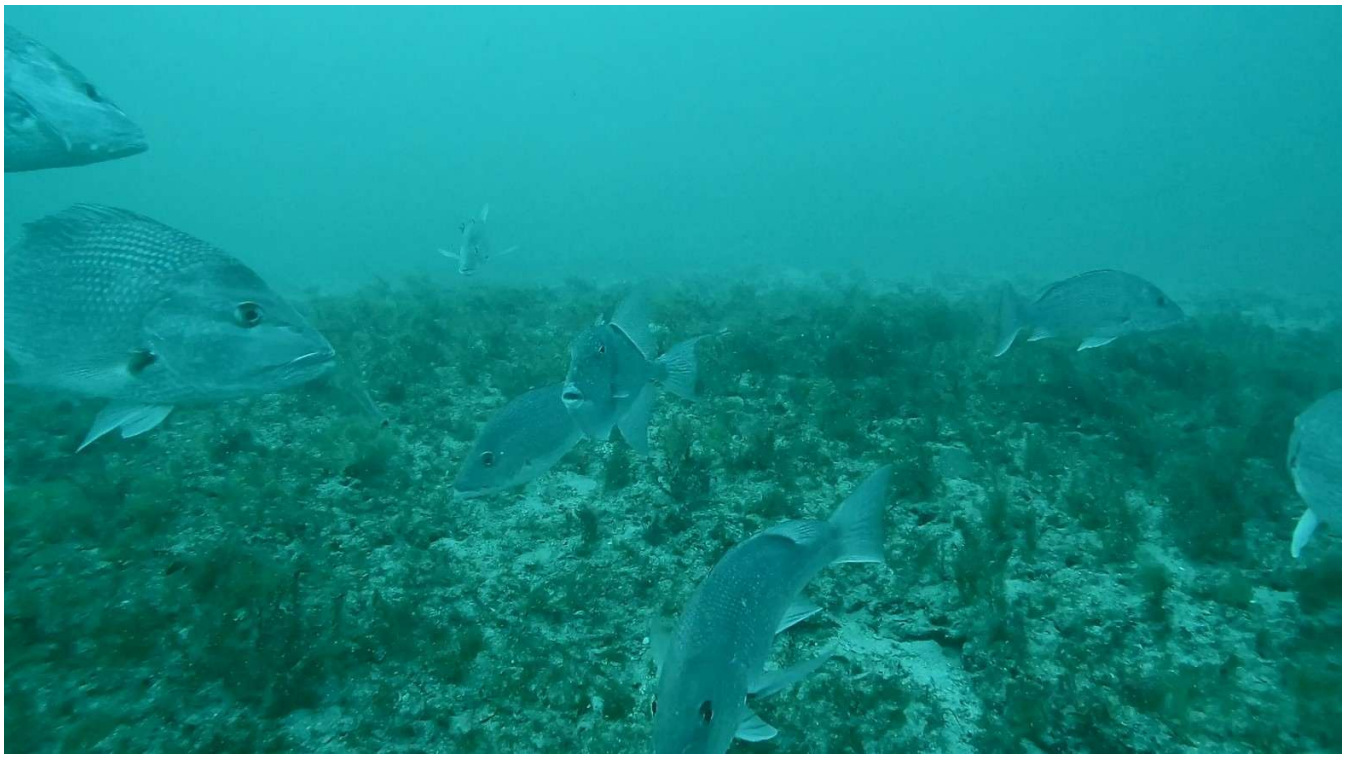

Final Report to the South Atlantic Red Snapper Research Program

UF UNIVERSITY of FLORIDA

NC STATE UNIVERSITY

TEXAS A&M UNIVERSITY CORPUS CHRISTI

USGS science for a changing world

NOAA

FLORIDA FISH AND WILDLIFE CONSERVATION COMMISSION

SOUTH CAROLINA DEPARTMENT OF NATURAL RESOURCES

Title Page

Project Title: Population Estimation of U.S. Atlantic Red Snapper, a Final Report to the South Atlantic Red Snapper Research Program

Date: March 30, 2026

NOAA Contract Number: NA20OAR4170471- R/CF-1a

How to cite this report:
Patterson III, W.F., D.S. Portnoy, and J.A. Buckel, editors. 2026. Population Estimation of U.S. Atlantic Red Snapper, Final Report to the South Atlantic Red Snapper Research Program. South Carolina Sea Grant, NOAA Sea Grant. 106 pp. plus appendices.

Table of Contents

Dedication

This study and final report are dedicated to the memory of our colleague, Kyle Shertzer, who passed away just prior to its completion. Kyle was a brilliant scientist, a valued collaborator, and a generous friend. His passing leaves a tremendous hole in the scientific capacity of our region. As significant as that loss is, it is nowhere near as acute as the one felt by his family and friends. Kyle is greatly missed by all who knew him.

Prologue

This report was assembled following the review of an earlier version by Center of International Experts and regional reviewers. A workshop was held in Charleston, South Carolina in January 2026 during which study team members presented the rationale, methods, results, and conclusions from approaches employed by the South Atlantic Red Snapper Research Program (SARSRP) study team to estimate red snapper population size. Study approaches estimated Atlantic red snapper population size with a Bayesian integrated hierarchical model (BHIM) that utilized red snapper density estimates derived from camera sampling and hardbottom habitat distribution estimates, and a close-kin mark-recapture (CKMR) approach that utilized the occurrence of half-sibling pairs (HSPs) from DNA sequencing data derived from fin clip samples. Reviewers asked questions of the study team and subsequently submitted reports addressing the Terms of Reference for the workshop. The SARSRP study team sincerely thanks the CIE and regional reviewers for the time, attention, and effort they put into the review of the SARSRP study and report. The study team found reviewer questions to be thoughtful and well-considered, and feels the report has been improved based on responses to reviewer comments and in places where additional analyses were performed to address them. Team responses and statements about additional analyses or specific revisions are listed below, as well as addressed in the text of Chapters 2 and 3. Additionally, an additional appendix chapter was added to the report. *Appendix V* contains a paper by Kehoe et al. (2025a) that examines the sensitivity of CKMR population estimates for elasmobranchs and teleosts to uncertainty in fish life history parameters via simulation analysis. Reviewers commented that a more focused simulation study on Atlantic red snapper CKMR model sensitivities would be beneficial, which is now provided as *Appendix XI* (Kehoe et al. 2025c).

Response to CIE Comments on Chapter 2: BHIM Population Estimation

The review panel indicated bottom habitat information used in the BHIM was too uncertain to provide a sufficiently reliable estimate of age 2+ absolute abundance. Reviewers also questioned whether the effective sampling area (ESA) of camera-traps estimated based on data from one region is applicable to other sampling regions. Lastly, they suggested the BHIM population estimate is not entirely independent from stock assessment data. Responses to these concerns and more minor issues are addressed below.

1. Minor typos were fixed and wording clarifications were made throughout the chapter.

2. Text was added to clarify the statistical methods related to the conditional autoregressive model formulation and remotely operated vehicle offset parameter (Methods, Results, and a new Supplemental Figure S1).

3. Discussion text was revised to further clarify the challenges posed by limited hardbottom information, discrepancies in the published hardbottom maps, and assumptions of effective sampling areas.
    a. Specific text on the limitations of hardbottom maps in the Discussion describes how a map known to be incorrect (i.e. The Nature Conservancy (TNC) alone map (Conley et al. 2017) that does not contain known Southeast Reef Fish Survey (SERFS) hardbottom sites) produced implausible (>99 million) and highly variable (<1 million vs >99 million) estimates of population size depending on model type. Additionally, maps that did contain the SERFS sampling areas (e.g., expert opinion (EO) map of Steward et al. 2022) gave less variable estimates of population size depending on map type used (e.g., combined TNC (all hardbottom confidence levels) plus EO map = ~7 million red snapper and combined TNC (high, very high hardbottom confidence levels) and EO map = ~5 million red snapper).
    b. A statement was included to address CIE reviewer concern that 'uncertainty in maps' was not included in our uncertainty in the BHIM-derived red snapper population size estimate was. This text reads, "Finally, analyzing multiple data sources in a single integrated model allows population estimates to account for the uncertainty associated with each data source (e.g., ESA, ROV offsets, camera-trap, and ROV count data). However, population estimates remained conditional on the chosen hardbottom mapping approach (e.g., composite, EO, TNC) and did not incorporate uncertainty from the map selection itself. Future work that integrates uncertainty across mapping products could help address this additional layer of variation; however, a comprehensive, high-resolution hardbottom mapping effort would ultimately provide the most robust foundation for estimating reef-associated fish abundance in the SEUSA."
    c. Specific text relative to the "ESA being based only on one region" includes the fact that the posterior distribution on ESA differed from the prior distribution of ESA (that was based on that one region). The Discussion text reads: "For our analysis, we found that ESA posterior distributions for camera-trap video samples diverged from priors in ecologically consistent patterns, with bait attraction expanding the ESA when currents flowed away from camera-traps and reducing the ESA when currents directed bait plumes behind camera-traps, highlighting the critical role of current-mediated bait plume effects on camera-trap count." However, we do acknowledge that although there was information in the count data that informed the posterior ESA estimates, those ESA estimates are fixed spatially and that this an area of future research: "Finally, we lacked information to allow the ROV offset and ESA parameters to vary across the study area. Instead, ROV offset and ESA parameters act as scaling factors affecting total population size. However, future research quantifying local, species-specific calibrations may identify processes important to unbiasedly estimating absolute abundance from underwater video surveys."

4. The study team agrees with the reviewers that the BHIM used some of the same data as the stock assessment, specifically SERFS camera counts of red snapper, thus the two methods are not completely independent. However, the BHIM estimate of abundance and spatial distribution of abundances only shared that single dataset in 2021 and 2022, integrated several other data sources not used in the stock assessment (e.g., ROV counts, effective sampling areas, hardbottom maps), and developed an population size estimation procedure that was independent of the stock assessment methods and many of the assumptions therein. As such, population size estimates from BHIM and the stock assessment remained largely independent.

Response to CIE Comments on Chapter 2: CKMR Population Estimation

The review panel stated the CKMR estimate is not independent of the stock assessment and concern was raised whether it can be used as an input to the next stock assessment. The panel also suggested uncertainty in age estimation via the age-length key, estimated stock age composition, and demographic parameters meant the estimated CV on the population estimate could be too low. The panel also questioned the assumption of equal sex-specific fecundity-at-age or fecundity-at-size and indicated this was not tested by the study team. Lastly, the panel suggested proving chromosome-level genome sequencing to assess the degree of linkage among the approximately 1,755 multiallelic haplotypic loci used to obtain the CKMR-derived population estimate. Study team responses are provided below, along with an indication of where changes were made in Chapter 3.

5. Some of the inputs to CKMR are data inputs that are also used in the stock assessment but are not products of the stock assessment. In all cases, life history parameters utilized were those evaluated to be the best scientific information available during the recent Southeastern Data, Assessment, and Review Data Workshop for Atlantic red snapper. An exception to this general statement are the data used to generate red snapper relative age composition for years 2104-2023, which were informed by SEDAR (2024) assessment output. To test how sensitive the CKMR model was to these relative (i.e. proportions not numbers at age) composition data, we also ran the CKMR under an equilibrium age composition, young-biased age composition, and old-biased age composition to produce estimates of population size (Methods, pages 75–76). (Results, pages 85–86) indicate changes to the age composition input had only mild effect with point estimates ranging from 1.29 million (biased old) to 1.91 million (biased young) among all scenarios examined, and 90% credible intervals overlapping for all scenarios. Lastly, CIE reviewer, Joe Powers, indicated a strength of the CKMR approach is it could be incorporated directly into the stock assessment model and the model's objective function, whereby the issue of independence would be moot.

6. Uncertainty in age estimation via the age-length key was in fact incorporated into the coefficient of variation on estimated population size (see page 71 for a description). The study team tested assumptions of stock age composition and aspects of demography which show fairly consistent results but did not include them in the estimate of uncertainty. One area which was not addressed in the previous draft of the report was what effect persistent differences in fecundity among individuals across years, if they existed, would have on estimated population size. An examination of this potential effect was added to the current study (Methods, pages 75–76) and results indicate persistent differences in fecundity among individuals across years, if they existed, would have only a minor effect on the population estimate (Results, 85–87) Additionally, the new simulation study focused solely on Atlantic red snapper CKMR (*Appendix XI*) clearly demonstrates error caused by even moderate levels of bias or imprecision in demographic inputs would be relatively minor.

7. The study team sequenced the entire mtDNA genome for 40 putative half-sibling pairs (HSPs) following the review workshop to examine the question about potential differences in realized fecundity between sexes (Methods, page 70). The mtDNA molecule is maternally inherited, such that maternal half-siblings inherit the same mtDNA (and hence the same mtDNA sequence), while paternal half-siblings carry mtDNA sequences that are not identical by descent, and therefore are expected to be different. This latter point, Atlantic red snapper mtDNA was highly variable with only 0.2% of unrelated pairs having matching mtDNA sequences, while 40% of related individuals did (Results, page 81). Results from mtDNA of HSPs indicated haplotype sharing among siblings was not significantly different from the expectation of 1:1. This demonstrates HSPs had an equal probability of sharing a mother or a father, thus suggesting realized fecundity was not significantly different for male versus female Atlantic red snapper. This inference is also consistent with the recent finding from the SEDAR 90 Data Workshop that red snapper display a sex ratio that is not significantly different than 1:1 across ages.

8. Simulation analyses examining the effect of bias or imprecision in life history parameters on CKMR-derived population estimates were streamlined, with changes being made to make the results and interpretation of the simulation study more directly applicable to the red snapper CMKR model utilized in Chapter 3. This revised simulation study now appears as report *Appendix XI*.

9. At the time of report submission, the red snapper epigenetic clock was still being optimized, thus could not be utilized to estimate the age composition of putative HSPs. The study team anticipates the optimization process will be completed in the first half of this 2026, making the clock available for a wide range of assessment applications, including estimating age composition for subsequent CKMR analyses. At that stage, age estimation for HSPs included

in Chapter 3 could be revisited, along with examination whether potential parent-offspring kin pairs exist among the study data.

10. The current red snapper genome is not a chromosome level assembly (L_{50} = 15,544), thus the team was unable to use it to directly assess physical linkage among haplotype loci. Red snapper heart tissue samples were collected by the study team in winter 2026 and are now undergoing genetic sequencing to assemble a chromosome-level genome for red snapper. Once completed, it could be utilized to examine genetic linkage as suggested by CIE reviewer, Daniel Ruzzante. This level of genome mapping will serve as a resource that can be used to refine myriad red snapper genetic and genomic studies. In the current study, potential issues in estimating the false negative rate caused by physical linkage were examined via simulation with results indicating very little potential effect on population estimation results (Discussion, page 90–92).

References

Conley, M.F., M.G. Anderson, N. Steinberg, and A. Barnett. 2017. The South Atlantic Bight Marine assessment: species, habitats and ecosystems. The Nature Conservancy, Eastern Conservation Science.

SEDAR. 2024. Stock Assessment of Red Snapper off the Southeastern United States – Update of SEDAR 73 Assessment. Technical report, SEFSC, Beaufort, NC. URL http://sedarweb.org/sedar-73.

Steward, D.N., A.B. Paxton, N.M. Bacheler, C.M. Schobernd, K. Mille, J. Renchen, Z. Harrison, J. Byrum, R. Martore, C. Brinton, K.L. Riley, J.C. Taylor, and G.T. Kellison. 2022. Quantifying spatial extents of artificial versus natural reefs in the seascape. Frontiers in Marine Science 9:980384.

Acknowledgements

This study was funded by South Carolina Sea Grant under the South Atlantic Red Snapper Research Program (SARSRP), which was initially appropriated by the U.S. Congress in 2020. We are thankful for the generous support provided by everyone at South Carolina Sea Grant, and particularly Susan Lovelace, Jocelyn Juliano, and Emily Osborne. We thank the SARSRP Steering Committee for constructive criticism and thoughtful comments during the process of starting the study and during annual update meetings. We also thank Representative Rutherford, the Congressional Sponsor of the SARSRP, and his staff members Amber Nejjari and Katie Ramos, for their support and open lines of communication. This project constitutes the largest cooperative research study with which any of the project team members have been associated. Every state fisheries agency from North Carolina to Florida has contributed significantly to this study, with an unprecedented amount of cooperation and collegiality devoted to the end goal of estimating red snapper population size. We are forever grateful for all their contributions and support. The study team has not attempted to sum the total amount of in-kind support provided to this work, in the form of personnel or ship time to collect samples, but it certainly has been many millions of dollars. Innumerable private anglers, charterboat and headboat captains and customers, and commercial fishermen provided us access to their catch or provided other invaluable data to this study. We have learned much more from them during this process than they would ever learn from us. We are incredibly grateful for their contributions, time, and shared knowledge of the Atlantic red snapper resource.

Executive Summary

The South Atlantic Red Snapper Research Program (SARSRP) was funded by the U.S. Congress in 2020 and thereafter administered by South Carolina Sea Grant. The primary goal of the SARSRP was to produce an estimate of age-2+ red snapper, *Lutjanus campechanus*, population size in the U.S. Atlantic from North Carolina to South Florida. The estimate was intended to be independent of the Southeast Data, Assessment, and Review (SEDAR) stock assessment, but subsequently inform and be incorporated into future stock assessments and fisheries management.

Our study team was based at the University of Florida, with significant research groups at North Carolina State University and Texas A&M University-Corpus Christi. Our team also had numerous members who are state or federal agency scientists, and we enjoyed extensive cooperation and help from various stakeholders in the region. The team proposed to produce two independent estimates of Atlantic red snapper population size. In the first approach, fish density estimates from Southeast Reef Fish Survey (SERFS) camera-trap and remotely operated vehicle video samples were integrated with hardbottom (natural reef) habitat and depth data across the study region in a Bayesian hierarchical integrated model (BHIM) framework. In the second approach, close-kin mark-recapture (CKMR) was used to estimate population size. Sequencing of DNA from red snapper fin clip samples (n = 14,085) collected during 2021–2023 revealed the frequency of half-sibling (HS) pairs across the study region. The HS pairs constitute recaptures of genetic marks passed from parents to offspring. Analysis of kin recaptures with CKMR models informed by life history parameters enabled our team to estimate red snapper population size.

The study team also went to great lengths to understand potential sources of uncertainty on BHIM or CKMR population size estimates, and to incorporate as many of those sources as possible into population size estimation procedures. A series of field or simulation modeling experiments was conducted to accomplish this. Details of those studies are presented in the various appendices of this report, while the most important implications with respect to BHIM or CKMR population estimates are discussed in Chapters 2 and 3, respectively.

Perhaps the greatest source of uncertainty in the entire study is the estimated distribution of hardbottom habitat on the southeastern U.S. Atlantic (SEUSA) continental shelf. This is key because BHIM red snapper population size estimates are heavily reliant on and sensitive to habitat distribution data and assumptions. There is extensive discussion in Chapter 2 about the different data sources utilized to inform previous habitat mapping efforts in the region, as well as the disparity in data quality within and among them. Based on different habitat modeling assumptions, estimates of red snapper population size ranged from 0.79 (coefficient of variation or CV = 0.46) to 99.95 (CV = 0.28) million fish among various model sensitivity runs. The habitat distribution estimate the study team felt was most defensible produced an age-2+ red snapper population estimate of 5.31 million fish, with CV = 0.39 (95%HDP = 2.33–10.02 million fish; HPD = Bayesian credible interval). This estimate applies to years 2021 and 2022, when BHIM sampling

occurred. The estimate's 95% credible interval does not overlap with the 2021–2022 mean age-2+ population size of 1.95 million fish from the SEDAR 73 update (73U) stock assessment, but there is considerable variance in the BHIM population estimate (Figure ES-1; SEDAR 2024). Furthermore, age-1 red snapper constituted 20% of caught in SERFS chevron traps in 2021 and 5% in 2022. The likely presence of age-1 red snapper in the count data from video samples collected with trap-mounted cameras, and the resulting positive bias of that, adds additional uncertainty to BHIM population size estimates.

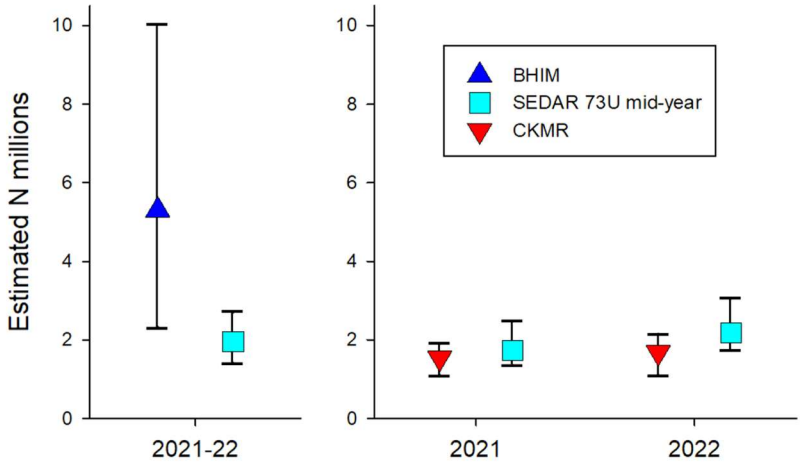

Figure ES-1. Estimates of Atlantic red snapper population size (± 95% credible intervals) produced in this study with a Bayesian hierarchical integrated model (BHIM) utilizing fish count data from video samples and close-kin mark-recapture (CKMR) from kinship analysis versus mid-year estimates from the SEDAR 73 update stock assessment.

The CKMR model produced a time series (2018–2023) of red snapper population estimates with annual CV ≤ 0.3. For 2021 and 2022, the BHIM years, the CKMR red snapper population estimate is 1.54 (CV = 0.17, 95%HPD = 1.10–2.14) and 1.68 (CV = 0.30, 95%HPD = 1.0–2.63) million fish, respectively. Therefore, estimated age-2+ red snapper population size from CKMR analysis is lower than the BHIM estimate, but not significantly different than estimates from the SEDAR 73U assessment (Figure ES-1). It is unclear, however, what effect estimated recreational removals (landings plus dead discards) being nearly 50% lower in the SEDAR 90 versus SEDAR 73U data will have on red snapper population estimates. For example, sensitivity analysis during SEDAR 73 demonstrated lower removals estimates had little effect on estimated fishing mortality but scaled population size downward. This may seem counterintuitive, but a larger population size would be required to produce higher landings or discards for the same fishing mortality rate, with the latter being informed by the age composition, not the magnitude, of removals.

The study team attempted to be good stewards of tax payer dollars and went well beyond the originally planned research to test assumptions, calibrate gear or estimate its effective sample area, or use data opportunistically to model important fishery parameters, such as red snapper release mortality. Data and analytical products produced during this work have already been incorporated into the SEDAR 90 assessment process, and the parallel process of incorporating CKMR into the assessment model should enable an even greater application of the data and methods developed during this study to be brought to bear for red snapper assessment, management, and conservation.

Table List

Figure List

Chapter 1

Overview of Atlantic Red Snapper Population Estimation under the South Atlantic Red Snapper Research Program

William F. Patterson III[1], David S. Portnoy[2], Jeffrey A. Buckel[3], Nathan M. Bacheler[4], Kyle W. Shertzer[4], and Walter J. Bubley[5]

[1]School of Forest, Fisheries, and Geomatics Sciences, University of Florida, 7922 NW 71st Street, Gainesville, Florida 32653, USA

[2]Marine Genomics Laboratory, Department of Life Sciences, Texas A&M University–Corpus Christi, 6300 Ocean Drive, Corpus Christi, TX 78412, USA

[3]Department of Applied Ecology, Center for Marine Sciences and Technology, North Carolina State University, Morehead City, NC, USA

[4]Southeast Fisheries Science Center, National Marine Fisheries Service, Beaufort, NC 28516, USA

[5]Marine Resources Research Unit, South Carolina Department of Natural Resources, Charleston, SC, USA

Introduction

Red snapper, *Lutjanus campechanus*, is an iconic, long-lived marine fish in Atlantic Ocean waters off the southeastern U.S. (SEUSA). A diversity of stakeholders target red snapper there, including members of commercial handline, for-hire charterboat and headboat, and private recreational fisheries. These fisheries started to develop in earnest in the middle of the 20th Century (SEDAR 2009), and by the 1980s there was concern about reduced spawning biomass in Atlantic red snapper. The South Atlantic Fishery Management Council (SAFMC), which is responsible for managing reef fishes and other fishery resources in federal waters on the SEUSA continental shelf, developed the Snapper Grouper Fishery Management Plan in 1983, with the first size limit for red snapper retention set at 12 inches (305 mm) total length (TL). That size limit was increased to 20 inches (508 mm) TL in 1992, with a daily bag limit in the recreational fishery of 2 fish per day. Those management measures followed the first stock assessment for Atlantic red snapper (Manooch III et al. 1998), which concluded the stock was depleted, had been unresponsive to initial management efforts, and fishing mortality should be reduced by nearly 70% to rebuild the stock.

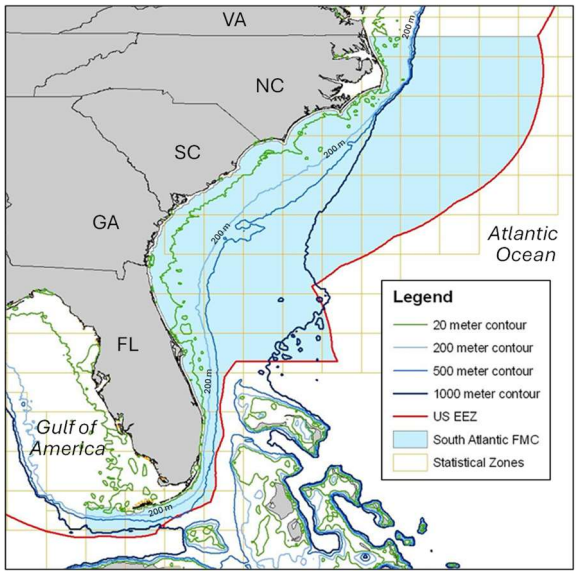

Figure 1-1. Map of the southeastern U.S. depicting Exclusive Economic Zone (EEZ) waters under the jurisdiction of the South Atlantic Fishery Management Council (blue), including continental shelf waters (200 m isobath) where red snapper occur. Source: SEDAR (2009).

The overfished status of red snapper, combined with its popularity as a prime target in the SEUSA snapper-grouper fishery, has resulted in considerable resources and scientific inquiry being devoted to understanding its life history and ecology, as well as the direct and indirect effects of fishing on its productivity. Many of those efforts have involved cooperative research among stakeholders, academic scientists, and federal and state agency scientists, with cooperative research being a running theme over the past two decades in efforts to improve the science behind red snapper assessment and management. Otolith ageing revealed maximum observed longevity to be 51 years (SEDAR 2009), while gonad histology indicated the age at maturity is only 2 years for this iteroparous (over multiple years) batch (multiple times in a year) spawner (Lowerre-

Barbieri et al. 2015). Early maturity, moderately fast growth over its first 10 years of life, and protracted spawning seasons impart a degree of resilience for Atlantic red snapper not typically seen in a long-lived periodic life history strategist (Winemiller and Rose 1992). That translates to a stock that has been able to produce strong estimated recruitment (large year classes) even while experiencing a truncated population age composition (SEDAR 2021, 2024).

The first integrated stock assessment for Atlantic red snapper occurred during Southeast, Data, Workshop, and Review (SEDAR) 15 in 2009, with SEDAR being the stock assessment peer review process utilized since 2002 by the South Atlantic, Gulf, and Caribbean Fishery Management Councils. The results of the SEDAR 15 assessment indicated the Atlantic red snapper stock had been overfished since the 1960s and overfishing was still occurring (SEDAR 2009). The SAFMC instituted a 35-year rebuilding plan and prohibited retention of red snapper starting in 2010, meaning a fishery closure was put in place. Following an update assessment in 2010, which showed some signs of strong recruitment, limited harvest was allowed again in 2012. Since then, however, the length of time the recreational fishery has been open in a given year has ranged from zero to 9 days, with management based on results of benchmark stock assessments, SEDAR 41 in 2017 (SEDAR 2017) and SEDAR 73 in 2021 (SEDAR 2021), along with update assessments following each benchmark.

Much consternation has been voiced by various stakeholders about red snapper assessment and management over the past 15 years. The SEDAR process allows for and encourages stakeholder participation and much of the cooperative research focused on red snapper over the past two decades started as stakeholder questions or input provided during data workshops for various SEDAR assessments. Resulting innovations include directed life history (Lowerre-Barbieri et al. 2015) and release mortality (Runde et al. 2021) studies, as well as studies or surveys aimed at estimating red snapper spatial distribution and population trends, or to better estimate landings. This included spatial expansion of fishery-independent camera-trap surveys in 2011, via the Southeast Reef Fish Survey (SERFS), to encompass SEUSA shelf areas from North Carolina to east central Florida (27N to 35N), which was partly needed to offset the lack of fishery-dependent data during fishery closures after 2010 (Williams and Carmichael 2009). A fishery-dependent longline survey also was conducted in 2010 and 2011 that found no evidence of a cryptic biomass of large (>800 mm TL), old (>age-10) red snapper on the SEUSA outer continental shelf (Mitchell et al. 2014). Lastly, Florida developed survey methods to estimate landings in the high-effort but short (≤9 d) recreational seasons that have existed since 2012 (Sauls et al. 2017), which was necessary given the inadequacy of the National Marine Fishery Service's (NMFS) Marine Recreational Information Program (MRIP) survey to estimate landings for such a short, pulsed fishery.

The most recently completed SEDAR benchmark stock assessment for Atlantic red snapper (SEDAR 73) was conducted in 2020-2021 (SEDAR 2021) and updated in 2024 (SEDAR 2024). Prior to that, and with the precedent of the Great Red Snapper Count (GRSC; Stunz et al. 2021) study being conducted in the Gulf of America (formerly Gulf of Mexico; hereafter, Gulf),

stakeholders expressed interest to the U.S. Congress for funding a similar population estimation study focused on Atlantic red snapper. In 2020, Congress allocated $1.5 million in funding toward the South Atlantic Red Snapper Research Program (SARSRP), which has been administered by South Carolina Sea Grant (SCSG). A request for proposals was issued by SCSG in October 2020 to solicit proposals to produce "an absolute estimate of abundance with an accompanying measure of uncertainty for the entire South Atlantic red snapper stock" to inform "future spawning stock assessments." Subsequent funding was made available by Congress through the SARSRP in 2021 and 2022 that totaled an additional $3.3 million.

In addition to estimating population size, SARSRP funding has been utilized by the study team to calibrate sampling gear, examine spatial and temporal trends in red snapper relative abundance, estimate red snapper release mortality, quantify stakeholder perceptions of habitat and red snapper distribution and compare to empirical and model-derived estimates, conduct tagging simulations, and test key assumptions of the population estimation approaches employed in the study. Those components are presented in appendix manuscripts that are briefly described below, cited in relevant places in report chapters, and can be accessed on the SCSG SARSRP webpage. The purpose of the appendices is to facilitate the review of population estimation while attempting to avoid an unwieldy report. Therefore, this report is focused on the Atlantic red snapper population estimation approaches and results, although it also briefly touches upon the process of integration of population estimation into the next SEDAR stock assessment.

Study Objectives and Approach

There were two primary objectives of this study. The first objective was to produce estimates of red snapper population size in U.S. waters of the Atlantic Ocean with two independent methods, while the second objective was to integrate independent population estimation into the Atlantic red snapper stock assessment model. With respect to estimating population size, the first method utilized fish count data in a Bayesian hierarchical integrated modeling (BHIM) framework, while the second utilized kinship relationships determined via DNA sequencing of fin clip samples in a close-kin mark-recapture (CKMR) framework. The data utilized in the BHIM approach were derived from standardized SERFS camera-trap sampling, as well as from fish count estimates produced with remotely operated vehicle (ROV) sampling at randomly sampled locations across the SEUSA shelf from North Carolina to south Florida (Figure 1-2). Two additional, complimentary studies were conducted to estimate the effective sample area of camera-trap gear such that red snapper count data could be expressed as density, which was critical for estimating total abundance, or population size (Zulian et al. 2024, Appendix I; Goldstein et al. 2025, Appendix II). The SERFS camera-trap data were utilized to examine temporal and spatial trends in red snapper abundance on the SEUSA shelf, while ROV data were used to test whether red snapper occur on unconsolidated habitats not targeted by the SERFS survey (Bacheler et al. 2025, Appendix III). That sampling was important given the large percentage of red snapper estimated to occur on unconsolidated habitats in the western Gulf during the Great Red Snapper Count study

in that region (Stunz et al. 2021). Once Atlantic red snapper density estimates were produced from either SERFS or ROV video samples, they were integrated with estimates of the distribution of hardbottom habitat and depth data across the continental shelf to estimate red snapper abundance at local, state-specific, and regional spatial scales, with the region abundance estimate constituting an estimate of SEUSA red snapper population size (see Chapter 2).

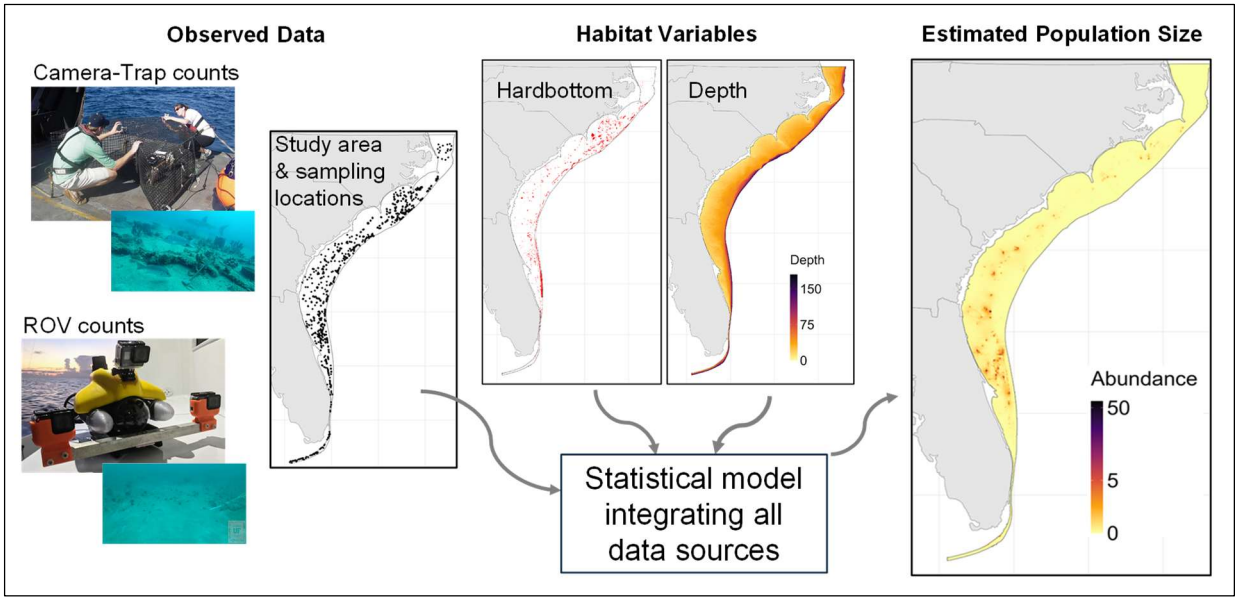

Figure 1-2. Conceptual diagram of how red snapper count and density estimates were produced using Southeast Reef Fish Survey camera-trap and remotely operated vehicle (ROV) fish count data which were then utilized in a Bayesian hierarchical integrated model (BHIM) with hardbottom habitat and depth data to predict local, state-specific, and regional estimates of abundance, with the region-wide estimate constituting an estimate of Atlantic red snapper population size.

The second method employed to estimate Atlantic red snapper population size was a genomic technique referred to as close-kin mark-recapture. The general concept of mark-recapture is straightforward and has a long history in fisheries and wildlife science to estimate population size. In the simplest example with traditional mark-recapture, individuals are randomly sampled across the spatial range of a population of interest and then artificial tags (e.g., anchor or dart tags in fisheries) are applied to mark those individuals. At some later time, after tagged individuals have mixed within the population of unmarked individuals, a second sample is taken. The estimate of population size is then calculated as the number of animals in the second sample divided by the fraction of tagged individuals, with key assumptions being animals do not lose their marks, all marks are recognized, the population is closed (i.e., no immigration or emigration), and births and deaths are balanced. For example, if those assumptions were met and 1,000 fish were captured in an initial sample, marked, and released, and then a second sample was taken sometime later and

another 1,000 were sampled and 10% of those fish were tagged, then the estimate of population size would be 10,000 (i.e., 1,000/0.1 = 10,000).

Close-kin mark-recapture is a variation on traditional mark-recapture with some important distinctions between the approaches. With CKMR, the marks utilized are genetic, specifically the composite genotype of each sampled individual derived from DNA sequencing (Figure 1-3). These genetic tags are never lost and can be recovered from live fish, fish sacrificed during scientific surveys, or from landings. Because these genetic marks are transferred from parents to offspring, they are partially shared among related individuals, or kin. When kin relationships, such as parent-offspring or half-sibling relationships, are identified in a sample of individuals of a population, they constitute a form of recapture based on these natural, genetic tags. Analyzing kin recaptures with CKMR models informed by life history information enables one to relate the number of kin observed in a sample to (absolute) population size (Skaug 2001; Bravington et al. 2016). Greater details of this approach are provided in Chapter 3, but the basic concept is the greater the number of related individuals (recaptures) in a given sample, the lower the estimated population size (Figure 1-4), which is similar to the example provided earlier for traditional tagging.

Figure 1-3. Illustration of the process of 1) taking a tissue sample from a fish in the field, 2) sequencing the DNA and filtering the sequence data through genomics pipelines, and 3) analysis of DNA sequence data to examine population structure and connectivity or to estimate population size via kinship analysis and CKMR.

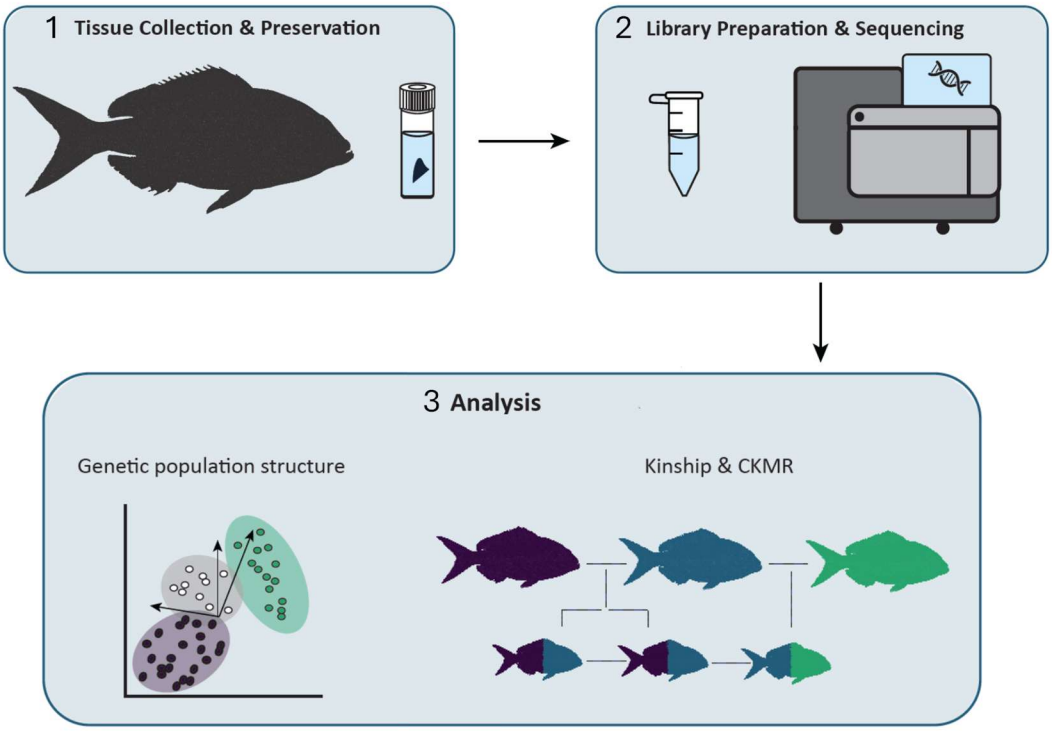

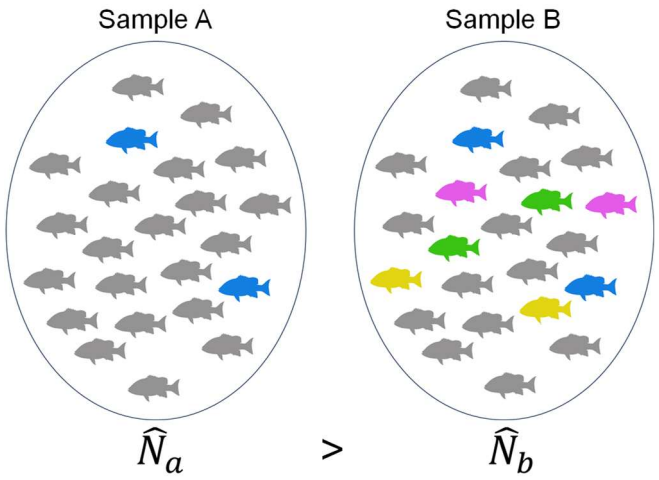

Figure 1-4. The general relationship between the proportion of kin pairs (like colored snapper) within a sample and the estimate of population size ($\widehat{N}$). The greater the number of kin pairs detected (i.e., "marks"), the lower the population estimate.

There are vast amounts of life history data available for Atlantic red snapper, as well as the numerous fishery-independent surveys and fishery-dependent sampling programs that encounter them. This combination makes red snapper an ideal species to apply CKMR to estimate population size. However, there are important assumptions that must be met. First, it is critical that samples are taken across the range of the population of interest and any genetic population structure is accounted for (Conn et al. 2020). To satisfy this assumption, we conducted an extensive population genetics analysis that demonstrated Atlantic and Gulf red snapper stocks were genetically distinct and there was no genetic structure within the Atlantic (Monroe et al. 2025; Appendix IV). Given the reliance on life history data in CKMR population estimation models, it is also important to understand the effect of bias or imprecision in estimated life history parameters on population estimates. Toward that end, an extensive, novel simulation analysis was done to examine the effect of error (bias or imprecision) on CKMR estimates for fishes with different life history strategies, including one based on Atlantic red snapper (Kehoe et al. 2025a, Appendix V). Results of that analysis indicate CKMR is fairly robust to even moderate bias or imprecision in life history parameters, although error in exponential fecundity functions can be problematic. In Chapter 3, details are presented why this is not likely an issue for estimating Atlantic red snapper population size with CKMR.

Integration Into Stock Assessment

The primary objective of the SARSRP was to produce an estimate of absolute abundance to validate or test the estimate derived from the Atlantic red snapper stock assessment. However, a secondary benefit of this approach would occur if the estimation procedure could be incorporated into the integrated assessment model. This would provide the model with an independent estimate of stock size, which would not only scale estimates of productivity but would also allow the model to estimate other parameters more freely, such as fishery selectivity or natural mortality (Punt et al. 2024; Fisch 2025). Therefore, the second primary objective of this study was to develop the

statistical methodology to incorporate CKMR estimation into the Beaufort Assessment Model (BAM) for Atlantic red snapper. This report focuses on population estimation, but the process of CKMR integration into BAM has occurred and is being tested through simulation (McLaughlin et al. 2025, Appendix VI). The parallel process of incorporating CKMR population estimation directly into the BAM red snapper stock assessment should make that process relatively seamless as the SEDAR 90 stock assessment moves forward.

Report Structure

This report is structured into four chapters, with additional, complimentary analyses presented in appendix manuscripts. The intent was to make the main body of the report informative and to the point with respect to Atlantic red snapper population estimation, while at the same time providing interested readers access to detailed analyses pertaining to gear calibration, assumption testing, or ongoing or planned future analyses. Following this introductory chapter is a chapter on BHIM population estimation (Chapter 2) and then a chapter on CKMR population size estimation chapter (Chapter 3). The final report chapter (Chapter 4) is a summary and conclusions chapter that juxtaposes and compares the population estimates produced with BHIM, CKMR, and the SEDAR73 updated stock assessment (SEDAR 2024). The sources of uncertainty in each estimate, including the one produced by the last stock assessment, are also discussed in an effort to reconcile as many differences as possible. The last section of the report focuses on the utility of CKMR population size estimation for Atlantic red snapper moving forward. A tremendous amount of time and effort has gone into developing the genomics tools, pipelines, and models required for CKMR population size estimation for Atlantic red snapper, as well as toward understanding and minimizing sources of uncertainty in CKMR population size estimation for this species and incorporating the CKMR machinery into the BAM assessment. Clearly, that will benefit other species who might be candidates for CKMR, but it also lays the groundwork for time series CKMR analysis for Atlantic red snapper. Lastly, we present a new approach to estimating the magnitude of Atlantic red snapper recreational discards, and potentially landings, that does not rely on Florida State Reef Fish Survey or uncertain MRIP data. Instead, the discard exploitation rate is estimated via conventional tagging and then multiplied by the CKMR population size estimate to estimate the magnitude of discards (Kehoe et al. 2025b, Appendix VII).

Contents of Report Appendices

Several supporting or complimentary studies were undertaken to test assumptions related to the BHIM or CKMR approaches to estimating Atlantic red snapper population size, to explore new, related lines of research leveraging results of this study, or to analyze data generated in ways that could enhance Atlantic red snapper stock assessment. These studies are presented as appendix manuscripts, some of which have already been published or are currently in review at scientific

journals. The appendices themselves can be accessed on the study website hosted by SCSG. A brief description of each appendix manuscript is provided below.

Appendix I

Zulian et al. (2024) Applying mark-resight, count, and telemetry data to estimate effective sampling area and fish density with stationary underwater cameras. Scaling fish counts to abundance requires fish density and total habitat area estimates. This can be problematic for fixed camera gear, such as SERFS camera-traps. This published paper describes a novel marked N-mixture model constructed to estimate the effective sample area (ESA) and density (fish/area) from repeated counts of unmarked and marked individuals observed in video collected with SERFS camera-traps. It integrates mark-capture, camera counts, and telemetry data of red snapper at a 1.6 km^2 reef off North Carolina to estimate the ESA of SERFS camera-traps.

Appendix II

Goldstein et al. (2025) An integrated approach to estimating the effective sampling area of baited underwater camera traps. This paper is currently in review and builds on the work described in Zulian et al. (2024). The study employed a spatial capture-recapture framework, where observed counts arise from red snapper movement and space use, to estimate SERFS camera-trap ESA. Information on movement from acoustic telemetry of tagged red snapper and counts from independent remotely operated vehicle (ROV) sampling is incorporated into ESA estimates via data integration. Not only does this approach provide estimates of camera-trap ESA for red snapper, it also provides a method to estimate the red snapper catchability for ROV sampling.

Appendix III

Bacheler et al. (2025) Spatiotemporal dynamics and habitat use of red snapper (*Lutjanus campechanus*) on the southeastern United States Atlantic continental shelf. This published study employed data from the SERFS camera-trap survey (2011–2022) and ROV sampling (2021–2023) on the SEUSA shelf to quantify temporal changes in red snapper relative abundance, patterns of spatial distribution, and habitat use. Results of generalized additive models indicate an approximately 1000 % increase in red snapper occurred in trap and video samples over the study period, while contemporary ROV sampling demonstrated red snapper are associated almost exclusively with natural hardbottom habitats on the SEUSA shelf, and rarely are observed on unconsolidated habitats in the region unless near (<100 m) reef habitat.

Appendix IV

Monroe et al. (2025) Genetic population structure of red snapper, *Lutjanus campechanus*, in the U.S. Atlantic and eastern Gulf of America. The study described in this draft manuscript assessed patterns of Atlantic red snapper genetic variation across 2,776 SNP-containing loci in fish (n = 307) sampled from continental shelf regions in the Gulf off southwest Florida and in the U.S.

Atlantic from North Carolina to east central Florida. Hierarchical analysis of molecular variance revealed significant heterogeneity attributable to differences between the Gulf and Atlantic, but no differences among sampling regions within the Atlantic were detected. Overall, results indicate red snapper in the Gulf and the Atlantic constitute separate genetic populations, while no genetic structure was observed among regions within the Atlantic. This has important implications for CKMR in that the Atlantic can be considered a separate genetic population from the Gulf, but CKMR could not estimate regional population sizes within the Atlantic.

Appendix V

Kehoe et al. (2025a) Sensitivity of CKMR population estimates to uncertainty in fish life history parameters examined via simulation analysis. This paper is currently in review at a scientific journal. The study it describes utilized simulation analysis to test the sensitivity of CKMR population analysis to bias or imprecision in fish life history parameters. Simulations were conducted for a model elasmobranch based on sandbar shark (*Carcharhinus plumbeus*) and a model bony fish based on Atlantic red snapper (*Lutjanus campechanus*). Results suggest bony fishes may need higher resolution age-based data inputs than elasmobranchs for accurate CKMR population estimation. Red snapper population estimates were robust to the levels of uncertainty explored, with an exception being a sensitivity to exponent choice for nonlinear fecundity functions. The recent Data Workshop for the ongoing SEDAR 90 Atlantic red snapper assessment concluded fecundity was best fit with a linear function, which alleviates a potential issue for the Atlantic red snapper CKMR model (Chapter 3).

Appendix VI

McLauglin et al. (2025) Incorporating close-kin mark-recapture data into an integrated stock assessment model for Southeast United States Atlantic red snapper (*Lutjanus campechanus*). This brief paper describes the simulation framework being utilized to test the integration of CKMR population estimation into the BAM Atlantic red snapper stock assessment. This process has been occurring parallel to the population estimation in the current study so independent CKMR-derived population estimates can be readily integrated into the SEDAR 90 red snapper stock assessment model. The primary objectives of this study are to evaluate whether inclusion of CKMR data improves estimates of absolute abundance or natural mortality(M). This work builds on a previous simulation study of Atlantic red snapper, which showed M can be estimated accurately within BAM, but only under a limited range of conditions. A growing body of literature suggests fitting stock assessment models with CKMR population estimation can enhance the precision and accuracy of estimates for both M and stock size (Hillary et al. 2018; Punt et al. 2024; Fisch 2025). The goal of this study is to test that for the BAM Atlantic red snapper model. Additional planned research will focus on assessing the feasibility of also incorporating results or modeling components from BHIM red snapper population estimation into the assessment model.

Appendix VII

Kehoe et al. (2025b) Estimating reef fish exploitation rates in catch-and-release fisheries with conventional and genetic tags. This paper is currently in review at a scientific journal. It details a simulation study in which conventional and genetic tagging data were simulated with age-structured population and individual-based tagging models to determine the tagging effort and angler participation required to precisely estimate the discard exploitation rate, or the fraction of a fish population that is caught-and-released. Models were parameterized with life history and fishery data from Atlantic red snapper. Results indicate conventionally tagging 2,500 fish per year would estimate the recreational catch-and-release probability, hence the discard rate, with a CV < 0.3. Genetic tagging was also able to produce precise estimates of the discard rate, but required participation from >2.5% (25,000 trips) of the total fishing effort, which is logistically prohibitive. Results suggest conventional tagging would perform better for estimating the discard mortality rate in fisheries such as Atlantic red snapper where catch is dominated by private vessels and is largely unobserved and decentralized. Combining conventional tagging with a CKMR-derived estimate of Atlantic red snapper would enable estimation of the total number of recreational discards.

Appendix VIII

Rudershausen et al. (2025a) Stakeholder insights corroborate habitat and reef fish abundance on the southeastern U.S. Atlantic continental shelf. This paper, which has been accepted for publication in Regional Studies in Marine Science, details an extensive cooperative research study in which commercial and for-hire recreational fishermen who target red snapper on the SEUSA shelf were asked to map the region they fish on the SEUSA shelf, categorize the extent of hardbottom habitat in 5 min latitude x 5 min longitude cells in their fishing region, and categorize the relative abundance of red snapper in those same cells. Results of spatial analysis applied to the data indicated habitat and red snapper distribution estimates were well-correlated with spatial patterns reported in Bacheler et al. (2025), as well as estimated with the BHIM in Chapter 2. Therefore, the perception of fisherman about the spatial distribution of the red snapper population on the SEUSA continental shelf closely matches empirical data collected during the SARSRP study, as well as BHIM modeling results presented in Chapter 2. Furthermore, results of this study demonstrate stakeholder insights could be used to corroborate fishery-independent survey data or provide information on the amounts and distribution of demersal marine resources where surveys do not occur. The latter has important implications for large or difficult-to-sample regions or emerging management issues.

Appendix IX

Rudershausen et al. (2025b) Discard mortality rates of red snapper after barotrauma and hook trauma: insights from using acoustic telemetry in the U.S. South Atlantic. This published paper details an analysis performed with three-dimensional telemetry data from red snapper (n = 79) that

were acoustically tagged in a natural reef area (depth = 38 m) off North Carolina. Some fish had been tagged and monitored in 2019, but the majority were acoustically tagged as part of the ESA analysis reported by Goldstein et al. (2025, Appendix II). Fate of released red snapper was inferred from three-dimensional movement patterns. Fate estimates indicated only 12.5% of fish released with descender devices suffered mortality, but release mortality was 93.7% for individuals that were deep-hooked. The goal of the Goldstein et al. (2025) study was not to estimate red snapper release mortality, but the study team took advantage of the available data to add valuable release mortality estimates to inform estimates of recreational release mortality.

Appendix X

Zimmermann et al. (2026) Post-release mortality of red snapper, *Lutjanus campechanus*, in U.S. Atlantic waters off northeast Florida estimated with three-dimensional acoustic telemetry. Like Rudershausen et al. (2025b), the analysis in this published paper took advantage of three-dimensional movement data of acoustically tagged red snapper from the Goldstein et al. (2025) study, but for red snapper (n = 65) tagged off northeastern Florida in summer 2024. Fish were released either at the surface or at depth with a descender device. Estimated release mortality was 27.9% for descended red snapper and 46.9% for surface-released fish. Results from Bayesian hurdle proportional hazards modeling indicate descended fish had significantly higher immediate survival, while smaller fish size and longer times out of water significantly decreased delayed survival. Study results reinforce best practice recommendations of minimizing air exposure and utilizing descender devices to mitigate post-release mortality in red snapper and other reef fishes. As with the Rudershausen et al. (2025b), results of this study add valuable release mortality estimates that were utilized during the SEDAR 90 Data Workshop to estimate red snapper recreational release mortality.

Appendix XI

Kehoe et al. (2025c) Sensitivity of CKMR-derived Atlantic red snapper population estimates to uncertainty in life history parameters. This manuscript was produced in response to Center for Independent Experts reviewer comments on *Appendix V*, which is a more general simulation study focused on elasmobranch and teleost life histories. *Appendix XI* focuses entirely and specifically on the Atlantic red snapper CKMR population model and tests via simulation the effects of bias or imprecision in various life history parameters (e.g., fecundity, mortality, and maturity at age) on red snapper population size estimates.

Chapter 1 References

Bacheler, N.M., W.F. Patterson III, J.H. Tarnecki, K.W. Shertzer, J.A. Buckel, N.J. Hostetter, K. Pacifici, V. Zulian, and W.J. Bubley. 2025. Spatiotemporal dynamics and habitat use of red snapper (*Lutjanus campechanus*) on the southeastern United States Atlantic continental shelf. Fisheries Research 281:107200; Appendix III in this report.

Bravington, M.V., H. J. Skaug, and E. C. Anderson. 2016. Close-Kin Mark-Recapture. Statistical Science 31:259–274.

Conn, P.B., M.V. Bravington, S. Baylis, and J.M. Ver Hoef. 2020. Robustness of close-kin mark–recapture estimators to dispersal limitation and spatially varying sampling probabilities. Ecology and Evolution 10:5558–5569.

Fisch, N. 2025. Expected improvements in precision when integrating opportunistic close-kin mark-recapture data into fisheries stock assessments. Fisheries Research 281:107222.

Goldstein, B.R., K. Pacifici, J.A. Buckel, N.M. Bacheler, E.M. Schliep, B. Reich, K.W. Shertzer, J.H. Tarnecki, W.F. Patterson III, and N.J. Hostetter. 2025. An integrated approach to estimating the effective sampling area of baited underwater cameras. Paper in Review; Appendix II in this report.

Hillary, R.M., M.V. Bravington, T.A. Patterson, P. Grewe, R. Bradford, P. Feutry, R. Gunasekera, V. Peddemors, J. Werry, M.P. Francis, C.A.J. Duffy, and B.D. Bruce. 2018. Genetic relatedness reveals total population size of white sharks in eastern Australia and New Zealand. Scientific Reports 8:2661.

Kehoe, L., E.C. Anderson, P.B. Conn, C.M. Hollenbeck, D.D. Chagaris, K.W. Shertzer, W.F. Patterson III, and D.S. Portnoy. 2025a. Evaluating the effect of uncertainty in life history parameters on close-kin mark-recapture estimates of fish population size through simulation. Draft Manuscript; Appendix V in this report.

Kehoe, L., K.W. Shertzer, M.V. Lauretta, J.A. Buckel, D.S. Portnoy, W.F. Patterson III, and D.D. Chagaris. 2025b. Estimating reef fish discard exploitation rates in catch and release fisheries with conventional or genetic tags. Paper in Review; Appendix VII in this report.

Lowerre-Barbieri, S., L. Crabtree, T. Switzer, S.W. Burnsed, and C. Guenther. 2015. Assessing reproductive resilience: an example with South Atlantic red snapper *Lutjanus campechanus*. Marine Ecology Progress Series 526:125–3141.

Manooch III, C.S., J.C. Potts, D.S. Vaughan, and M.L. Burton. 1998. Population assessment of the red snapper from the southeastern United States. Fisheries Research 38:19–32.

McLaughlin, P.S, E.C. Anderson, P.B. Conn, M.D. Damiano, C.M. Hollenbeck, A.A. Monroe, W.F. Patterson III, D.S. Portnoy, K.W. Shertzer, and M.T. Vincent. 2025. Incorporating close-kin mark-recapture data into an integrated stock assessment model for southeast United States Atlantic red snapper (*Lutjanus campechanus*). Draft Manuscript; Appendix VI in this report.

Mitchell W.A., T.G. Kellison, N.M. Bacheler, J.C. Potts, and C.M. Schobernd. 2014. Depth-related distribution of post-juvenile red snapper in southeastern U.S. Atlantic Ocean waters: ontogenetic patterns and implications for management. Marine and Coastal Fisheries 6:142–155.

Monroe, A., C.M. Hollenbeck, C.L. Lanoue, W.F. Patterson III, and D.S. Portnoy. 2025. Genetic population structure of red snapper, *Lutjanus campechanus*, in the U.S. Atlantic and eastern Gulf of America. Draft Manuscript; Appendix IV in this report.

Punt, A.E., R. Thomson, L.R. Little, P. Bessell-Browne, P. Burch, and M. Bravington. 2024. Including close-kin mark-recapture data in statistical catch-at-age stock assessments and management strategies. Fisheries Research 276:107057.

Rudershausen, P.J., B.J. Runde, R.M. Tharp, J.H. Merrell, N.M. Bacheler, W.F. Patterson III, and J.A. Buckel. 2025b. Discard mortality rates of Red Snapper after barotrauma and hook trauma: insights from using acoustic telemetry in the U.S. Atlantic. North American Journal of Fisheries Management 45:270–282; Appendix IX in this report.

Rudershausen, P.J., C.M. Schobernd, N.M. Bacheler, N.J. Hostetter, K. Pacifici, W.F. Patterson III, B.J. Runde, and J.A. Buckel. 2025a. Stakeholder insights corroborate habitat and reef fish abundance on the southeastern U.S. Atlantic continental shelf. In Press at Regional Studies in Marine Science; Appendix VIII in this report.

Runde, B.J., N.M. Bacheler, K.W. Shertzer, P.J. Rudershausen, B. Sauls, and J.A. Buckel. 2021. Discard mortality of red snapper released with descender devices in the U.S. South Atlantic. Marine and Coastal Fisheries 13:478–95.

Sauls, B.J., R.P. Cody, and S.J. Strelcheck. 2017. Survey methods for estimating red snapper landings in a high-effort recreational fishery managed with a small annual catch limit. North American Journal of Fisheries Management 37:302–313.

SEDAR. 2009. SEDAR 15 Stock Assessment Report 1 (SAR 1) South Atlantic Red Snapper. SEDAR, North Charleston, SC, 2009. https://sedarweb.org/assessments/sedar-15/

SEDAR. 2017. SEDAR 41 South Atlantic Red Snapper Assessment Report – Revision 1. SEDAR, North Charleston SC. 805 pp. http://sedarweb.org/sedar-41

SEDAR. 2021. SEDAR 73 South Atlantic Red Snapper Stock Assessment Report. SEDAR, North Charleston, SC. 194 pp. https://sedarweb.org/sedar-73

SEDAR. 2024. Stock Assessment of Red Snapper off the Southeastern United States – Update of SEDAR 73 Assessment. SEFSC, Beaufort, NC. http://sedarweb.org/sedar-73.

Skaug, H.J. 2001. Allele-sharing methods for estimation of population size. Biometrics 57: 750–756.

Stunz, G.W., W.F. Patterson III, S.P. Powers, J.H. Cowan, Jr., J.R. Rooker, R.A. Ahrens, K. Boswell, L. Carleton, M. Catalano, J.M. Drymon, J. Hoenig, R. Leaf, V. Lecours, S. Murawski, D. Portnoy, E. Saillant, L.S. Stokes, and R.J.D. Wells. 2021. The Great Red Snapper Count: Estimating the Absolute Abundance of Age-2+ Red Snapper (*Lutjanus*

campechanus) in the U.S. Gulf of Mexico. Mississippi-Alabama Sea Grant Consortium, NOAA Sea Grant. 408 pages.

Williams, E.H. and J. Carmichael. 2009. Final Report of the South Atlantic Fishery Independent Monitoring Program Workshop. Beaufort, North Carolina.

Winemiller, K.O. and K.A. Rose. 1992. Patterns of life-history diversification in North American fishes: implications for population regulation. Canadian Journal of Fisheries and Aquatic Sciences 49:2196–2218.

Zimmermann, S., L. Kehoe, M.A. Taylor, J.H. Tarnecki, N.M. Bacheler, Z.A. Siders, and W.F. Patterson III. 2026. Post-release mortality of red snapper, *Lutjanus campechanus*, in Atlantic waters off northeast Florida estimated with three-dimensional acoustic telemetry. Fisheries Research 294:107703; Appendix X in this report.

Zulian, V., K. Pacifici, N.M. Bacheler, J.A. Buckel, W.F. Patterson III, B.R. Reich, K.W. Shertzer, and N.J. Hostetter. 2024. Applying mark-resight, count, and telemetry data to estimate effective sampling area and fish density with stationary underwater cameras. Canadian Journal of Fisheries and Aquatic Sciences 82:1–11; Appendix I in this report.

Chapter 2

Bayesian Hierarchical Integrated Modeling to Estimate Red Snapper (*Lutjanus campechanus*) Population Size in the U.S. Atlantic

Christopher A. Custer[1a], Krishna Pacifici[2], Jeffrey A. Buckel[3], Brian J. Reich[4], Erin M. Schliep[4], Nathan M. Bacheler[5], Kyle W. Shertzer[5], Benjamin R. Goldstein[2], J. Christopher Taylor[6], Walter J. Bubley[7], Joseph H. Tarnecki[8], William F. Patterson III[8], Nathan J. Hostetter[9]

[1]North Carolina Cooperative Fish and Wildlife Research Unit, Department of Applied Ecology, North Carolina State University, Raleigh, NC, USA
[2]Department of Forestry and Environmental Resources, North Carolina State University, Raleigh, NC, USA
[3]Department of Applied Ecology, Center for Marine Sciences and Technology, North Carolina State University, Morehead City, NC, USA
[4]Department of Statistics, North Carolina State University, Raleigh, NC, USA
[5]Southeast Fisheries Science Center, National Marine Fisheries Service, Beaufort, NC, USA
[6]National Centers for Coastal Ocean Science, National Ocean Service, National Oceanic and Atmospheric Administration, Beaufort, NC, USA
[7]Marine Resources Research Institute, South Carolina Department of Natural Resources, Charleston, SC, USA
[8]School of Forest, Fisheries, and Geomatics Sciences, University of Florida, Gainesville, FL, USA
[9]U.S. Geological Survey, North Carolina Cooperative Fish and Wildlife Research Unit, Department of Applied Ecology, North Carolina State University, Raleigh, NC, USA

[a] Current address: U.S. Geological Survey, Virginia and West Virginia Water Science Center

Abstract

Spatial variation in fish abundance is driven by interacting processes across multiple spatial scales, making large-area abundance estimation challenging. Recent advances to integrate multiple survey methods and data sources provide new opportunities to expand spatial coverage, overcome logistical constraints, and leverage existing monitoring programs to quantify total abundance (i.e., population size) and its spatial drivers. This may be especially advantageous in a stock assessment context where an independent estimate of stock size may free assessment models to estimate mortality or other parameters more accurately. Herein, we estimated the population size of red snapper (*Lutjanus campechanus*), an important fishery species, across a 112,511 km^2 region of the southeastern U.S. Atlantic (SEUSA) continental shelf during 2021–2022. We developed a spatially explicit hierarchical model that incorporated fine-scale landscape covariates (e.g., depth, hardbottom presence) and a broader spatial model to capture regional variation not explained by local features. The model integrated data from baited underwater camera traps, video collected via remotely operated vehicle transects, seafloor mapping and predictive modeling, and gear-specific effective sampling areas. We estimate a population size of 5.31 million age-2+ red snapper (95% highest posterior density interval: 2.33–10.02 million) occurred on the SEUSA continental shelf during the study period. A quadratic relationship over depth and hardbottom metrics were significant predictors of local density, underscoring the importance of high-resolution seafloor mapping. Regional patterns indicate higher red snapper densities occurred off northeastern Florida with a general decline with increasing latitude, but there were localized areas of relatively high abundance in Georgia, South Carolina, and central North Carolina. Our integrative approach combined prior information for parameter values from directed research studies, targeted surveys across heterogeneous landscapes and fishery-independent data from ongoing research and monitoring programs. This approach demonstrates a generalizable framework for overcoming persistent challenges in estimating absolute abundance of marine fish populations across large spatial scales.

Introduction

Estimating abundance of fish and wildlife populations across broad spatial scales presents substantial challenges, largely due to the effort and resources required to collect sufficient data (Chrysafi and Kuparinen 2016; Stunz et al. 2021; Bruce et al. 2025). Increasingly, studies are investigating opportunities to leverage multiple survey platforms to address these logistical challenges and capitalize on existing monitoring programs, legacy data sources, and cost-effective survey approaches (Pacifici et al. 2017; Robinson et al. 2017; Schaub et al. 2024). However, integrating data from diverse and often disparate sources requires careful consideration of sampling design, underlying assumptions, potential biases, and the intended scope of inference. Variability in spatial and temporal coverage, sampling intensity, and detectability can further complicate analyses, underscoring the need for robust sampling designs and statistical frameworks (Maunder and Punt 2013; Zipkin et al. 2021; Schaub et al. 2024). In response to these challenges, methods to integrate multiple data sources continue to expand and create new opportunities to address persistent challenges and complex ecological questions in macrosystems ecology (Fei et al. 2016; Zipkin et al. 2021).

A wide range of methods are used to estimate abundance, with approaches varying based on the logistical constraints of data collection and assumptions made about the target population (e.g., spatial distribution, movement during surveys; Williams et al. 2002). Methods range from simple count-based indices to sophisticated hierarchical models that explicitly account for ecological and sampling complexities (refer to reviews in Williams et al. 2002; Kéry and Royle 2020). In recent years, camera-traps and video-based survey methods have rapidly expanded in applications across terrestrial and aquatic systems (e.g., Cove et al. 2021; Bicknell et al. 2016; Delisle et al. 2021; Bruce et al. 2025). However, estimating absolute abundance or density from camera data remains challenging as animals often cannot be individually identified, and movement into and out of the field of view can confound the effective sampling area (ESA), detection probability, and spatial reference of abundance estimates (Chandler and Royle 2013; Moeller et al. 2018; Amburgey et al. 2021; Zulian et al. 2025). These challenges are particularly pronounced in marine environments, where highly mobile marine fish rarely possess unique external identifiers and often move rapidly into and out of the camera's field of view. Despite these hurdles, methodological advances continue to improve our ability to infer absolute abundance from camera-based data in aquatic systems (Coggins et al. 2014; Shertzer et al. 2016; Shertzer et al. 2020; Garner et al. 2022; Bacheler et al. 2023; Zulian et al. 2025), and expand the role of camera surveys in fisheries-independent monitoring and spatial population assessments (Bicknell et al. 2016; Gwinn et al. 2019).

Red snapper (*Lutjanus campechanus*) is an important species for commercial and recreational fisheries in the southeastern United States, with economic and ecological significance that extends across the Atlantic and Gulf of America (formerly Gulf of Mexico; hereafter, Gulf) regions (Cowan Jr 2011; Shertzer et al. 2024; Bacheler et al. 2025). While the Atlantic and Gulf stocks are managed separately, both have experienced overfishing leading to population declines

(Hood et al. 2007; Schwartzkopf et al. 2017; Shertzer et al. 2024). In response to these findings, stringent management measures and stock rebuilding programs were introduced in both regions (DeVictor et al. 2009; Cowan et al. 2011; Cowan Jr 2011; Karnauskas et al. 2022). Research indicates these measures have improved the sustainability of the Gulf fishery, yet uncertainty remains about the status of red snapper in the southeastern United States Atlantic (SEUSA; Karnauskas et al. 2022). Current abundance estimates of Atlantic red snapper are provided in stock assessments that integrate catch-at-age, life history, and abundance index data (SEDAR 2021, 2024). Stock assessment abundance estimates are critical for management decisions. However, verifying inferences using alternative approaches and data sources is crucial to independently evaluate abundance and inform management decisions related to the stock's long-term viability.

Here, we estimated the population size of age 2+ red snapper in the SEUSA by integrating multiple fishery-independent sampling methods. Specifically, our data included underwater camera-traps from the Southeast Reef Fish Survey (SERFS), transect video collected via a remotely operated vehicle (ROV), previously published maps that quantified the distribution and extent of hardbottom habitat (Steward et al. 2022; Bacheler et al. 2025), and results from localized experiments to inform sampling gear efficiencies (e.g., effective sampling areas, imperfect detection). We developed a spatially explicit process model to estimate SEUSA red snapper population size based on fine-scale landscape covariates (e.g., depth, hardbottom presence and configuration at ~90 × 90 m resolution), along with a broader spatial model to account for local-to-regional variation not captured by fine-scale features. We paired this with survey-specific observation models that addressed the distinct sampling characteristics of each gear type and method. This approach of combining localized experiments to evaluate sampling gear efficiencies, targeting samples across diverse habitats, and the integration of research and monitoring datasets focused on high-abundance areas illustrates a general framework for designing fishery-independent studies capable of overcoming the persistent challenges in estimating absolute abundance of marine fish populations and provides regional and state-specific estimates of red snapper abundances across the SEUSA.

Methods

Study Area and Surveys

We estimated age-2+ red snapper abundance along the SEUSA coast from North Carolina to the Florida Keys (Figures 2-1, 2-2). The study area covered approximately 112,500 km^2, encompassing the northern to southern extent of the South Atlantic Fishery Management Council's jurisdiction. The study area was designed to cover depths of 10 to 150 m (>99.5% of the study area); however a small proportion of locations (<0.5% of the study area) had depths that were <10 or >150 m (range 0 to 179 m; Figure 2-1). Red snapper count data were obtained from two fishery-independent surveys conducted during 2021–2022: (1) SERFS baited camera-traps (2,434 samples; hereafter camera-trap), and (2) remotely operated vehicle (ROV) video survey (436 samples; hereafter ROV; Table 1).

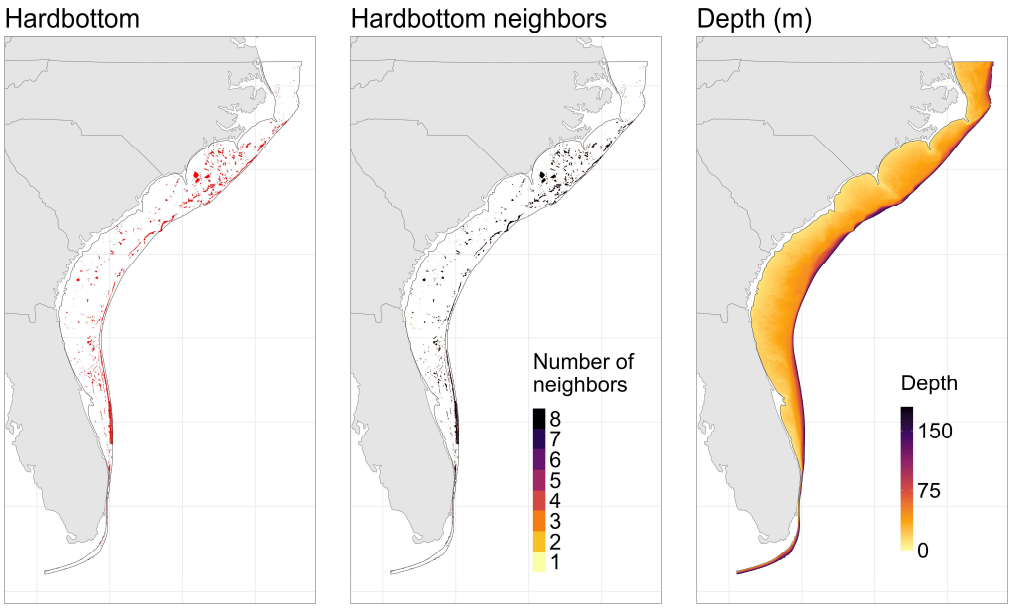

Figure 2-1. Maps of habitat covariates at ~90×90-m grid cells across the study region (black outline). Hardbottom cells are those with predicted hardbottom by the expert opinion map (see Steward et al. 2022) or The Nature Conservancy - South Atlantic Bight Marine Assessment map (High or Very High confidence levels; see Conley et al. 2017). Hardbottom neighbors is the number of neighboring grid cells with hardbottom (queen's case, maximum of 8), and depth in m.

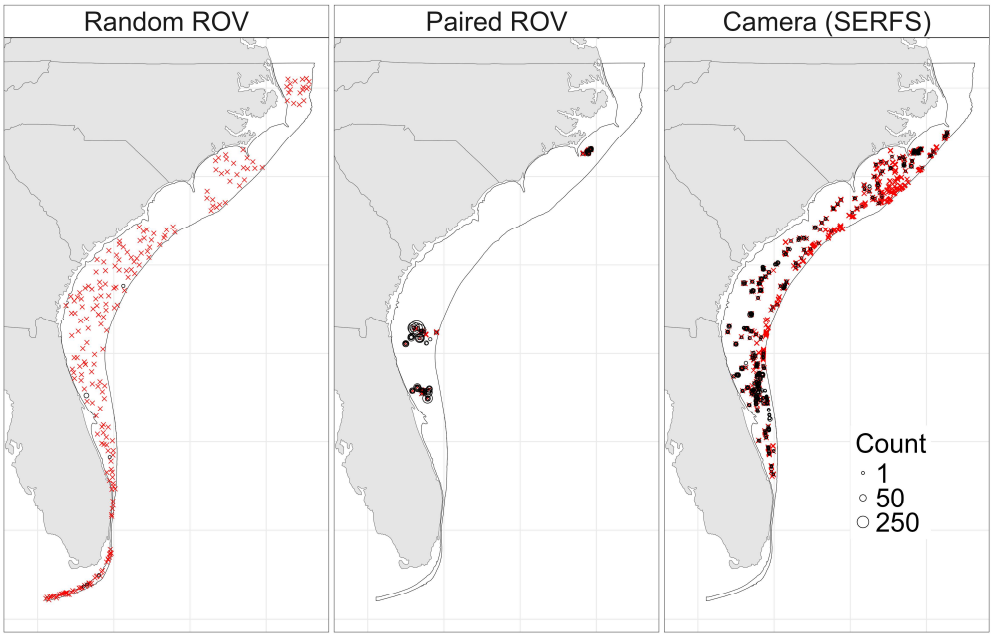

Figure 2-2. Maps of red snapper sampling sites by sampling design across the study region (black outline). Point shapes indicate whether red snapper were observed, with black circles for detections and red Xs for non-detections. Circle size is scaled to the number of red snapper counted at remotely operated vehicle (ROV) sites or the mean count across 41 picture frames for camera-trap sites.

Camera-trap samples followed SERFS sampling protocols described in detail by Bacheler et al. (2025), and summarized here. We sampled across the SEUSA continental shelf and upper slope between Cape Hatteras, North Carolina, and St. Lucie Inlet, Florida, using chevron traps (trap volume = 1.7 × 1.5 × 0.6 m; 0.91 m^3) baited with *Brevoortia* spp and with two attached cameras during April-September 2021 (n=1,384) and 2022 (n=1,050; Figure 2-2; Smart et al. 2015; Bacheler et al. 2023). GoPro® Hero3+ or Hero4 cameras were mounted on top of chevron traps and recorded video at 1080p resolution and 30 frames per second across a 123° linear field of view. Red snapper were then counted in each of 41 snapshots spaced 30 seconds apart, beginning 10 minutes after the trap reached the seafloor and spanning a total of 20 minutes (Schobernd et al. 2014; Bacheler et al. 2023). Current direction was estimated as "away", "sideways", or "towards" based on the movement of visible particles in the water relative to the view field of the video camera over the trap mouth (Bacheler et al. 2025). Our analysis focused on the camera counts and not the catches of red snapper in the traps as we developed methods to estimate density and absolute abundance from camera counts but not trap catches (described below). SERFS sampling locations were chosen via simple random sampling from approximately 4,300 potential sites assumed to have reef structure (Smart et al. 2015; Steward et al. 2022; Cao et al. 2024).

The ROV survey ($n = 436$) sampled red snapper throughout the entire study area, from the Florida Keys (24'N , 81'W) to the Nags Head, North Carolina (36'N, 74'W; Figure 2-2). At each site, one ($n = 5$) or two ($n = 431$) 100-meter transects were conducted at approximately 1–2m above the seafloor (see Bacheler et al. 2025 for more details). Samples were conducted during June-August 2021 ($n = 262$ samples) and June-October 2022 ($n = 174$ samples). We used two methods to select ROV sample sites: (1) randomly selected locations (n = 231; hereafter *random ROV*) and (2) sites paired with SERFS camera-trap locations ($n = 205$; hereafter *paired ROV*). For random sites, the study area was divided into six regions, and within each region, sites were selected by generating random integer latitudes and longitudes, then random decimal degrees within the specified depth range. ROV transects were conducted as close as possible to the selected GPS coordinates, considering sea conditions (Bacheler et al. 2025). In contrast, paired ROV sites were co-located near SERFS camera-trap locations to maximize spatial overlap between ROV and camera-trap samples, providing data to inform parameters linking the two sampling methods [see Section 2.3 in Bacheler et al. (2025)]. Paired sites therefore occurred in areas of high red snapper abundance (Figure 2-2). Video readers quantified the total number of red snapper observed in the video footage from each transect, providing both red snapper counts and estimates of the area sampled, which were derived from the ROV's height above the seafloor, camera angle, and transect length (Patterson et al. 2014; Garner et al. 2022).

Habitat Data

Red snapper are associated with hard structures such as reefs, rocks, and areas of high relief, collectively termed hardbottom (Chatterjee et al. 2024; Bacheler et al. 2025). For our analyses, we divided the study area into $G = 14{,}658{,}041$ grid cells of approximately 90 × 90 m

($g \in 1, \ldots, G$) following Pickens and Taylor (2020). We then developed a composite hardbottom map using maps from Steward et al. (2022) and Conley et al. (2017). A grid cell was classified as hardbottom if either the expert opinion map (hereafter EO map) in Steward et al. (2022) or The Nature Conservancy's South Atlantic Bight Marine Assessment map (hereafter TNC map; Conley et al. 2017) indicated hardbottom presence. Otherwise, a grid cell was classified as not having hardbottom. For the TNC map, we restricted hardbottom to areas listed as high or very high confidence of hardbottom presence (Conley et al. 2017). Combining the EO map and TNC map was necessary as no comprehensive survey of reef habitat from North Carolina to southern Florida exists in the literature. We combined the two maps to address limitations of each: (1) the EO map was not developed for areas north of Cape Hatteras, North Carolina or south of St. Lucie Inlet, Florida, but it served as the basis for selecting SERFS sampling locations; and (2) the TNC map covered the entire study area but classified the majority of SERFS sampling locations as non-hardbottom. The EO map was created in 2022 by two experts who delineated reef boundaries using multiple data sources, and many hardbottom areas they identified have since been confirmed with multibeam or side-scan sonar surveys (Steward et al. 2022). The TNC map was generated from a synthesis of depth, seafloor complexity, geology, and sediment data, with details provided in Steward et al. (2022) and Conley et al. (2017). Additionally, to account for red snapper use of areas adjacent to hardbottom (Bohaboy et al. 2022; Lowerre-Barbieri et al. 2025), we included the number of neighboring grid cells (using queen's case connectivity, with a maximum of 8) containing hardbottom as a habitat structure potentially affecting abundance. To account for potential nonlinear patterns in red snapper abundance across depth gradients, we included both depth and its quadratic term (depth^2) in the model (Mitchell et al. 2014; Bacheler et al. 2016).

Abundance Model

We define λ_g as the expected density of red snapper in grid cell g. Expected absolute abundance (hereafter abundance) in grid cell g is thus $\lambda_g \times area_g$, and total abundance across the SEUSA is $\Lambda = \sum_{g=1}^{G} \lambda_g \times area_g$. We modeled red snapper expected density as

$$\log(\lambda_g) = \beta_0 + \mathrm{X}_g\boldsymbol{\beta} + \alpha_g, \qquad \text{(equation 2-1)}$$

where $\mathrm{X}_g = (X_{g1}, \ldots, X_{gp})$ are the p habitat covariates associated with each grid cell g (hardbottom presence, number of hardbottom neighbors, depth, depth^2), $\boldsymbol{\beta}$ is the p-length vector of estimated habitat coefficients, and α_g are spatial random effects included to explain spatial variation not captured by the covariates. The spatial random effects α_g were modeled using a conditional autoregressive (CAR) prior (Gelfand et al. 2010). Due to the large number of grid cells (> 14 million), we define the CAR prior on a coarser grid of subregions, described below (~5.5 x 5.5 km; or 0.05 x 0.05 degrees) to ensure a computationally tractable adjacency matrix. The size of the subregions was selected so the number of subregions exceeds the number of sampled sites

to preserve the spatial information in the data (Gelfand et al. 2010). This parsimonious approach ensures that the total number of parameters to estimate is small relative to the number of observations (i.e. only the parameters of the CAR prior are estimated, τ) while simultaneously allowing for information to be shared across a subregion via spatial correlation. Let the spatial domain be buffered by 0.25 degrees and partitioned in R subregions (R = 7,861) with $\alpha_g = a_r$ if grid cell g is in subregion r. The CAR prior for $\mathbf{a} = (a_1, \ldots, a_R)^T$ is multivariate normal with mean zero and inverse covariance $\tau(\mathbf{M} - \mathbf{D})$, with scale parameter $\tau^{-1/2}$, adjacency matrix $\mathbf{D}$ ($D_{rs} = 1$ if subregions r and s are adjacent and zero otherwise, and $D_{rr} = 0$), and $\mathbf{M}$ the diagonal matrix with diagonal element r equal to the number of subregions adjacent to subregion r. To identify the intercept parameter β_0, we impose the constraint that the spatial random effects sum to zero. Together, this approach allows red snapper abundance to vary as a function of local covariates at the grid cell level, while also addressing broader spatial patterns unexplained by covariates (e.g., regional abundance patterns; Bacheler et al. 2025).

We estimated abundance using the two previously described data sources: (1) SERFS camera-traps and (2) ROV video samples. To integrate information across both data sources, we jointly modeled the ROV and camera-trap data in terms of the underlying density parameters λ_g with additional terms to account for systematic differences between gear types and sampling designs.

For the ROV data, let Y_i be the number of red snapper observed by the ROV at site $i \in \{1, \ldots, I\}$ (summed across transects at site i) and the index of the grid cell that includes ROV site i is $g_i \in \{1, \ldots, G\}$. We modeled the ROV data as

$$Y_i \sim \text{Poisson}(\mu_i), \qquad \text{(equation 2-2)}$$

$$\mu_i = \lambda_{g_i} \times \text{area}_i \times \exp(\gamma_{\text{paired}} \times E_i) \times \gamma_{\text{rov}}. \qquad \text{(equation 2-3)}$$

Here, λ_{g_i} is the expected red snapper density in the grid cell containing site i, and $area_i$ is the fixed and known ROV sampling area (in km^2) at site i. We included two additional terms to account for ROV-specific sampling designs. First, $\gamma_{\text{paired}} \times E_i$ adjusts for paired sampling design effects, where $E_i = 1$ if site i was a paired ROV site that was purposefully placed near a camera-trap location with anticipated high red snapper abundance (and $E_i = 0$, otherwise). This offset parameter is applied to the ROV abundance model to explain the higher counts at paired sites (due to sampling bias) while preserving the true underlying density in that grid cell and minimizing the effects of this bias on estimates from random ROV sites. Here, we expected a result of $\gamma_{\text{paired}} > 0$ as we preferentially selected sites with high abundances to inform model parameters linking the ROV and camera-trap sample methods at paired sites. Second, γ_{rov} is an estimated offset that adjusts for differences in detection or sampling efficiency specific to the ROV. If $\gamma_{rov} \neq 1$, ROV counts deviate from expected counts based on the grid cell density. We applied an informative prior distribution from Goldstein et al. (2025), which indicates ROV counts may be elevated

($\gamma_{rov} > 1$) due to attraction of red snapper to the ROV, landscape mismatches between camera-trap drop locations and landscapes along the 100 m transects, or other mechanisms. We assigned $\gamma_{rov} \sim \text{Gamma}(shape = 30.24, rate = 6.55)$ reflecting a prior mean and standard deviation of 4.6 and 0.84, respectively (Goldstein et al. 2025).

For the camera-trap data, let W_{jf} be the number of red snapper observed in frame $f \in \{1,\ldots,41\}$ of camera-trap site $j \in \{1,\ldots,J\}$. We modeled camera-trap data using an N-mixture framework (Royle 2004), where

$$N_j \sim \text{Poisson}(\lambda_{g_j} ESA_j), \quad \text{(equation 2-4)}$$

$$W_{jf} \sim \text{Binomial}(p_{jf}, N_j), \quad \text{(equation 2-5)}$$

$$p_{jf} \sim \text{Beta}(z_1 z_2, (1 - z_1) z_2). \quad \text{(equation 2-6)}$$

Here, N_j is the latent number of red snapper available to be sampled during the 20-minute camera-trap deployment at site j, and λ_{g_j} is the expected red snapper density in the grid cell containing camera-trap site j. The effective sampling area, ESA_j, represents the latent area sampled by the camera-trap across the 20-minute sampling period at site j, and p_{jf} is the detection probability, modeled with a Beta distribution defined by hyperparameters z_1 and z_2 (defined in Section 2.4).

Unlike the ROV data, the effective sampling area for camera-traps is unknown because fish may enter or leave the field of view during the 30-second intervals between frames across the 20-minute sample period. Therefore, we treated ESA_j as a latent parameter with an informative prior derived from an independent camera–ROV–telemetry study that estimated ESA values using baited camera-traps similar to those used here (Goldstein et al. 2025). Effective sampling areas of camera-traps were assigned to one of three prior distributions based on current direction (b_d): $ESA_j = b_1$ if the current was flowing away from the camera-trap, b_2 if the current was flowing sideways to the camera-trap, and b_3 if the current was flowing towards the camera-trap. Incorporating current direction specific $ESAs$ accounts for a form of bait attraction and aggregation. For example, we expect larger $ESAs$ when the current direction pushes the bait plume in front of the camera compared to behind the camera not because fish density is locally higher (λ_{g_j}), but because fish are aggregating in front of the camera (ESA_j; Bacheler et al. 2022b; Zulian et al. 2025; Goldstein et al. 2025). We defined prior distributions based on results from Goldstein et al. (2025) where $b_d \sim \text{Gamma}(shape = k_d, rate = \theta_d)$, with k_d and θ_d set so that the prior means in km^2 of b_1, b_2 and b_3 were 0.0105, 0.0091, and 0.0088, and standard deviations were 0.0016, 0.0015, and 0.0016, respectively. Finally, there is the potential for bias in camera-trap counts due to red snapper entering the chevron trap and no longer being available for detection by the camera-traps. This bias is likely small or non-existent for several reasons. First, the frequency of occurrence of red snapper in the camera-trap data is twice that of occurrence in chevron traps (Bacheler et al. 2022a) meaning that around half of the positive camera-trap counts had no chevron

trap catch. Second, camera-traps sample minutes 10 to 30 of a trap soak which generally lasts 90 minutes or more; given that chevron trap catch increases with soak time, most red snapper may go into traps after the camera sampling occurs (N.M. Bacheler, pers. comm.).

Model Fitting and Predictions

We fit the abundance model in a Bayesian framework. As previously described, we assigned informative priors to the ROV offset (γ_{rov}) and camera-trap effective sampling areas (**b**), while the remaining parameters were given vague prior distributions. Specifically, we assigned $N(0, sd = 10)$ priors to β_0, $\beta_1, \ldots, \beta_p$, and γ_{paired}, $\tau \sim$ Half-Cauchy(0,1), $z_1 \sim$ Beta(1,1), and $z_2 \sim$ Half-Cauchy(0,1).

All analyses were conducted using R (R Core Team 2024). The model was fit with the NIMBLE package (de Valpine et al. 2017). We ran 3 chains of 250,000 total iterations with the first 50,000 iterations discarded as burn-in. Due to file size (>14 million grid cells), we thinned each chain to every 200th sample thus retaining 3,000 posterior samples for inference and prediction. We verified convergence using traceplots and $\hat{R}$ <1.1 (Gelman et al. 2013). We summarize posterior distributions using medians and the 95% highest posterior density interval (HPD) using the hdi function from the HDInterval package (Meredith and Kruschke 2022) We predicted expected fish abundance, $\lambda_g area_g$, for each grid cell across the study region. Study area abundance was then the sum of all grid cells, and state-specific abundance estimates were derived as the sum of grid cells within the state boundaries defined for fishery management in the South Atlantic Exclusive Economic Zone (NOAA 2025).

We compared our estimate of red snapper abundance to estimates of abundance from the most recent Atlantic red snapper stock assessment (SEDAR 2024). We assumed estimates reflected age-2+ red snapper; however, in 2021 nearly 20% of the chevron trap catch was age-1 fish but it was less than 5% in 2022 (SEDAR 2024). As such, SERFS camera-trap data included age-1 fish and our estimate of red snapper abundance includes some unknown proportion of age-1 red snapper. Thus, we compare our estimate of abundance to stock assessment estimates of both age-1+ and age-2+ red snapper.

Furthermore, we refit the model under three alternative scenarios to evaluate the sensitivity of total abundance estimates to hardbottom map selection and assumptions. First, we used a hardbottom map derived solely from the TNC map (ignoring the EO map). Second, we again used the TNC map but added a preferential sampling parameter (Conn et al. 2016) to account for SERFS sites being selected based on assumed hardbottom presence. Third, we fit the model defined in Section 2.3, but developed the composite map (TNC + EO) using all confidence levels of the TNC map (i.e., not restricting the map to high and very high confidence levels). This was not intended as a comprehensive evaluation of assumptions; rather, it highlights the importance of underlying hardbottom maps for estimating red snapper abundance in the SEUSA.

Results

Surveys

During 2021–2022, researchers conducted a total of 436 ROV samples (205 paired and 231 random) and sampled 2,434 sites with camera-traps across the study area (Table 2-1; Figure 2-2). Of the 231 random ROV samples, only 3% ($n = 6$) detected red snapper. In contrast, paired ROV and camera-trap samples, both targeting areas with hardbottom, detected red snapper at 46% and 35% of sites, respectively. Observed current directions at the camera-traps were 700 away (28.8%), 1,119 sideways (46.0%), 615 towards (25.2%).

After merging the EO and TNC hardbottom maps, 5.4% of the study area grid-cells were classified as hardbottom (Figure 2-1). The total area surveyed by ROV transects was 0.71 km^2, representing 0.0006% of the total study area. Using posterior median estimates of effective sampling areas (ESA), the 2,434 camera-trap sites covered 25.93 km^2, or 0.023% of the study area. Combined, the two sampling methods surveyed 0.024% of the total area (Figure 2-2).

Table 2-1. Summary of red snapper count data by sampling method. *Sites* is the number of sampled sites (percentage of total sites). *Sites observed* is the number of sampled sites with at least one red snapper detected, along with the percentage of sites containing observations for that design. *Mean* is the average count across all sampled sites, while *Mean observed* is the mean count across only those sampled sites where at least one red snapper was observed.

Method	Sites (%)	Sites observed (%)	Mean (Mean observed)
Random ROV	231 (8%)	6 (3%)	0.11 (3.8)
Paired ROV	205 (7%)	95 (46%)	14.98 (32.3)
Camera-trap (SERFS)	2434 (85%)	852 (35%)	0.46 (1.3)

Random ROV samples provided the primary data source for estimating abundance in non-hardbottom regions (Table 2-2). The influence of adjacent hardbottom habitat on red snapper presence and abundance was evident in ROV data, with red snapper detections and counts substantially higher at non-hardbottom sites bordered by at least one hardbottom grid cell (mean count = 1.20) compared to non-hardbottom locations with 0 neighboring hardbottom cells (mean count = 0.02; Table 2-2A). In contrast, SERFS camera-trap samples were the primary source of data for hardbottom regions, with 2,418 video samples conducted at sites classified as hardbottom, all of which had at least one neighboring hardbottom cell (Table 2-2B). Camera-trap sites with predicted hardbottom detected red snapper during 847 of the 2418 samples, with a mean count of 0.46 red snapper per sample (Table 2-2B). Finally, mean red snapper counts at paired ROV sites were considerably higher than those from other sampling designs (15.05 individuals per site; Table 2-2C), consistent with the paired sampling objective to target locations with higher densities to inform model parameters linking the two survey methods (γ_{rov}, γ_{paired}, ESA). In total across all gears, the detection of red snapper increased with the presence of hardbottom (0.04 to 0.36) and

hardbottom neighbors (0.03 to 0.36; Table 2-2D).

Covariate Effects

Depth and the number of hardbottom neighbors were significantly associated with red snapper density (95% HPD intervals did not overlap zero for β estimates; Table 2-3). The quadratic depth relationship indicated a peak in red snapper density near depths of approximately 40-50 m, with sharp declines in shallower and deeper waters (Figure 2-3). Red snapper density also increased significantly with the number of neighboring hardbottom cells (0.30; 95% HPD 0.13 – 0.48; Table 2-3), consistent with patterns in the raw data where non-hardbottom sites adjacent to hardbottom showed notably higher counts (Table 2-2). In contrast, the binary presence of hardbottom within a grid cell was not significantly related to density (-0.95; 95% HPD -2.20 – 0.32; Table 2-3). However, this likely reflects the spatial clustering of hardbottom features, as more than 99% of hardbottom cells had at least one neighboring hardbottom cell (790,254 out of 792,123; Figure 2-1). The spatial random effects supported regional structure, where red snapper abundances were higher than expected from the habitat covariates alone throughout sections of central and northern Florida and Georgia, and lower than expected in portions of South Carolina and North Carolina (Figure S1).

Table 2-2. Summary of red snapper count data (means) by sampling method, hardbottom presence at a site (HB), and hardbottom neighbors (HBn). Numbers in parentheses indicate number of sites where ≥1 red snapper was observed relative to the total number of sites sampled. Section (D) (Total) does not report mean counts, as these values are not directly comparable across survey methods.

A) ROV random (n=231)

	HBn=0	HBn>0	Total
HB=0	0.02 (3/192 = 0.02)	1.20 (2/15 = 0.13)	0.11 (5/207 = 0.02)
HB=1	0.00 (0/1 = 0.00)	0.04 (1/23 = 0.04)	0.04 (1/24 = 0.04)

B) Camera-trap (n=2,434)

	HBn=0	HBn>0	Total
HB=0	0.36 (4/14 = 0.29)	0.20 (1/2 = 0.50)	0.34 (5/16 = 0.31)
HB=1	NA (0/0 = NA)	0.46 (847/2418 = 0.35)	0.46 (847/2418 = 0.35)

C) ROV paired (n=205)

	HBn=0	HBn>0	Total
HB=0	NA (0/0 = NA)	0.00 (0/1 = 0.00)	0.00 (0/1 = 0.00)
HB=1	NA (0/0 = NA)	15.05 (95/204 = 0.47)	15.05 (95/204 = 0.47)

D) Total (n=2,870)

	HBn=0	HBn>0	Total
HB=0	7/206 = 0.03	3/18 = 0.17	10/224 = 0.04
HB=1	0/1 = 0.00	943/2645 = 0.36	943/2646 = 0.36
Total	7/207 = 0.03	946/2663 = 0.36	

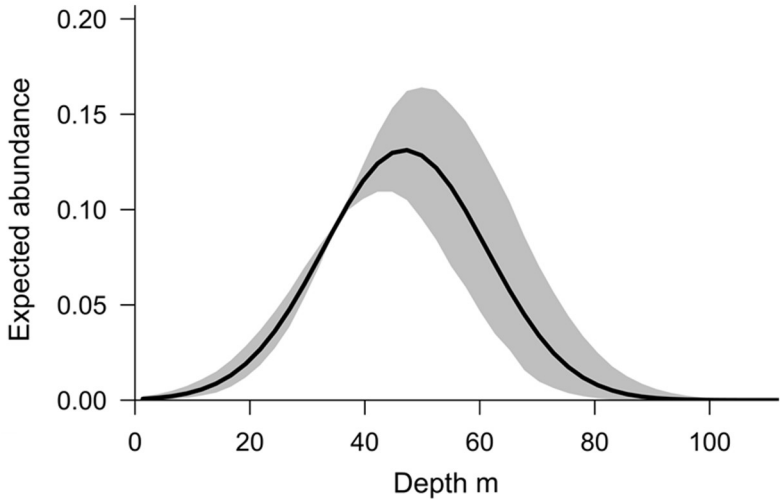

Figure 2-3. Effect of water depth on expected red snapper abundance per ~90×90-m grid cell across the study region. Median predictions (black line) and 95% highest posterior density intervals (gray shading) are shown; all other covariates held at mean values.

Table 2-3. Summary of parameter estimates from the red snapper population estimation model (posterior medians and 95% highest posterior density [HPD] intervals). Values include the log-scale intercept (β_0), effects of hardbottom presence in the grid cell (β_{hb}), number of hardbottom neighbors ($\beta_{neighbors}$), depth (β_{depth}), depth^2 (β_{depth2}), paired sampling offset (γ_{paired}), remotely operated vehicle offset (γ_{rov}), effective sampling areas of camera-traps by current direction i (ESA_i; in km^2), the precision parameter for the conditional autoregressive (CAR) prior (τ), and parameters controlling the mean and precision of detection probability in the camera-trap samples (z_1, and z_2, respectively). For abundance parameters, estimates are on the log-scale except γ_{rov} and ESA_i, which are multipliers on the natural scale (see Methods: *Abundance Model*).

Parameters	Median	95% HPD
β_0	2.44	(1.60, 3.21)
β_{hb}	-0.95	(-2.20, 0.32)
$\beta_{neighbors}$	0.30	(0.13, 0.48)
β_{depth}	-1.47	(-1.93, -0.93)
β_{depth2}	-1.64	(-2.11, -1.19)
γ_{paired}	2.47	(1.83, 2.95)
γ_{rov}	2.28	(1.17, 3.65)
ESA_{away}	0.016	(0.012, 0.019)
$ESA_{sideways}$	0.009	(0.007, 0.011)
$ESA_{towards}$	0.007	(0.005, 0.008)
τ	0.21	(0.17, 0.26)
z_1	0.190	(0.186, 0.194)
z_2	5.55	(5.26, 5.87)

Posterior inference for the ROV offset parameter (γ_{rov}) yielded a median of 2.28 (95% HPD: 1.17 – 3.65), indicating elevated counts relative to underlying density. However, the posterior distribution was substantially attenuated relative to the prior (median = 4.6), reflecting strong data influence and shrinkage toward no effect (Figure 2-4). As anticipated, the ROV paired sampling parameter (γ_{paired}) indicated ROV counts were substantially higher than expected densities at paired sites (2.47; 95% HPD 1.83 – 2.95), consistent with the sampling design objective of selecting high-density locations to inform parameters linking the camera-trap and ROV methods) (Table 2-3). Effective sampling area (ESA) estimates for camera-traps were generally consistent with their prior distributions, though posterior differences among current directions became more pronounced. Specifically, ESA estimates were lower when current flowed toward the camera (0.007 km^2) and higher when current flowed away (0.016 km^2) relative to their prior distributions (Figure 2-4). Hyperparameter estimates for camera-trap detection probability (z_1 and z_2; Table 2-3) indicated detection probability at the camera-traps was generally low and variable among sites (approximate hyperparameter detection probability median = 0.15; 95% HPD <0.01 – 0.50). Taken together with ESA results, the low and variable detection probabilities were consistent with the assumption that red snapper frequently moved into and out of the camera-trap field of view during the 20-minute sampling period, resulting in both an effective sampling area that was larger than the camera-trap field of view and the same red snapper not being consistently detected in all frames.

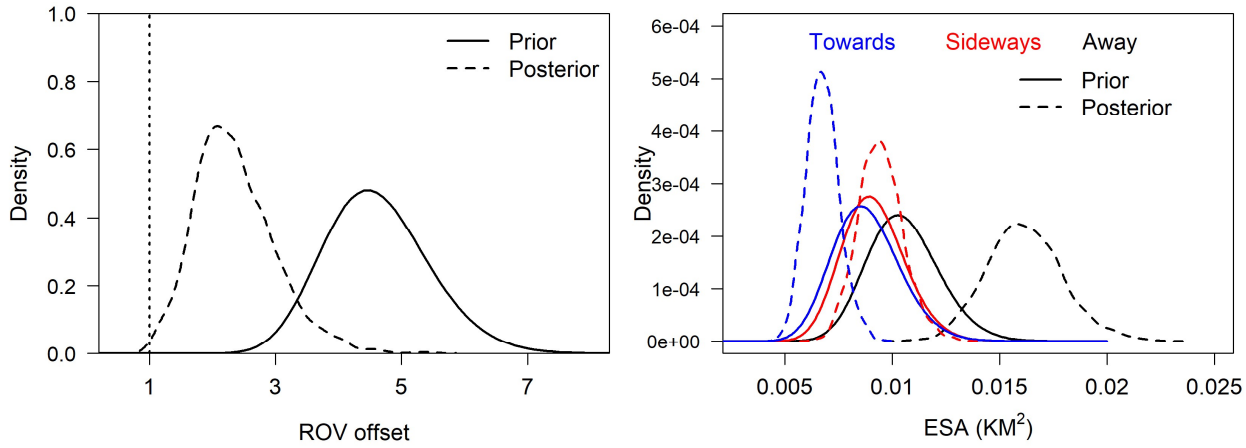

Figure 2-4. Prior and posterior distributions for (left) the remotely operated vehicle (ROV) offset parameter and (right) camera-trap effective sampling area (ESA) parameters for the three current directions. Prior distributions were derived from an independent camera–ROV–telemetry study that estimated ESA and ROV offset parameters using baited camera-trap systems similar to those used in the study herein (Goldstein et al. 2025). In the ROV offset panel, values greater than 1.0 indicate that the ROV detected more fish than expected based on the grid cell density.

Estimated Population Size

Total abundance (population size) in the 112,511 km^2 study area was estimated at 5.31 million red snapper (95% HPD 2.33 – 10.02 million; coefficient of variation = 0.39; Figure 2-5). Predicted abundance at the local scale varied greatly across the study area, ranging from 0 – 60 individuals per ~90 x 90 m grid cell (Figure 2-5). Of the 14.66 million grid cells, 13.79 million (94%) had predicted abundances of fewer than 0.5 individuals per cell (Figure 2-6), a pattern consistent with the approximately 95% of the study area classified as non-hardbottom habitat (Figure 2-1). In contrast, only 0.2% of grid cells (n = 30,002) had predicted abundances of 5 or more individuals per cell (Figures 2-5, 2-6).

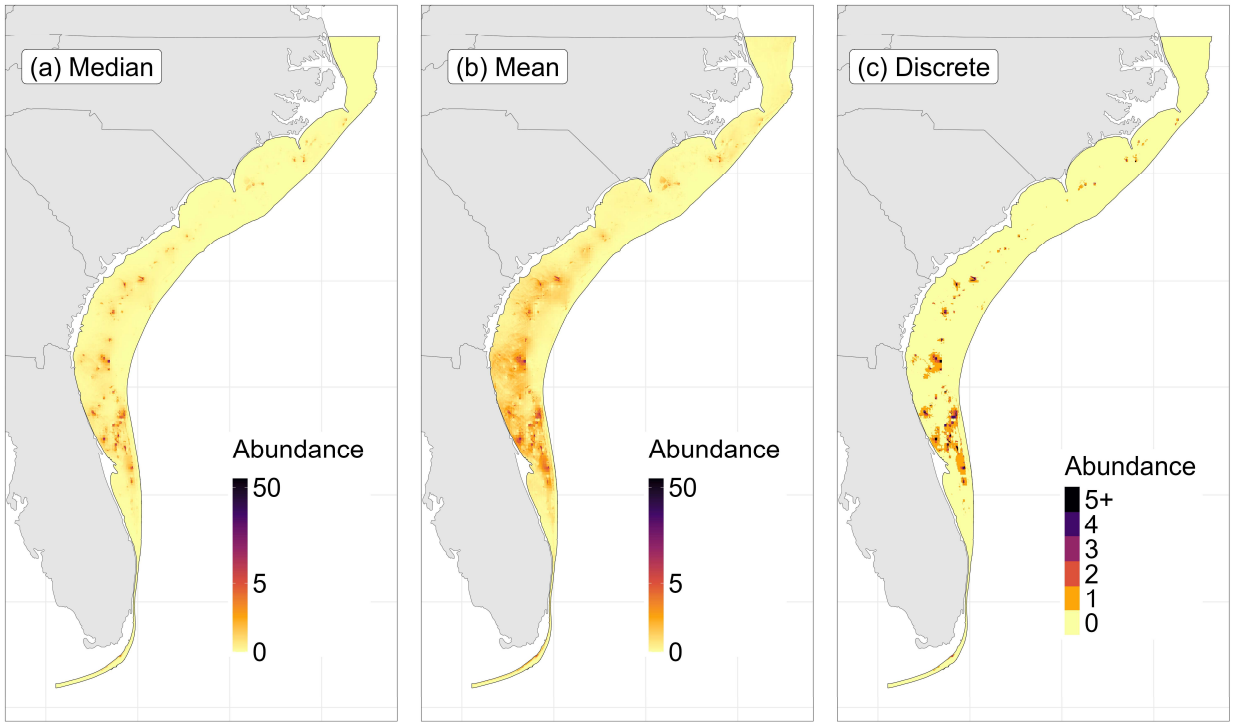

Figure 2-5. Predicted red snapper abundance per ~90×90-m grid cell across study region. Maps show posterior medians (left), means (middle), and discretized medians (right). Population estimate across region = 5.31 x 10^6 fish (95% highest posterior density: 2.33–10.02 x 10^6).

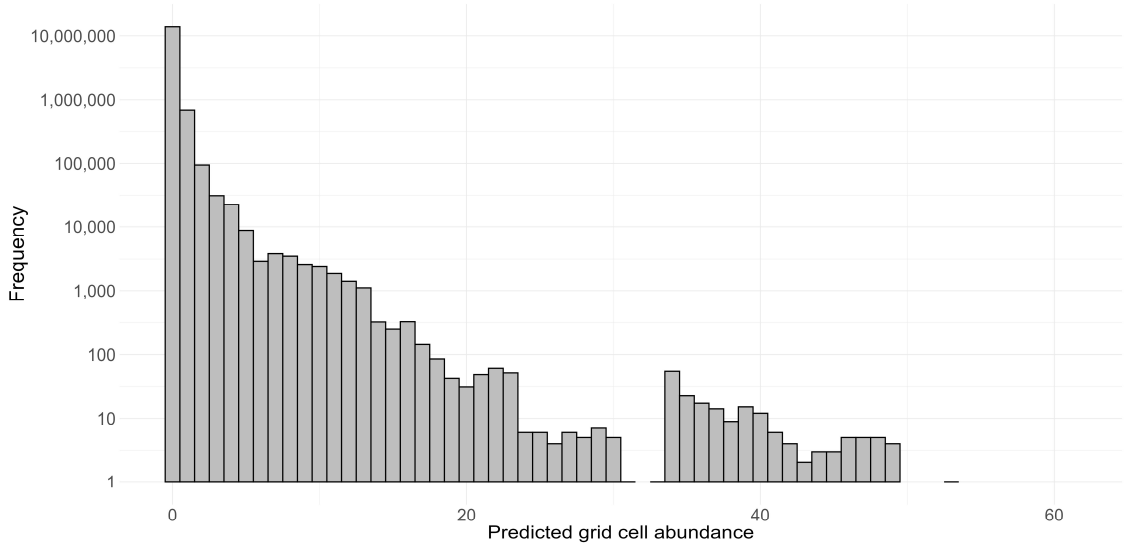

Figure 2-6. Histogram of median predicted red snapper abundance per ~90 x 90-m grid cell across the study region. The y-axis is displayed on the log_{10} scale. For example, predicted abundance was <0.5 red snapper per cell in 13.79 million of the 14.66 million grid cells, ~1 red snapper per grid cell in 0.69 million grid cells, and ≥5 red snapper per cell for 30,002 grid cells. See Figure 2-5 for mapped predictions.

Expected abundance was highest off the coast of northeastern Florida, with additional localized areas of higher abundance off the coasts of Georgia, South Carolina, and southern North Carolina (Figure 2-5). In northern Florida, expected abundance exceeded 5 individuals per grid cell in numerous locations but areas of higher abundance declined steadily with increasing latitude, remaining at or below 3 individuals per cell farther north even in the highest abundance locations (Figure 2-5). Large areas of near-zero expected abundance appeared throughout northern regions of the study area, closely mirroring the distribution of observed data (Figure 2-7). By state, the highest estimated abundance occurred in Florida (3.06 million; 95% HPD 1.28 – 5.91 million), followed by Georgia (0.96 million; 95% HPD 0.27 – 1.91 million), South Carolina (0.75 million; 95% HPD 0.26 – 1.52 million), and North Carolina (0.51 million; 95% HPD 0.19 – 1.23 million; Table 2-4).

If we assume our total red snapper population estimate (5.31 million) only consisted of age-2+ red snapper, then it is above the median of the 2021 and 2022 estimates of age-2+ red snapper (2.02 million) from the updated Atlantic red snapper stock assessment (SEDAR 2024). However, the lower bound (95%HPD) of our estimate (2.33 million) falls within the 95% bounds for the 2021 and 2022 stock assessment estimates (1.54 to 2.76 million). The average of the medians and 95% bounds for age-1+ red snapper population size from the updated SEDAR 73 assessment for 2021 and 2022 are 3.11 million (2.29 to 4.37 million), which also overlaps with the bounds of our estimate.

Table 2-4. Estimated red snapper population size by state, including area (km^2), hardbottom areas (km^2), posterior median population size (millions), 95% highest posterior density (HPD) interval, and %total population size. Estimates for Florida are presented as total and subdivided into northeastern Florida (NEFL; state waters north of 28N), east central Florida (ECFL; 28N to Miami), and southeastern Florida (SEFL; Miami to the southern boundary of the study area).

State	Total area km^2	Hardbottom area km^2	Median population size millions	95% HPD	%Total population size
NC	36,912	2,503	0.51	(0.19, 1.23)	9.66
SC	25,414	847	0.75	(0.26, 1.52)	14.20
GA	17,361	390	0.96	(0.27, 1.91)	18.18
FL	32,823	2,372	3.06	(1.28, 5.91)	57.95
NEFL	26,037	1,594	2.91	(1.16, 5.69)	55.11
ECFL	4,943	696	0.08	(0.02, 0.20)	1.52
SEFL	1,843	82	0.04	(<0.01, 0.14)	0.01

Population size estimates exceeded 99.95 million red snapper (coefficient of variation, CV = 0.28) when the model was refit using only the TNC map to delineate hardbottom habitat. In contrast, population estimates declined to 0.79 million (CV = 0.46) individuals when the model incorporated both the TNC map and a preferential sampling parameter for SERFS sites. The inflated abundance in the former case arose because the TNC map classified more than 50% of SERFS sites as non-hardbottom. This discrepancy led the model to estimate higher red snapper densities in non-hardbottom areas, which comprise the majority of the study region (Table 2-4). Conversely, including the preferential sampling effect led the model to attribute elevated counts at SERFS sites to targeted site selection rather than to higher abundances associated with hardbottom, resulting in substantially reduced population estimates. Finally, using all confidence levels of the TNC map to develop the composite map increased predicted hardbottom across the study area from ~5.4% to ~13%, but assigned SERFS sites to hardbottom areas in the same way as the original composite map. Based on this revised hardbottom map, total red snapper abundance was estimated at 7.22 million individuals (95% HPD 3.37 - 12.01 million; CV = 0.32).

Discussion

To address challenges in estimating absolute fish abundance from video surveys, we implemented a Bayesian hierarchical model that integrated count data from multiple survey types. Demonstrated here with red snapper across the SEUSA shelf, we estimated a total abundance that exceeded those from the most recent stock assessment (SEDAR 2024), although with substantial uncertainty (posterior median = 5.31 million; 95% HPD: 2.33 - 10.02 million). Our survey design and statistical modeling approaches addressed numerous critical uncertainties and information needs (e.g., effective sampling areas, survey-specific sampling designs) to convert camera-trap and ROV video counts (i.e., relative abundance) into estimates of absolute abundance. While our integrated modeling approach addresses many longstanding obstacles in abundance estimation, important data limitations remain, including: 1) survey effort was extensive (>2,800 sites), yet covered <0.1% of the total study area; and 2) the lack of a comprehensive hardbottom habitat map across the SEUSA adds substantial uncertainty when estimating abundance for a reef-associated species like red snapper (Steward et al. 2022). Despite these challenges, our framework for integrating multiple sampling methods demonstrates how an intensive short-term survey and experiments (ROV and telemetry-based estimates of camera-trap ESAs and ROV offsets; Zulian et al. 2024, Appendix I; Goldstein et al. 2025, Appendix II) can supplement long-running research and monitoring programs to estimate fish abundance and inform management needs at multiple spatial scales (Maunder 2003; Maunder and Punt 2013; Schaub et al. 2024).

Our findings reinforce previous work showing that red snapper use a range of habitats but are generally more abundant on or near hardbottom features (Patterson et al. 2014; Dance and Rooker 2019; Bohaboy et al. 2022; Bacheler et al. 2025; Lowerre-Barbieri et al. 2025). We found a significant positive association between red snapper density and the number of neighboring hardbottom cells, even when the focal cell lacked hardbottom. This indicates that red snapper frequently use adjacent non-hardbottom habitats, likely for foraging or movement between reef structures - a pattern supported by diet and movement studies (McCawley and Cowan Jr 2007; Tarnecki and Patterson 2015; Bohaboy et al. 2022; Bacheler et al. 2025). Occupancy modeling using SERFS camera-trap data found that local reef features were not strong predictors of red snapper presence, supporting the view that they are reef habitat generalists (Coggins et al. 2014). Red snapper tend to remain within approximately 100 m of hardbottom and their use of nearby non-hardbottom areas may be driven by foraging opportunities in sandy or soft-bottom habitats (McCawley and Cowan Jr 2007; Tarnecki and Patterson 2015; Bacheler et al. 2021; Bohaboy et al. 2022; Chatterjee et al. 2024). Moreover, relative abundance has been found to be highest in areas with moderate structured habitat, (around 20-70% of the visual substrate that was hardbottom or reef), underscoring the importance of both hardbottom and its surrounding habitat (i.e. patchy and not continuous; Bacheler et al. 2025). Research into the degree and duration of red snapper use in transitional habitats (e.g., Topping and Szedlmayer 2011; Tharp et al. 2024; Lowerre-Barbieri et al. 2025) can help optimize survey design and enhance the accuracy of spatially explicit abundance estimates (Scoulding et al. 2023; Schaub et al. 2024; Grüss et al. 2025). Given the

amount and demonstrated use of non-hardbottom habitat, inclusion of these areas in future sampling efforts – especially those within close proximity to hardbottom – provides opportunities to improve spatial coverage, refine abundance models, and better detect population-level changes.

This study highlights the importance of diversifying the spatial distribution of sampling locations, particularly in under-sampled regions. Monitoring programs often focus on areas of high abundances, which can obscure broad-scale trends, limit inferences to non-surveyed areas, and potentially mask changes (declines or increases) in overall abundance due to hyperstability (e.g., stable catch rates despite declining populations; Erisman et al. 2011; Ward et al. 2013). By combining SERFS camera-trap samples that target known reef locations with ROV samples spanning the broader continental shelf, we achieved a more comprehensive sampling design that leveraged the strengths of both methods while addressing critical gaps in coverage and inference. In the estimate of red snapper abundance in the Gulf (Stunz et al. 2021), red snapper were observed at higher absolute abundances on uncharacterized habitats (i.e. unknown if sand, mud, artificial and natural reefs, or other) which substantially altered total abundance estimates as these areas, although having low densities, covered vast areas of the Gulf (Stunz et al. 2021). We did not have an uncharacterized habitat covariate in our analysis but low densities of red snapper found at non-hardbottom neighbor cells were not applied uniformly to the large non-hardbottom neighbor area as red snapper densities were modeled at both a local (~90 x 90 m grid cell; count models) and coarser grid cell (~5 x 5 km; CAR model). In our study, camera-trap sampling efforts were limited to areas with assumed hardbottom habitat (i.e., hardbottom habitat was frequently unobserved on camera but assumed nearby), whereas ROV samples documented low red snapper counts at non-hardbottom areas, further highlighting the importance of comprehensive spatial sampling when assessing range-wide abundance.

The sensitivity of our estimate of SEUSA red snapper population size to the choice of assumed hardbottom map also reinforces the importance of more expansive sampling and mapping efforts. For example, using only the TNC map resulted in the majority of the SERFS camera-trap sites being placed in non-hardbottom grid cells and thus substantial numbers of red snapper being associated with non-hardbottom areas. Given the large expanse of non-hardbottom areas in the SEUSA, abundance estimates when using only the TNC map were substantially inflated, reaching implausible estimates of >99 million fish. In contrast, we explored modeling SERFS sites as a form of preferential sampling (i.e., SERFS sites were selected because of expert opinion regarding local hardbottom, not the TNC map; Conn et al. 2016). Here, preferential sampling and hardbottom effects became confounded, resulting in estimates of <1 million fish as the model attributed increased counts to preferential site selection and not increased abundance on and near hardbottom locations. Our composite hardbottom layer, combining EO and TNC maps, helped mitigate these issues, returning relationships that reflected the data of increasing red snapper abundance in grid cells with increasing number of hardbottom neighbors and at moderate depths. However, total expected abundance remained sensitive to the amount of hardbottom included in the composite map. Using a composite map with all predicted hardbottom from the TNC map (~13% total

hardbottom) yielded an abundance estimate of 7.22 million, whereas restricting TNC-predicted hardbottom to areas with high or very high confidence resulted in total hardbottom percentage (~5%) closer to estimates in Steward et al. (2022) (~3%) and reduced the abundance estimate to 5.31 million. Finally, analyzing multiple data sources in a single integrated model allows population estimates to account for the uncertainty associated with each data source (e.g., ESA, ROV offsets, camera-trap and ROV count data). However, population estimates remained conditional on the chosen hardbottom mapping approach (e.g., composite, EO, TNC) and did not incorporate uncertainty from the map selection itself. Future work that integrates uncertainty across mapping products could help address this additional layer of variation; however, a comprehensive, high-resolution hardbottom mapping effort will ultimately provide the most robust foundation for estimating reef-associated fish abundance in the SEUSA.

Quantifying habitat in patchy networks is challenging. Our composite map of hardbottom addressed important needs in our study, but differs from previously published individual maps (Steward et al. 2022; Pickens and Taylor 2020). For example, we reported approximately 5% total hardbottom in the SEUSA study area, which is slightly higher than the approximately 3% reported in Steward et al. (2022) that evaluated a different region (Cape Hatteras, NC to St Lucie Inlet, FL and depths up to 200 m) and did not reconcile conflicting hardbottom predictions among maps. Further, given our primary objective of abundance estimation, we discretized the study area into grid cells of approximately 90 x 90 m. We classified a grid cell as hardbottom if any portion of it was predicted to contain hardbottom habitat. While this binary classification simplifies spatial analysis, it inherently reduces the resolution of habitat complexity. Hardbottom habitats in the SEUSA can be highly heterogeneous, and this complexity can occur at spatial scales smaller than our grid resolution. In addition to not including this fine scale patchiness, our model also did not include three dimensional substrate relief that has been shown to be a significant predictor of red snapper abundance (Bacheler et al. 2016). As such, our approach may obscure fine-scale structural variation that could be ecologically relevant. We also excluded the artificial reef habitat map because its estimated extent ($\sim 3 km^2$) represented a negligible portion of the sampling region (<0.01%; Steward et al. 2022) and was not targeted during sampling. Given the central role of habitat in predicting reef fish abundances, mapping and validating hardbottom features with greater resolution remains critical for improving abundance estimation models for reef fishes in the SEUSA and beyond. Lastly, we did not have a comprehensive spatial map of water temperature and clarity both of which have been shown to influence the abundance of red snapper (Bacheler et al. 2025).

Within the limits of current habitat data, red snapper abundance was highest in northern Florida and declined with increasing latitude, although areas of higher abundance were also detected off Georgia, South Carolina, and central North Carolina. This nested spatial structure, characterized by broad regional gradients and localized deviations, is consistent with expectations for a temperate, reef-associated fish species like red snapper (Bacheler et al. 2016; Cao et al. 2024). Our hierarchical modeling framework effectively captured this spatial complexity, where

grid cell-level covariates identified higher densities at moderate depths and in areas with higher numbers of hardbottom neighbors, while the conditional autoregressive spatial random effects accounted for residual regional variation not attributable to localized habitat features. For example, despite comparable depth and substrate conditions in Florida and North Carolina, sites in Florida generally exhibited higher red snapper abundance, suggesting the influence of broader-scale ecological or oceanographic drivers. This emergent pattern of regional-scale gradients and localized abundance hotspots is consistent with prior analyses of red snapper distribution (Bacheler et al. 2025), reinforcing the utility of multi-scale spatial modeling for assessing population structure over broad spatial extents. However, further investigations into the mechanistic basis for broader-scale effects, such as physiological constraints associated with abiotic factors (e.g., effects of upwelling; Hyun and He 2010), drivers of spatial recruitment patterns (Karnauskas et al. 2022), and spawning habitat availability and use, could be critical for forecasting species responses to spatially explicit management strategies and climate-induced environmental change.

Inclusion of ESA was required for estimating absolute abundance; however, the ESA would not be identifiable from count data alone and requires informative prior knowledge to constrain the model. This limitation is inherent to hierarchical models that attempt to separate detection from abundance, particularly when using unmarked video survey data. For our analysis, we found that ESA posterior distributions for camera-trap video samples diverged from priors in ecologically consistent patterns, with bait attraction expanding the ESA when currents flowed away from camera-traps and reducing the ESA when currents directed bait plumes behind camera-traps, highlighting the critical role of current-mediated bait plume effects on camera-trap counts (Coggins et al. 2014; Bacheler et al. 2022b; Zulian et al. 2025; Goldstein et al. 2025). The ROV offset (median γ_{rov} = 2.28) shifted closer to 1.0 relative to the prior mean of 4.6, indicating reduced differences between ROV and camera-trap densities. This reduction may reflect the broader range of densities and habitat types sampled in this study compared to previous work integrating ROV and camera-trap data (Goldstein et al. 2025). The estimated ROV offset (~2.3) also aligns with previous empirical findings on red snapper responses to ROVs at small spatial scales (<5 m; Garner et al. 2022). While red snapper responses were not significantly different during ROV transects and control periods at medium (~15 m; determined with sonar) or large (~100 m; determined from telemetry) spatial scales, Garner et al. (2022) concluded red snapper may be attracted to the ROV at the typical spatial scales of ROV transects in our study (2 m above bottom with a ~9 m transect width). Finally, we lacked information to allow the ROV offset and ESA parameters to vary across the study area. Instead, ROV offset and ESA parameters act as scaling factors affecting total abundance. However, future research quantifying local, species-specific calibrations may identify processes important to unbiasedly estimating absolute abundance from underwater video surveys.

We estimated spatially explicit abundance and habitat associations of red snapper across a >112,000 km^2 region spanning North Carolina to Florida by integrating fishery-independent data from underwater camera-traps, ROV video transects, and habitat mapping. Our modeling framework incorporated knowledge and uncertainty on camera-trap ESAs and ROV-camera count

disparities (ROV offsets) to convert relative counts into estimates of absolute abundance. This integration of multiple survey types within a hierarchical Bayesian model allowed us to account for gear-specific detection processes and spatial heterogeneity, providing a robust approach to abundance estimation in reef-associated species. Our findings reinforce the importance of spatially complex and heterogeneous reef habitat for red snapper – patterns which have important implications for survey design and habitat-based management.

Despite these advances, the lack of a comprehensive, high-resolution seafloor habitat map remains a major limitation for predicting regional abundance. Like other broad-scale studies, our analysis relied on predicted rather than directly observed hardbottom, introducing substantial uncertainty into abundance estimates for habitat-associated species. While recent progress has improved our ability to estimate red snapper density and absolute abundance from video data (Zulian et al. 2025; Goldstein et al. 2025; herein), the reliability of regional estimates ultimately depends on the accuracy of habitat maps (Steward et al. 2022). Improved seafloor mapping would enhance both the characterization of sampled sites and the prediction surface, benefiting not only red snapper assessments but also abundance modeling for other reef fish species in the Southeast U.S. Atlantic. More broadly, our integrated, multi-survey modeling approach offers a transferable framework for estimating fish abundance in other systems, particularly where traditional survey methods are limited or where multiple data sources must be reconciled. These methods can complement traditional stock assessments by providing independent, spatially resolved metrics essential for ecosystem-based fisheries management.

Chapter 2 Acknowledgments

Funding for this study was principally provided by the South Carolina Sea Grant through the South Atlantic Research Program. We thank S. Lovelace and J. Juliano for administering this program and facilitating our study, and M. Lauretta for helpful comments on an earlier draft. This work would not have been possible without the large field and video reading effort by the Southeast Reef Fish Survey (SERFS) and University of Florida staff and numerous volunteers. The funding for SERFS sampling and video reads was from the National Marine Fisheries Service, while funding for the modeling and ROV data was provided by South Carolina Sea Grant via the South Atlantic Red Snapper Research Program. Data availability requests can be sent to the topic specific author: SERFS camera-trap data (N. Bacheler), ROV video data (W. Patterson). Any use of trade, firm, or product names is for descriptive purposes only and does not imply endorsement by the U.S. government. The scientific results and conclusions, as well as any views and opinions expressed herein, are those of the authors and the U.S. Geological Survey, but do not necessarily reflect those of the National Oceanic and Atmospheric Administration.

Chapter 2 References

Amburgey, S.M., A.A. Yackel Adams, B. Gardner, N.J. Hostetter, S.R. Siers, B.T. McClintock, and S.J. Converse. 2021. Evaluation of camera trap-based abundance estimators for unmarked populations. Ecological Applications 31:e02410.

Bacheler, N.M., K.W. Shertzer, Z.H. Schobernd, and L.G. Coggins. 2023. Calibration of fish counts in video surveys: a case study from the Southeast Reef Fish Survey. Frontiers in Marine Science 10:1183955.

Bacheler, N.M., K.W. Shertzer, B J. Runde, P.J. Rudershausen, and J.A. Buckel. 2021. Environmental conditions, diel period, and fish size influence the horizontal and vertical movements of red snapper. Scientific Reports 11:9580.

Bacheler, N.M., B.J. Runde, K.W. Shertzer, J.A. Buckel, and P.J. Rudershausen. 2022b. Fine-scale behavior of red snapper (*Lutjanus campechanus*) around bait: approach distances, bait plume dynamics, and effective fishing area. Canadian Journal of Fisheries and Aquatic Sciences 79:458–471.

Bacheler, N.M., Z.D. Gillum, K.C. Gregalis, E.P. Pickett, C.M. Schobernd, Z.H. Schobernd, B.Z. Teer, T.I. Smart, and W.J. Bubley. 2022a. Comparison of video and traps for detecting reef fishes and quantifying species richness in the continental shelf waters of the southeast USA. Marine Ecology Progress Series 698:111-123.

Bacheler, N.M., Z.H. Schobernd, D.J. Berrane, C.M. Schobernd, W.A. Mitchell, B.Z. Teer, K.C. Gregalis, and D.M. Glasgow. 2016. Spatial distribution of reef fish species along the southeast US Atlantic coast inferred from underwater video survey data. PLoS ONE 11:e0162653.

Bacheler, N.M., W.F. Patterson III, J.H. Tarnecki, K.W. Shertzer, J.A. Buckel, N.J. Hostetter, K. Pacifici, V. Zulian, and W.J. Bubley. 2025. Spatiotemporal dynamics and habitat use of red snapper (*Lutjanus campechanus*) on the southeastern United States Atlantic continental shelf. Fisheries Research 281:107200.

Bicknell, A.W., B.J. Godley, E.V. Sheehan, S.C. Votier, and M.J. Witt. 2016. Camera technology for monitoring marine biodiversity and human impact. Frontiers in Ecology and the Environment 14:424–432.

Bohaboy, E.C., S.L. Cass-Calay, and W.F. Patterson III. 2022. Fine-scale movement of northern Gulf of Mexico red snapper and gray triggerfish estimated with three-dimensional acoustic telemetry. Scientific Reports 12:14274.

Bruce, T., Z. Amir, B.L. Allen, B.F. Alting, and M.S. Luskin. 2025. Large-scale and long- term wildlife research and monitoring using camera traps: a continental synthesis. Biological Reviews 100:530–555.

Cao, J., J.K. Craig, and M.D. Damiano. 2024. Spatiotemporal dynamics of Atlantic reef fishes off the southeastern US coast. Ecosphere 15:e4868.

Chandler, R.B. and J.A. Royle. 2013. Spatially explicit models for inference about density in unmarked or partially marked populations. The Annals of Applied Statistics 7:936–954.

Chatterjee, N., D. Wolfson, D. Kim, J. Velez, S. Freeman, N.M. Bacheler, K. Shertzer, J.C. Taylor, and J. Fieberg. 2024. Modelling individual variability in habitat selection and movement using integrated step-selection analysis. Methods in Ecology and Evolution 15:1034–1047.

Chrysafi, A. and A. Kuparinen. 2016. Assessing abundance of populations with limited data: Lessons learned from data-poor fisheries stock assessment. Environmental Reviews 24:25–38.

Coggins, L.G. J., N.M. Bacheler, and D.C. Gwinn. 2014. Occupancy models for monitoring marine fish: a Bayesian hierarchical approach to model imperfect detection with a novel gear combination. PLoS ONE 9:e108302.

Conley, M.F., M.G. Anderson, N. Steinberg, and A. Barnett. 2017. The South Atlantic Bight Marine assessment: species, habitats and ecosystems. The Nature Conservancy, Eastern Conservation Science.

Conn, P.B., J.T. Thorson, and D.S. Johnson. 2016. Confronting preferential sampling when analysing population distributions: diagnosis and model-based triage. Methods in Ecology and Evolution 8:1535–1546.

Cove, M. V., R. Kays, H. Bontrager, C. Bresnan, M. Lasky, et al., and W. J. McShea. 2021. SNAPSHOT USA 2019: a coordinated national camera trap survey of the United States. Ecology 102:e03353.

Cowan, J., C. Grimes, W.F. Patterson III, C.B. Walters, A.C. Jones, W.J. Lindberg, D.J. Sheehy, W.E. Pine III, J.E. Powers, M.D. Campbell, K.C. Lindeman, S.L. Diamond, R. Hillborn, H.T. Gibson, and K.A. Rose. 2011. Red snapper management in the Gulf of Mexico: science- or faith-based? Reviews in Fish Biology and Fisheries 21:187–204.

Cowan Jr, J.H. 2011. Red snapper in the Gulf of Mexico and US South Atlantic: data, doubt, and debate. Fisheries 36:319–331.

Dance, M.A. and J.R. Rooker. 2019. Cross-shelf habitat shifts by red snapper (*Lutjanus campechanus*) in the Gulf of Mexico. PLoS One 14:e0213506.

de Valpine, P., D. Turek, C.J. Paciorek, C. Anderson-Bergman, D.T. Lang, and R. Bodik. 2017. Programming with models: writing statistical algorithms for general model structures with NIMBLE. Journal of Computational and Graphical Statistics 26:403–413.

Delisle, Z.J., E.A. Flaherty, M.R. Nobbe, C.M. Wzientek, and R.K. Swihart. 2021. Next-generation camera trapping: systematic review of historic trends suggests keys to expanded research applications in ecology and conservation. Frontiers in Ecology and Evolution 9:617996.

DeVictor, R., K. Gore, S. Holiman, M. Jepson, J. McGovern, N. Mehta, and J. Waters, 2009. Interim Rule to Address Overfishing of Red Snapper in the South Atlantic Region. URL https://repository.library.noaa.gov/view/noaa/21148.

Erisman, B.E., L.G. Allen, J.T. Claisse, D.J. Pondella, E.F. Miller, and J.H. Murray. 2011. The illusion of plenty: hyperstability masks collapses in two recreational fisheries that target

fish spawning aggregations. Canadian Journal of Fisheries and Aquatic Sciences 68:1705–1716.

Fei, S., Q. Guo, and K. Potter. 2016. Macrosystems ecology: novel methods and new understanding of multi-scale patterns and processes. Landscape Ecology 31:1–6.

Garner, S.B., R. Ahrens, K.M. Boswell, M.D. Campbell, D. Correa, J.H. Tarnecki, and W. F. Patterson III. 2022. A multidisciplinary approach to estimating red snapper, *Lutjanus campechanus*, behavioral response to mobile camera and sonar sampling gears. Fisheries Re- search 246:106155.

Gelfand, A.E., P. Diggle, P. Guttorp, and M. Fuentes. 2010. Handbook of Spatial Statistics (1st Edition). CRC press.

Gelman, A., J.B. Carlin, H.S. Stern, D.B. Dunson, A. Vehtari, and D.B. Rubin. 2013. Bayesian data analysis (3rd edition). Chapman and Hall/CRC, Boca Raton.

Goldstein, B.R., K. Pacifici, J.A. Buckel, N.M. Bacheler, E.M. Schliep, B.J. Reich, K.W. Shertzer, W.F. Patterson III, J.H. Tarnecki, and N.J. Hostetter. 2025. An integrated approach to estimating the effective sampling area of baited underwater camera traps. Appendix in: Estimation of Southeastern United States Atlantic Red Snapper Abundance. W.F. Patterson III et al. (editors).

Grüss, A., R.L. O'Driscoll, J.T. Thorson, J.R. McKenzie, S.L. Ballara, and A.R. Charsley. 2025. Impacts of different types of data integration on the predictions of spatio-temporal models: A fishery application and simulation experiment. Fisheries Research 284:107321.

Gwinn, D.C., N.M. Bacheler, and K.W. Shertzer. 2019. Integrating underwater video into traditional fisheries indices using a hierarchical formulation of a state-space model. Fisheries Research 219:105309.

Hood, P.B., A.J. Strelcheck, and P. Steele. 2007. A history of red snapper management in the Gulf of Mexico. Pages 241–256 *in* Population ecology and fisheries of U.S. Gulf of Mexico red snapper, volume 60. American Fisheries Society, 5410 Grosvenor Ln. Ste. 110 Bethesda MD 20814.

Hyun, K.H. and R. He. 2010. Coastal upwelling in the South Atlantic Bight: A revisit of the 2003 cold event using long term observations and model hindcast solutions. Journal of Marine Systems 83:1–13.

Karnauskas, M., K.W. Shertzer, C.B. Paris, N.A. Farmer, T.S. Switzer, S.K. Lowerre-Barbieri, G.T. Kellison, R. He, and A.C. Vaz. 2022. Source–sink recruitment of red snapper: Connectivity between the Gulf of Mexico and Atlantic Ocean. Fisheries Oceanography 31:571–586.

Kéry, M. and J.A. Royle. 2020. Applied hierarchical modeling in ecology: Analysis of distribution, abundance and species richness in R and BUGS: Volume 2: Dynamic and advanced models. Academic Press.

Lowerre-Barbieri, S.K., K. Wall, C. Friess, S. Keenan, C. Lembke, J. Tarnecki, L.J. Williams-

Grove, and W.F. Patterson III. 2025. Movement traits important to conservation and fisheries management: an example with red snapper. Scientific Reports 15:4614.

Maunder, M.N. 2003. Paradigm shifts in fisheries stock assessment: from integrated analysis to Bayesian analysis and back again. Natural Resource Modeling 16:465–475.

Maunder, M.N. and A.E. Punt. 2013. A review of integrated analysis in fisheries stock assessment. Fisheries Research 142:61–74.

McCawley, J.R. and J.H. Cowan Jr., 2007. Seasonal and size specific diet and prey demand of red snapper on Alabama artificial reefs. Pages 71–96 *in* American Fisheries Society Symposium, volume 60.

Meredith, M. and J. Kruschke. 2022. HDInterval: Highest (Posterior) Density Intervals. URL https://CRAN.R-project.org/package=HDInterval.

Mitchell, W.A., G.T. Kellison, N.M. Bacheler, J.C. Potts, C.M. Schobernd, and L.F. Hale. 2014. Depth-related distribution of post juvenile red snapper in southeastern U.S. Atlantic Ocean waters: ontogenic patterns and implications for management. Marine and Coastal Fisheries 6:142–155.

Moeller, A.K., P.M. Lukacs, and J.S. Horne. 2018. Three novel methods to estimate abundance of unmarked animals using remote cameras. Ecosphere 9:e02331.

NOAA. 2025. Defined Fishery Management Areas Off South Atlantic States Map GIS Data. URL https://www.fisheries.noaa.gov/resource/map/defined-fishery-management-areas-south-atlantic-states-map-gis-data.

Pacifici, K., B.J. Reich, D.A. W. Miller, B. Gardner, G. Stauffer, S. Singh, A. McKerrow, and J.A. Collazo. 2017. Integrating multiple data sources in species distribution modeling: a framework for data fusion. Ecology 98:840–850.

Patterson III, W.F., J.H. Tarnecki, D.T. Addis, and L.R. Barbieri, 2014. Reef fish community structure at natural versus artificial reefs in the northern Gulf of Mexico. Pages 4–8 *in* Proceedings of the Gulf and Caribbean Fisheries Institute, volume 66.

Pickens, B. and J. Taylor. 2020. Regional Essential Fish Habitat geospatial assessment and framework for offshore sand features. https://repository.library.noaa.gov/view/noaa/23696

R Core Team, 2024. R: A Language and Environment for Statistical Computing. R Foundation for Statistical Computing, Vienna, Austria. URL https://www.R-project.org/.

Robinson, N.M., W.A. Nelson, M.J. Costello, J.E. Sutherland, and C.J. Lundquist. 2017. A systematic review of marine-based species distribution models (SDMs) with recommendations for best practice. Frontiers in Marine Science 4:296834.

Royle, J.A. 2004. N-Mixture models for estimating population size from spatially replicated counts. Biometrics 60:108–115.

Schaub, M., M.N. Maunder, M. Kéry, J.T. Thorson, E.K. Jacobson, and A.E. Punt. 2024. Lessons to be learned by comparing integrated fisheries stock assessment models (SAMs) with integrated population models (IPMs). Fisheries Research 272:106925.

Schobernd, Z.H., N.M. Bacheler, and P.B. Conn. 2014. Examining the utility of alternative video monitoring metrics for indexing reef fish abundance. Canadian Journal of Fisheries and Aquatic Sciences 71:464–471.

Schwartzkopf, B.D., T.A. Langland, and J.H. Cowan Jr. 2017. Habitat selection important for red snapper feeding ecology in the northwestern Gulf of Mexico. Marine and Coastal Fisheries 9:373–387.

Scoulding, B., S. Gastauer, J.C. Taylor, K.M. Boswell, D.V. Fairclough, G. Jackson, P. Sullivan, K. Shertzer, F. Campanella, N. Bacheler, M. Campbell, R. Domokos, Z. Schobernd, T.S. Switzer, N. Jarvis, B.M. Crisafulli, C. Untiedt, and P.G. Fernandes. 2023. Estimating abundance of fish associated with structured habitats by combining acoustics and optics. Journal of Applied Ecology 60:1274–1285.

SEDAR. 2021. SEDAR 73 South Atlantic Red Snapper Stock Assessment Report. Technical report, SEDAR, North Charleston, SC. URL http://sedarweb.org/sedar-73.

SEDAR. 2024. Stock Assessment of Red Snapper off the Southeastern United States – Update of SEDAR 73 Assessment. Technical report, SEFSC, Beaufort, NC. URL http://sedarweb.org/sedar-73.

Shertzer, K., S. Crosson, E. Williams, J. Cao, R. DeVictor, C. Dumas, and G. Nesslage. 2024. Fishery management strategies for Red Snapper in the southeastern U.S. Atlantic: a spatial population model to compare approaches. North American Journal of Fisheries Management 44:113–131.

Shertzer, K.W., N.M. Bacheler, L.G. Coggins Jr, and J. Fieberg. 2016. Relating trap capture to abundance: a hierarchical state-space model applied to black sea bass (*Centropristis striata*). ICES Journal of Marine Science 73:512–519.

Shertzer, K.W., N.M. Bacheler, W.E. Pine III, B.J. Runde, J.A. Buckel, P.J. Rudershausen, and J. H. MacMahan. 2020. Estimating population abundance at a site in the open ocean: combining information from conventional and telemetry tags with application to gray triggerfish (*Balistes capriscus*). Canadian Journal of Fisheries and Aquatic Sciences 77:34–43.

Smart, T.I., M.J. Reichert, J.C. Ballenger, W.J. Bubley, and D.M. Wyanski. 2015. Overview of sampling gears and standard protocols used by the Southeast Reef Fish Survey and its partners. SEDAR41-RD58. https://sedarweb.org/assessments/sedar-41/

Steward, D. N., A.B. Paxton, N.M. Bacheler, C.M. Schobernd, K. Mille, J. Renchen, Z. Harrison, J. Byrum, R. Martore, C. Brinton, K.L. Riley, J.C. Taylor, and G.T. Kellison. 2022. Quantifying spatial extents of artificial versus natural reefs in the seascape. Frontiers in Marine Science 9:980384.

Stunz, G.W., W.F. Patterson III, S.P. Powers, J.H. Cowan, Jr., J.R. Rooker, R.A. Ahrens, K. Boswell, L. Carleton, M. Catalano, J.M. Drymon, J. Hoenig, R. Leaf, V. Lecours, S. Murawski, D. Portnoy, E. Saillant, L.S. Stokes, and R.J.D. Wells. 2021. The Great Red Snapper Count: Estimating the absolute abundance of age-2+ Red Snapper (*Lutjanus*

campechanus) in the US Gulf of Mexico. Technical report, Mississippi-Alabama Sea Grant Consortium, NOAA Sea Grant.

Tarnecki, J.H. and W.F. Patterson III. 2015. Changes in red snapper diet and trophic ecology following the Deepwater Horizon oil spill. Marine and Coastal Fisheries 7:135–147.

Tharp, R.M., N.J. Hostetter, A.B. Paxton, J.C. Taylor, and J.A. Buckel. 2024. Artificial structure selection by economically important reef fishes at North Carolina artificial reefs. Frontiers in Marine Science 11:1373494.

Topping, D.T. and S.T. Szedlmayer. 2011. Site fidelity, residence time and movements of red snapper *Lutjanus campechanus* estimated with long-term acoustic monitoring. Marine Ecology Progress Series 437:183–200.

Ward, H.G., P.J. Askey, and J.R. Post. 2013. A mechanistic understanding of hyperstability in catch per unit effort and density-dependent catchability in a multistock recreational fishery. Canadian Journal of Fisheries and Aquatic Sciences 70:1542–1550.

Williams, B.K., J.D. Nichols, and M.J. Conroy. 2002. Analysis and management of animal populations. Academic Press, San Diego.

Zipkin, E.F., E.R. Zylstra, A.D. Wright, S.P. Saunders, A.O. Finley, M.C. Dietze, M.S. Itter, and M.W. Tingley. 2021. Addressing data integration challenges to link ecological processes across scales. Frontiers in Ecology and the Environment 19:30–38.

Zulian, V., K. Pacifici, N.M. Bacheler, J.A. Buckel, W.F. Patterson III, B.J. Reich, K.W. Shertzer, and N.J. Hostetter. 2025. Applying mark-resight, count, and telemetry data to estimate effective sampling area and fish density with stationary underwater cameras. Canadian Journal of Fisheries and Aquatic Sciences 82:1–11.

Supplementary material

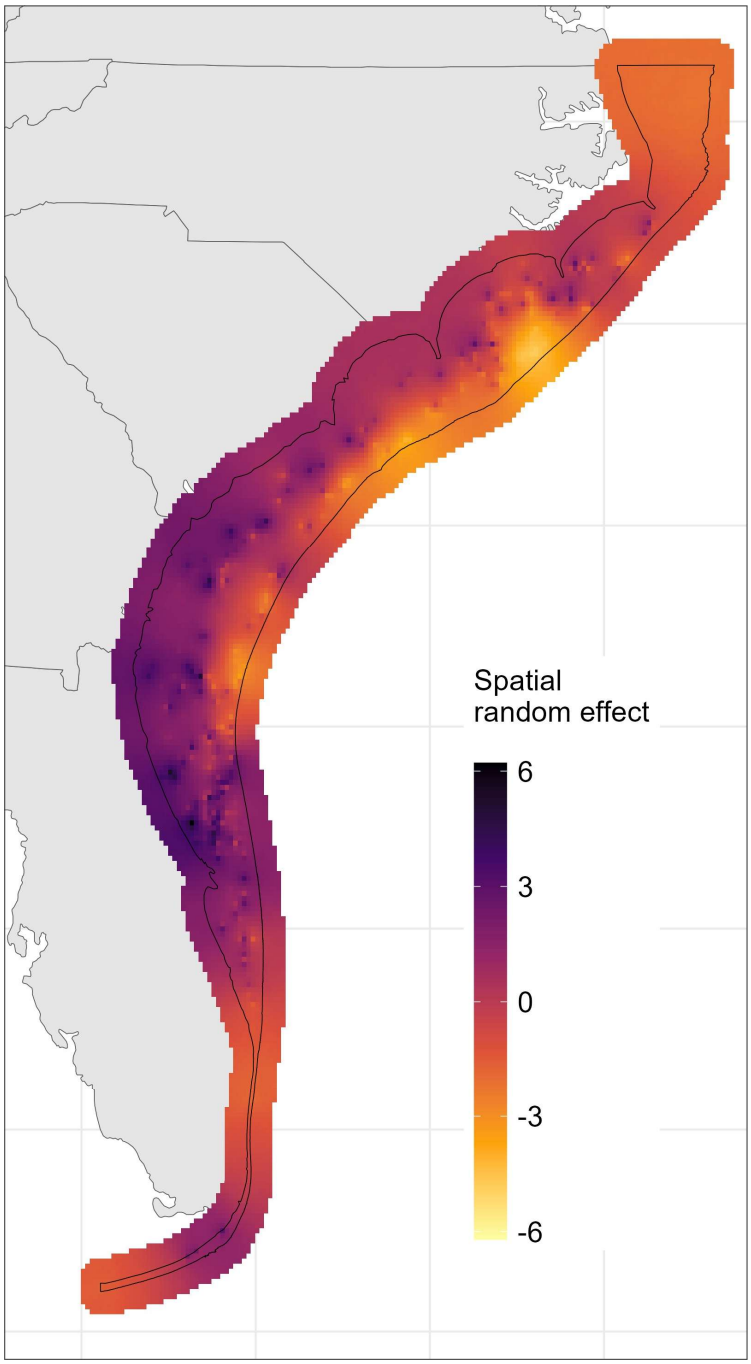

Figure S1: Estimated spatial random effects for red snapper abundance per ~5.5×5.5-km grid cell across the buffered southeastern U.S. Atlantic study region. Values are the posterior mean for each grid cell (α_g).

Chapter 3

Estimation of Red Snapper, *Lutjanus campechanus*, Population Size in the U.S. Atlantic via Close-Kin Mark-Recapture

David S. Portnoy[1], Eric C. Anderson[2], Alison Monroe[1], Kyle W. Shertzer[3], Christopher M. Hollenbeck[1], D. Nick Weber[1], Katherine L. Lanoue[1], Katie Gabe[1], Nathan M. Bacheler[3], Walter J. Bubley[4], Jeffrey A. Buckel[5], Ted Switzer[6], and William F. Patterson III[7]

[1]Marine Genomics Laboratory, Department of Life Sciences, Texas A&M University–Corpus Christi, Corpus Christi, TX, USA

[2] Department of Biology and Department of Fisheries, Wildlife and Conservation Biology, Colorado State University, Fort Collins, CO, USA

[3]Southeast Fisheries Science Center, National Marine Fisheries Service, Beaufort, NC, USA

[4]Marine Resources Research Institute, South Carolina Department of Natural Resources, Charleston, SC, USA

[5]Department of Applied Ecology, Center for Marine Sciences and Technology, North Carolina State University, Morehead City, NC, USA

[6]Florida Fish and Wildlife Commission, Fish and Wildlife Research Institute, St. Petersburg, FL, USA

[7]School of Forest, Fisheries, and Geomatics Sciences, University of Florida, , Gainesville, FL, USA

Abstract

Red snapper, *Lutjanus campechanus*, is an iconic marine fish that supports commercial and recreational fisheries in U.S. waters of the Atlantic Ocean (Atlantic) from North Carolina through South Florida. The stock has been estimated to be overfished since the 1960s despite fishery closures in 2010-2011 and limited harvest since 2012. The greatest source of annual removals is estimated to be dead discards in the multi-species recreational reef fish fishery, which drive the red snapper stock assessment despite being poorly estimated. Here, close-kin mark-recapture (CKMR) was used to generate a benchmark estimate of absolute abundance for age-2+ Atlantic red snapper to anchor the stock assessment, but also as an input to future studies aimed at estimating the magnitude of recreational discards. Fish were sampled from fishery-independent surveys and fishery landings in 2021-2023. In total, 14,085 individual red snapper were genotyped using a genotyping in thousands by sequencing (GT-seq) panel designed to identify a subset of candidate kin pairs. Double-digest restriction site-associated DNA sequencing (ddRAD seq) was then used to define final kin categories using 1,755 multiallelic haplotyped loci. Final CKMR estimates were made using cross-cohort half-sibling pairs with an age-structured model. Due to evidence of increasing abundance prior to 2019, three different approaches to CKMR population estimation were performed. Approach 1 included all samples, approach 2 included only pairs where the second-born individual was in the 2019-2023 cohort, and approach 3 used a model that allowed for population size change. Population estimates from approaches 1 and 2 were similar (approach 1: 1.42 million, CV 17%; approach 2: 1.52 million, CV 19%). The range of annual population estimates from approach 3 (2018: 1.33 million, CV 33%; 2019: 1.37 million, CV 22%; 2020: 1.45 million, CV 17%; 2021: 1.54 million, CV 21%; 2022: 1.68 million, CV 30%) suggested population expansion, but overall results were consistent with the other two approaches. Study results provide an important benchmark estimate of absolute abundance for red snapper in the Atlantic that was previously unavailable for assessment and management. More broadly, the study demonstrates the utility (and challenges) of half-sibling based CKMR approaches for estimating absolute abundance of managed bony fishes for which large population sizes and wide distributions preclude the use of other methods.

Keywords: CKMR, population size estimation, managed fisheries, fisheries assessment

Introduction

Estimating population size is performed in population ecology and fisheries using a variety of techniques. Among the more common of these approaches are those utilizing mark-recapture, typically via conventional tagging studies. Genetic mark-recapture methodologies are a modern variation of mark-recapture that are similar to traditional mark-recapture methodologies in many ways, yet some important differences also exist. A genetic mark is the composite genotype of an individual across some number of characterized loci and is natural and permanent (Palsbøll 1999). Therefore, it can be recovered from a fully processed carcass, or in the case of live animals, from minimally invasive tissue samples, minimizing handling stress and avoiding issues with tag loss that make traditional mark-recapture studies challenging (Taberlet et al. 1999). Initial attempts at genetic mark-recapture resembled traditional tag-based mark-recapture study designs, in that census estimates were based on the capture and recapture of specific individuals for which a genetic mark was generated (Woods et al. 1999; Miller et al. 2015; Palsbøll et al. 1997). In terrestrial systems, fecal samples, fur, or feathers often have been utilized to avoid animal capture entirely (Lukacs and Burnham 2005). However, for dispersive marine organisms with relatively large census sizes, the probability of recapturing an individual will often be fairly low, requiring intense sampling effort (Marcy-Quay et al. 2020).

Genetic marks are transmitted from parent to offspring, thus are partially shared between related individuals, considerably expanding the scope of what may be considered a "recapture" to closely related individuals (i.e., kin). Combining kin recaptures with models informed by life history information to relate the number of kin to absolute (versus relative) population size is a recent technique known as close-kin mark-recapture (CKMR, Skaug 2001; Bravington et al. 2016a). This approach offers great promise for generating population size estimates that are accurate and precise for marine organisms of management interest provided the required life history data (age- and sex-specific mortality, age- and sex-specific fecundity, age-at-maturity) are available.

The probability is 1.0, or 100%, that an individual in a sample has one mother and one father. In an idealized population model where adult reproductive contribution is equal, the probability that one individual has the same mother as another is $1/N_{\text{adult\_females}}$. The probability that those same two individuals have the same father is $1/N_{\text{adult\_males}}$. Ignoring full siblings, the probability that two individuals are half-siblings is $1/N_{\text{adult\_females}} + 1/N_{\text{adult\_males}}$. If the sex ratio is equal, then $N_{\text{adult\_females}} = N_{\text{adult\_males}} = 0.5\text{N}$, such that the probability of being a half-sibling (either maternal or paternal) is $4/N_{\text{adult}}$. If m pairwise comparisons are made from individuals sampled from the population, then the expected number of half-sibling pairs (K) is $4m/(N_{\text{adult}})$. Solving for N_{adult} yields $N_{\text{adult}} = 4m/K$, and substituting the observed for the expected number of half-sibling pairs in that equation provides a simple estimate of N_{adult} (hereafter, census size or N_c).

In real populations, however, adult contribution is not equal because it is dependent on realized fecundity across sexes and ages. Therefore, probabilities for each comparison must be adjusted to account for effects arising from age, year, and sex through the use of a population

dynamics model accounting for adult abundance, size-specific mortality, and size-specific fecundity (Bravington et al. 2016a). Additionally, the effects of annual random variation in reproductive success among breeders must be controlled by only making comparisons between samples from different cohorts (Bravington et al. 2016a). Therefore, a properly executed CKMR study requires: 1) parameterized life history data, 2) accurately aged samples, 3) a sample size and design that can provide sufficient kin pairs among all the pairwise comparisons made between samples, and 4) sufficient resolution in genetic data to accurately characterize kin relationships.

While CKMR has not yet been widely applied, it has seen increasing use to estimate population size for marine and anadromous species, particularly fishes. The first large-scale CKMR estimate of abundance was made for southern bluefin tuna (Bravington et al. 2016b). Since then, the method has been applied to a variety of aquatic species of conservation and management concern, including great white shark (Hillary et al. 2018), brook trout (Ruzzante et al. 2019), Atlantic salmon (Wacker et al. 2021), Arctic grayling (Prystupa et al. 2021), blue skate (DeLaval et al. 2023), speartooth shark (Patterson et al. 2022), thornback ray (Trenkel et al. 2022) and bearded seals (Taras et al. 2024). While the results of these studies differ in terms of accuracy and precision due largely to details of experimental design, they collectively demonstrate the great promise this method has for providing census size estimates that could be used to support stock assessment and management for a variety of fished species.

Here, a large-scale effort was used to apply CKMR to estimate the population size of red snapper, *Lutjanus campechanus*, in United States' (U.S.) Atlantic waters from North Carolina to South Florida. Red snapper is a long-lived species distributed across a variety of shelf habitats in the western Atlantic (Camber 1955; Bacheler et al. 2016). This species is highly sought as a food fish and supports valuable commercial and recreational fisheries in U.S. waters of the Gulf of America (Gulf) and Atlantic (Atlantic) from North Carolina through Florida. In the Atlantic, management is difficult because a large component of the effort comes from private recreational anglers during times of the year closed to harvest, thus discards are an important source of fishery removals for the stock (Shertzer et al. 2019). Consequently, uncertainty has led to a cautionary approach to management and in recent years very short red snapper seasons (SEDAR 2021; Bacheler et al. 2025). Generation of a benchmark estimate of population size is a straightforward first step towards improving assessment and management, as it can be used to better understand trends in abundance, but can also be used as an input to tagging studies aimed at understanding the magnitude of recreational discards (Kehoe et al. 2025b, Appendix VII). While generating an estimate of population size for a widely distributed species with population sizes in the millions using traditional methods (e.g., conventional tag-based mark-recapture) is an ambitious pursuit, given access to appropriate tissue samples, it is a task well-suited for CKMR approaches (Skaug 2001; Bravington et al. 2016a).

This chapter is focused on the study designed and conducted to produce an independent estimate of the population size of age-2+ red snapper on the U.S. Atlantic continental shelf from North Carolina through South Florida with CKMR. Complementary studies were conducted either

to test population structure assumptions of CKMR (Monroe et al. 2025; Appendix IV), or to examine effects of bias or imprecision in life history parameter estimates on CKMR-derived estimates of red snapper population size (Kehoe et al. 2025c; Appendix XI). Their results indicate the red snapper population in the Atlantic is genetically distinct from the Gulf, with no significant genetic differences among red snapper sampled from North Carolina to Florida, and CKMR is robust to moderate levels of imprecision or bias in red snapper biological parameter estimates. For the CKMR study itself, simulation was first utilized to estimate the number of tissue samples required to estimate red snapper population size with a coefficient of variation ≤0.3, with the target population size being 3x the then-current stock assessment-derived population estimate (SEDAR 2021). Thereafter, a three-year study was conducted to collect fin clip tissue samples from fishery landings and fishery-independent samples, followed by DNA sequencing and kinship analysis, and finally statistical modeling to estimate red snapper population size. To our knowledge, this is the largest CKMR population estimation study conducted in U.S. waters and one of the larger ones conducted around the globe. Furthermore, the degree to which population structure assumptions were checked and the extensive testing done to assess the sensitivity of the red snapper population estimate to error (bias or imprecision) in population parameter estimates greatly reduces potential uncertainty in the reported Atlantic red snapper population size estimate.

Methods

Sample Size Estimation

Forward simulations were conducted with *CKMRpop* (Anderson 2025a) in *R* (R Core Team 2024), with the model parameterized with Atlantic red snapper life history data, to estimate fin clip sample sizes required to estimate age-2+ population size with a coefficient of variation (CV) ≤0.3. Simulations were run twenty times each for population sizes of 5×10^5, 1×10^6, and 1.5×10^6 individuals. This range in population size was chosen because there were approximately 5×10^5 age-2+ red snapper estimated to be in the U.S. Atlantic in the most recent assessment (SEDAR 2017) at the time, with a population size of 1.5×10^6 being 3x the SEDAR (2017) population size estimate to provide a conservative buffer for population expansion.

Population size was estimated with an annual sample size of 2,500 and 5,000 individuals per year for two sampling years, which originally was the planned duration of the study. Only half-siblings sampled across cohorts were used to estimate N_{adult}. Estimation of N_{adult} followed the pseudo-likelihood approach of Bravington et al. (2016a). Briefly, for each pair of samples the probability of being half-siblings for a given N_{adult} was calculated, accounting for age at sampling, year of sampling, the expected age structure of the population, and age-specific variation in reproductive success. All probabilities were then combined into a likelihood of observing the number of recorded half-siblings for a given population size and the suite of Atlantic red snapper life history parameters. Likelihoods were evaluated for population sizes between 5×10^5 and 1.5×10^6, normalized, and used to construct posterior probability distributions. The estimated N_{adult}

and CV was then calculated for each posterior distribution and averaged across all 20 runs for each combination of N_{adult} and sample size.

Sample Collection

Red snapper fin clips were sampled from fisheries-independent and -dependent sources along the U.S. Atlantic Coast between Port St. Lucie, Florida and Cape Hatteras, North Carolina during 2021-2023 (Figures 3-1, 3-2). Metadata for all sampled individuals can be found at https://github.com/marinegenomicslab/Red-Snapper-CKMR/. Sampling was carried out by a variety of academic, state and federal partners, with the majority of samples coming from randomized fishery-independent trap or vertical line surveys conducted by NOAA Fisheries, Beaufort Laboratory, South Carolina Department of Natural Resources (SCDNR), and the Florida Fish and Wildlife Conservation Commission (FWC).

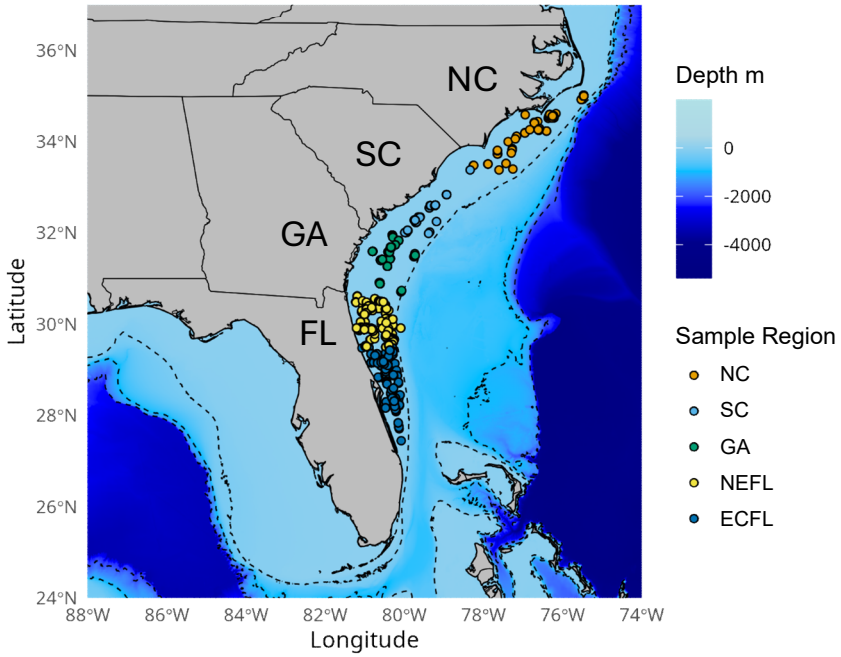

Figure 3-1A. Distribution of Atlantic red snapper sampling in 2021. Colors indicate groupings based on state lines: North Carolina (NC), South Carolina (SC), Georgia (GA), northeastern Florida (NEFL), and east central Florida (ECFL) split arbitrarily at 29.5°N

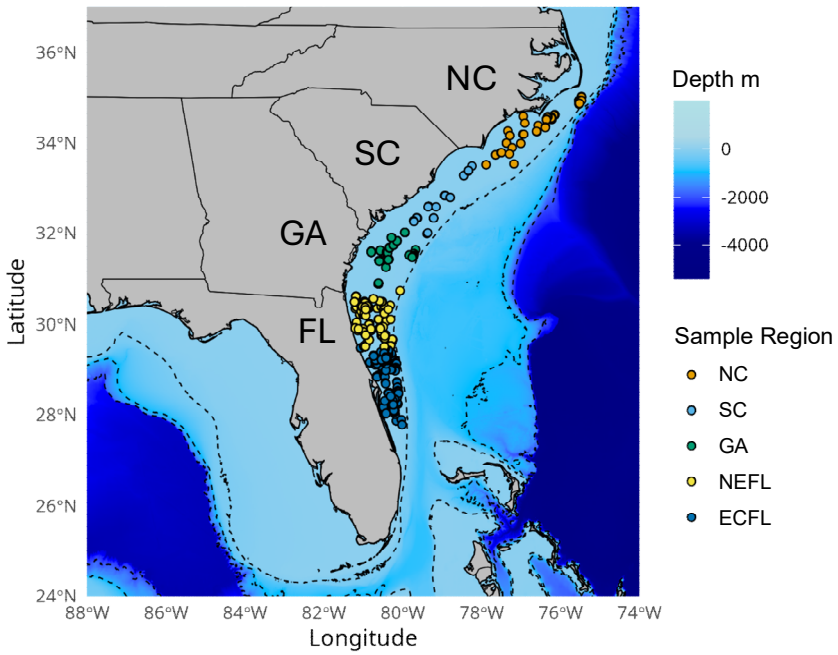

Figure 3-1B. Distribution of Atlantic red snapper sampling in 2022. Colors indicate groupings based on state lines: North Carolina (NC), South Carolina (SC), Georgia (GA), northeastern Florida (NEFL), and east central Florida (ECFL) split arbitrarily at 29.5°N

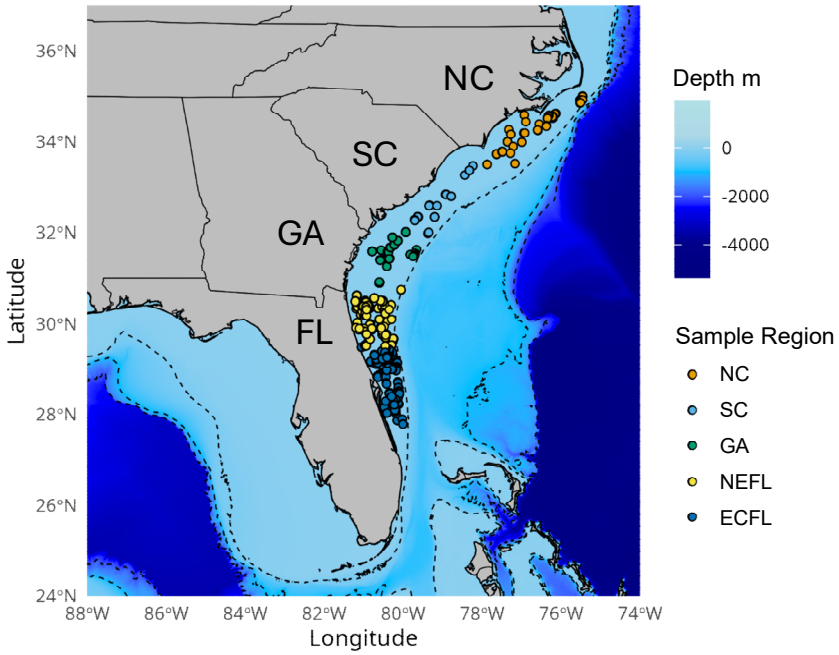

Figure 3-1C. Distribution of Atlantic red snapper sampling in 2023. Colors indicate groupings based on state lines: North Carolina (NC), South Carolina (SC), Georgia (GA), northeastern Florida (NEFL), and east central Florida (ECFL) split arbitrarily at 29.5°N.

All fin clips were collected using sterile scissors or razor blades, placed in 1.5-ml cryovials, and immersed in salt-saturated DMSO buffer (Seutin et al. 1991); paired fin clips were sampled from most individuals. Fin clips were sent to the Marine Genomics Laboratory at Texas A&M University - Corpus Christi where they were stored at room temperature until time of extraction. When possible, otoliths were also collected and sent to SCDNR or FWC where they were sectioned and aged using well-established protocols.

GT-seq Panel Design and Optimization

Candidate SNP-containing loci were identified from a previously published double digest restriction-site associated DNA sequencing (ddRAD) data set (Portnoy et al. 2022) using *dDocent* (Puritz et al. 2014) to map reads and call SNPs. Data were rigorously filtered for quality and missing data with *VCFtools* (Danecek et al. 2011), following recommendations made by O'Leary et al. (2018). Filtered loci were then haplotyped with *RADhaplotyper*, further screened for the potential presence of paralogs (Willis et al. 2017), and filtered by observed heterozygosity and minor allele frequency. Finally, loci were ranked by the Shannon's diversity index and the top 500 loci were selected for possible primer design. Primers were designed using *Primer3* (Untergasser et al. 2012) with a specific set of target parameters (melting temperature: 57-65°C, insert size: 110-190 bp, primer size: 18-25 bp). *PrimerPooler* (Brown et al. 2017) was then used to screen for interactions between primers with a Delta G threshold of -7 and to make sure no loci mapped to multiple regions of the genome. A final set of 452 specific PCR1 primers was ordered from Integrated DNA Technologies (IDT). For PCR2, 96 unique 'i5' primers were used to identify individuals in a plate and 24 unique 'i7' primers used to identify plates were designed and ordered from IDT following Campbell et al. (2015). This allowed for the simultaneous genotyping of up to 2,304 individuals on a single sequencing run.

DNA was extracted from 20 haphazardly selected individuals using Mag-Bind Blood and Tissue DNA kits (Omega Bio-Tek), quantified using an AccuBlue High Sensitivity Kit (Biotium) on a Spectramax M2 Microplate Reader (Molecular Devices), and diluted to a concentration of 5-20 ng/ml. Primers for PCR1 were resuspended using 1x TE buffer to a concentration of 100 mM, and 1 ml of each primer was then pooled and diluted to a concentration of 200 nM per primer. Primers for PCR2 were also resuspended to a 100 mM concentration using 1x TE buffer and then diluted to 10 mM aliquots for use in the second PCR reaction.

Sequencing via GT-seq was conducted following the methods of Campbell et al. (2015), with a slight modification to the PCR1 cycling protocol. Reaction conditions involved denaturation at 95 °C for 15 min; followed by 20 cycles of denaturation at 95 °C for 30 sec, annealing at 57 °C for 30 sec, and extension at 72 °C for 2 min; followed by 10 cycles of denaturation at 95 °C for 30 sec, annealing at 65 °C for 30 sec, and extension at 72 °C for 30 sec; followed by a 4 °C hold. Products from PCR1 were diluted in Milli-Q water at a 1:20 ratio and used in the PCR2 reaction which incorporates the unique indexes and Illumina adaptors (i.e., i5 and i7 primers).

After PCR2, the product was quantified as above and equal ng of product from each test individual were pooled into a single tube. A 50 ml aliquot was taken of this sample and cleaned using AMPureXP beads (Agilent), with a dual-sided 0.4x and 0.7x and a third 0.7x clean. The final product was quantified using a Qubit High Sensitivity DNA kit (Thermo Fisher) and run on a fragment analyzer to check the size distribution of the fragments. Libraries were sequenced at the Field Museum in Chicago, IL, USA by the Pritzker Laboratory on a MiSeq using the reagent nano (300-cycle) v2 kit (Illumina).

Demultiplexed amplicon data were analyzed using custom lab scripts. Reads were mapped to a reduced representation reference using *BWA*, SNPs were called using *Freebayes*, and microhaplotypes were identified and filtered using *microhaplot* (https://github.com/ngthomas/microhaplot). Rates of primer cross-hybridization and overamplification were calculated and loci were removed on the basis of high hybridization rates, high or low amplification, or departure from the expectations of Hardy-Weinberg equilibrium (HWE). The panel was considered optimized when total on-target reads accounted for more than 70% of sequenced reads, and more than 90% of the targeted loci passed variant calling and filtering. The final panel consisted of 322 microhaplotype loci.

Amplicon Genotyping and Filtering

All fin clip samples were run through the above protocol using the final GT-seq panel. DNA was extracted with Chelex resin 100 (BioRad) to reduce costs. With this method, a small piece of fin clip (< 3 mm^2) was combined with 100 ml of 10% Chelex dissolved in MilliQ water and 5 ml of proteinase K. They were then placed on the thermocycler with a program of 90 minutes at 60 °C followed by 15 minutes at 95 °C. The plate of DNA extractions was vortexed to ensure proper digestion, and the supernatant was used as the DNA input in PCR1 at a ratio of 1:1 with MilliQ water. Each well of a 96-well plate received a unique i5 primer, while each plate received a different i7 primer in the second PCR to allow for pooled sequencing of all samples. All individuals in a plate were pooled and each pooled plate was cleaned separately. After cleaning, each pooled plate was quantified using the Qubit kit, normalized to a concentration of 15 nM, and equal volumes of each were used to create a final sequencing library that contained all individuals. This was all done in batches of ten plates, leading to ~960 samples being sequenced together on one run. Sequencing was carried out on a MiSeq (Illumina) using the v2 300-cyle kit at the Field Museum in Chicago, IL, USA by the Pritzker Laboratory.

Demultiplexed fastq files were trimmed with *fastp*, forward and reverse sequences were flashed together, and mapped to the reduced reference genome using *BWA*. Microhaplotypes were called and filtered using *microtyper* (Delomas et al. 2023). Genotypes were then imported into *R* and individuals and loci were filtered out based on missing data. Expected and observed genotype frequencies were visualized using *whoa* (Anderson 2021). The degree of departure from the expectation of HWE was quantified for each genotype using the *z*-score computed by *whoa*. This is simply the difference between observed and expected genotype frequency divided by the

standard deviation expected under HWE. Loci were filtered out if any one of their genotypes had a z value <-5 or >10.

Kinship Estimation

Identification of kin pairs was done in two stages. Likely kin pairs were first identified using the amplicon genotypes, and then these were subsequently confirmed as kin (or not) by ddRAD sequencing of the likely pairs. This strategy was selected because GT-seq enables the efficient mass genotyping of thousands of samples for <$10 per sample, but only for hundreds of genetic markers, making assignment to kin group tenuous. Conversely, ddRAD provides data from thousands of genetic markers, allowing for high-resolution assignment of kin groups, but is considerably more expensive at >$25 per sample.

Using the amplicon genotypes, *CKMRsim*, a Monte Carlo method based simulator and kinship log-likelihood calculation in R (Anderson 2025b; Baetscher et al. 2019; Bootsma et al. 2020), was used to calculate log-likelihoods for four different pairwise kin relationship categories: parent offspring, L(PO), full-sibling, L(FS), half-sibling, L(HS), and half-avuncular, L(HA), as well as for the unrelated category L(U). The Monte Carlo simulation features of *CKMRsim* were used to simulate the expected distributions of various log-likelihood ratios [for example $\Lambda_{HS/U}$ = L(HS)/L(U)] to determine thresholds for selecting likely kin, and calculating false-positive rates (rate at which pairs of individuals are incorrectly included in a target kin category; FPRs) and false-negative rates (rate at which pairs of individuals are incorrectly excluded from a target kin category; FNRs) associated with using such thresholds.

The distribution of log-likelihood ratios is affected by the number of missing loci per individual, thus a new functionality was developed in *CKMRsim* to account for this type of missing data. First, fast routines were implemented for counting the number of shared loci (NSL) in a pair. Across nearly 100 million pairs, most pairs shared just under 100 loci (Figure 3-2). Secondly, existing functionality was utilized in *CKMRsim* to simulate pairs with a given NSL according to the actual patterns of missing data observed across all the pairs with that same value of NSL. Physical linkage among markers must be accounted for in kinship inference; however, the genome assembly for red snapper is not at a chromosome-level and the locations of the markers within the genome are not known. To deal with this, during simulations markers were randomly placed within a genome of 24 linkage groups ranging in size from 75 to 43 centimorgans (cM) with a total genetic length of 1350 cM, as reported by Norrell et al. (2020). Parameters of the genotyping error model were tuned so simulations of unrelated pairs fit closely to the observed data for both $\Lambda_{PO/U}$ and $\Lambda_{HS/U}$ (Figure 3-3). The genotyping model chosen was *CKMRsim*'s "ge_model_microhap_1" with an allele miscall rate of 0.001 and an allele dropout rate of 0.01 per gene copy (0.02 per locus).

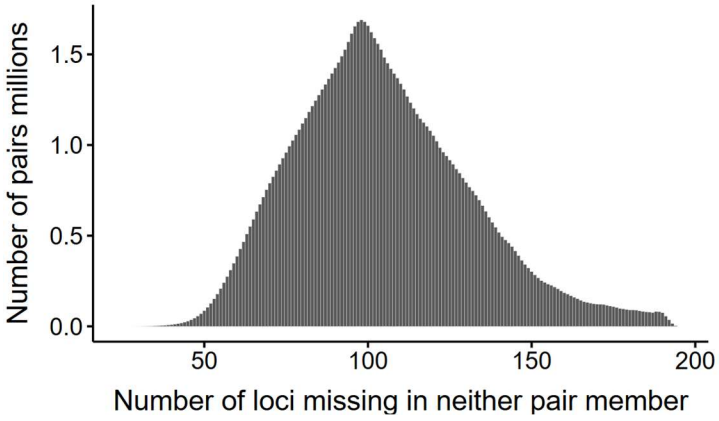

Figure 3-2. Distribution of pairs (y-axis) having the number of shared loci (NSL) on the x-axis from the 14,085 red snapper genotyped with the GT-seq panel.

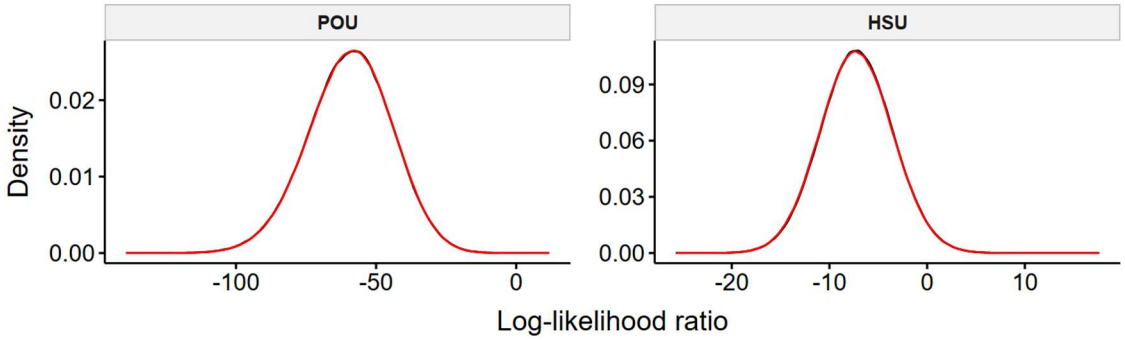

Figure 3-3. Observed and simulated (for unrelated pairs) distributions of $\Lambda_{PO/U}$ (on the left) and $\Lambda_{HS/U}$ (on the right). The observed density line is in red and the simulated line is in black. Result is shown for NSL = 120.

Thresholds were set for $\Lambda_{PO/U}$ and $\Lambda_{FS/U}$ to yield FPRs of 1 x 10^{-10}, so the chance that any U pairs exceed that threshold is small (~1/100). By contrast, HS pairs are much more difficult to distinguish from U pairs, and since all pairs were confirmed with ddRAD seq data, error could be tolerated at this stage. The $\Lambda_{HS/U}$ threshold was set to 1 x 10^{-6}, such that approximately 100 U pairs would be expected to exceed that threshold. For all candidate pairs at this stage, FNR (which depends on the amount of missing data) was recorded to account for it in the CKMR model. Individuals belonging to all pairs that exceeded the above thresholds with the amplicon sequencing genotypes were sequenced using a full complement of ddRAD seq markers, and *CKMRsim* was used again to confirm the pairwise relationships.

In the second round of *CKMRsim* use, with the ddRAD data, only four high-confidence PO pairs were confirmed. Therefore, only HS pairs were used for the CKMR population estimation. The set of "likely HS pair candidates" to be used in the CKMR estimate were defined as those which 1) were candidate HS pairs from the GT-seq experiment; 2) had 100 or more NSLs from the GT-seq panel; and, 3) had $\Lambda_{HS/HAN} > 0$, $\Lambda_{HS/FS} > 0$, and $\Lambda_{HS/PO} > 0$. The FNRs associated with

this filtering were calculated using *CKMRsim* and recorded as FNR_{ddRAD}. The pairs in this "likely HS pair candidates" set were then used in the CKMR analysis to estimate red snapper population size.

MtDNA Sequencing and Sex of Potential Kin Pairs Shared-Parent

The entire mitochondrial genome (mtDNA) was amplified for a subset of HS candidate pairs and a set of samples that were unrelated to test the assumption there was no sex bias in realized reproductive success. Briefly, DNA was extracted using Mag-Bind Tissue DNA kits (Omega Bio-Tek) and prepared using a modified protocol for whole genome sequencing with the Illumina DNA Prep Kit (Jones et al. 2023). Genomic DNA was both cut and ligated with Illumina bead-linked chemistry. Tagged DNA fragments were PCR amplified using Phusion Taq polymerase and a unique combination of i5 and i7 indexed flowcell adaptors, allowing samples to be pooled and sequenced together on an Illumina NovaSeq X. Samples were combined into two separate libraries.

Because there is significant length variation among mtDNA available publicly, the mtDNA of the individual with the highest sequencing read depth was *de novo* assembled using the default settings in the *MitoZ* v3.6 pipeline (Meng et al. 2019) and used as the reference for subsequent analysis. Sequences were aligned to that reference and variant sites were detected using *freebayes* v1.0.2 (Garrison and Marth 2012) and *bcftools* v 1.17 (Danecek et al. 2021) was used to find a consensus sequence for each individual. Consensus sequences were aligned using MUSCLE v 5.3 (Edgar 2022) and indels removed for further evaluation. If the depth at a base for a given sample was less than 10, or if the percent of alternative allele counts was 25 to 75 percent of the depth, an ambiguous base was used in the consensus sequence for that sample. Consensus sequences with over 20 ambiguous bases were removed from the dataset. Haplotype diversity (H_d), nucleotide diversity (π), and number of pairwise differences (p) were calculated using Arlequin with one member of each of the kin pairs removed from the dataset. Because mtDNA is inherited maternally, kin sharing haplotypes were assumed to be maternally related whereas kin with different haplotypes were assumed to be paternally related. A binomial test was then used to test whether the observed ratio of kin who shared haplotype to kin who did not shared haplotypes was different than a ratio of 1:1.

CKMR Pseudolikelihoods

A central element of the pseudolikelihood is the HS kinship probability, which is formulated in terms of the expected relative reproductive output (ERRO) and $N_{a,t}$, the abundance of age-a individuals at time t. ERRO for age a at time t is proportional to the product of percent maturity (P), fecundity (Fec) and the relative proportion of individuals of age a at time t, which can be calculated from estimates of mortality or input directly as age composition data:

$$\mathrm{ERRO}_{a,\mathrm{t}} = \frac{P_a \mathrm{Fec}_a R_{a,t}}{\sum_a P_a \mathrm{Fec}_a R_{a,t}}. \qquad \text{(equation 3-1)}$$

This quantity is the same for male and female adults, given the assumption of balanced sex ratios and reproductive output.

Given a pair of samples with birth years b_1 and b_2, respectively, such that b_1 is the birth year of the first born (i.e., $b_1<b_2$), and the difference between birth years is $b_2 - b_1 = d$, the probability that individual *1* and *2* are HSs $[P(\mathrm{HS}|b_1 b_2, \mathrm{N}, \Theta)]$ can be calculated as:

$$P(\mathrm{HS}|b_1 b_2, \mathrm{N}, \Theta) = \sum_{a=1}^{a=20-d} \left(\mathrm{ERRO}_{a,b_1} \times \mathrm{ERRO}_{a+d,b_2} \left[\prod_{k=a+1}^{a+d} S_k \right] \frac{4}{N_{a+d,b_2}} \right) \qquad \text{(equation 3-2)}$$

This occurs because the pair will only be HSs if:

1. individuals *1* and *2* were born d years apart, i.e., individual *1* was born to an a-year-old at time b_1 and individual 2 was born to an $a+d$-year-old at time b_2. This is reflected in the product $\mathrm{ERRO}_{a,b_1} \times \mathrm{ERRO}_{a+d,b_2}$
2. the parent of individual *1* survived for the d years until the time of individual *2*'s birth, reflected in the product

$$\prod_{k=a+1}^{a+d} S_k \qquad \text{(equation 3-3)}$$

3. the parent of individual 2 is exactly a single, specific individual (the parent of 1, to be precise) from amongst the N_{a+d,b_2} adults of age $a+d$ at time b_2 that have the same expected reproductive output, reflected in the term $1/N_{a+d,b_2}$.

The sum over a in the expression accounts for the fact that we must consider all possible ages of the shared parent of individual 1 and 2. The factor of 4 accounts for the parent being either a male or a female, with an even sex ratio and similar survival and reproductive success between sexes for N_{a+d} reproductive adults (male or female) of age $a+d$ at the time of individual *2*'s birth (b_2).

CKMR Model Description and Parameterization

An age-structured model indexed by year was adopted for CKMR estimation of Atlantic red snapper population size, with population parameters available either from the most recent stock assessment (SEDAR 2024) or from the Data Workshop of the ongoing SEDAR 90 stock assessment process (SEDAR 2025; Table 3-1). In the demographic model, the maximum age of a fish is considered to be 20 years, with any older fish being combined into the 20-year category, thus making it a 20+ group. The demographic model was parameterized with age composition data from the SEDAR 73 update assessment (Table 3-2, SEDAR 2024) for all age groups in years 2014-2023, and with year-specific annual survival rates taken from estimates of total instantaneous

mortality rate (SEDAR 2024; Table 3-3), while Atlantic red snapper life-history characteristics and parameters were derived from inputs to the SEDAR 90 Data Workshop (SEDAR 2025; Table 3-1). Relative fecundity as a function of age was assumed to be linear with average weight within an age class and constant across years and was calculated as (mass at age)/Σ(mass at age) as recommended because of uncertainty in modeling fecundity in terms of total egg production (SEDAR 2025, Section 2.3.4). Age-specific relative reproductive output of males was assumed to scale with age the same as the fecundity of females. The proportion of females mature at age was assumed to be the same for males. A sex ratio of 1:1 was used throughout.

Table 3-1. Estimates of Atlantic red snapper life-history characteristics and parameters from the SEDAR 90 Data Workshop (SEDAR 2025). M = instantaneous natural mortality, Prop mature = proportion mature females.

Age y	Total length mm	Mass kg	M:F sex ratio	M y^{-1}	Prop mature
1	316.4	0.49	1:1	0.270	0.139
2	434.3	1.27	1:1	0.197	0.676
3	527.9	2.28	1:1	0.162	0.925
4	602.3	3.38	1:1	0.142	0.985
5	661.4	4.47	1:1	0.129	0.997
6	708.4	5.49	1:1	0.121	0.999
7	745.7	6.40	1:1	0.115	1.000
8	775.4	7.20	1:1	0.110	1.000
9	798.9	7.87	1:1	0.107	1.000
10	817.6	8.43	1:1	0.105	1.000
11	832.5	8.90	1:1	0.103	1.000
12	844.3	9.28	1:1	0.101	1.000
13	853.7	9.60	1:1	0.100	1.000
14	861.2	9.85	1:1	0.099	1.000
15	867.1	10.05	1:1	0.099	1.000
16	871.8	10.22	1:1	0.098	1.000
17	875.6	10.35	1:1	0.098	1.000
18	878.5	10.45	1:1	0.097	1.000
19	880.9	10.54	1:1	0.097	1.000
20	882.8	10.61	1:1	0.097	1.000

Table 3-2. Annual estimates of Atlantic red snapper mid-year proportional age composition from the SEDAR 73 update stock assessment (SEDAR 2024).

Year	Age-1	Age-2	Age-3	Age-4	Age-5	Age-6	Age-7	Age-8	Age-9	Age-10
2014	0.63351	0.17606	0.05775	0.04071	0.01559	0.00891	0.02674	0.01767	0.01483	0.00049
2015	0.51619	0.30297	0.08186	0.02686	0.01977	0.00813	0.00494	0.01535	0.01032	0.00874
2016	0.41435	0.29682	0.16738	0.04690	0.01714	0.01417	0.00632	0.00401	0.01275	0.00866
2017	0.49747	0.20978	0.14108	0.07917	0.02413	0.00988	0.00892	0.00418	0.00272	0.00874
2018	0.33877	0.32651	0.13055	0.08875	0.05447	0.01851	0.00820	0.00773	0.00370	0.00243
2019	0.51807	0.16831	0.14892	0.05739	0.04149	0.02850	0.01065	0.00498	0.00482	0.00234
2020	0.37911	0.32048	0.09809	0.08645	0.03582	0.02871	0.02136	0.00835	0.00399	0.00390
2021	0.48673	0.19786	0.15556	0.04625	0.04311	0.01980	0.01733	0.01357	0.00544	0.00263
2022	0.21983	0.37406	0.14785	0.11693	0.03687	0.03721	0.01818	0.01649	0.01314	0.00531
2023	0.08641	0.20064	0.32392	0.12666	0.10712	0.03716	0.04038	0.02057	0.01903	0.01531

Year	Age-11	Age-12	Age-13	Age-14	Age-15	Age-16	Age-17	Age-18	Age-19	Age-20
2014	0.00065	0.00149	0.00111	0.00113	0.00141	0.00079	0.00043	0.00016	0.00010	0.00048
2015	0.00029	0.00038	0.00088	0.00066	0.00067	0.00084	0.00047	0.00026	0.00010	0.00034
2016	0.00736	0.00025	0.00032	0.00075	0.00056	0.00057	0.00071	0.00040	0.00022	0.00037
2017	0.00597	0.00509	0.00017	0.00022	0.00052	0.00039	0.00039	0.00049	0.00028	0.00041
2018	0.00784	0.00536	0.00457	0.00015	0.00020	0.00047	0.00035	0.00035	0.00044	0.00062
2019	0.00155	0.00499	0.00342	0.00292	0.00010	0.00013	0.00030	0.00022	0.00023	0.00068
2020	0.00190	0.00126	0.00407	0.00279	0.00238	0.00008	0.00011	0.00024	0.00018	0.00074
2021	0.00259	0.00126	0.00084	0.00271	0.00185	0.00158	0.00005	0.00007	0.00016	0.00062
2022	0.00258	0.00254	0.00124	0.00082	0.00266	0.00183	0.00156	0.00005	0.00007	0.00077
2023	0.00621	0.00302	0.00298	0.00146	0.00097	0.00313	0.00215	0.00184	0.00006	0.00098

Table 3-3. Estimates of Atlantic red snapper total instantaneous mortality (y^{-1}) from the SEDAR73 update stock assessment (SEDAR 2024).

Year	Age-1	Age-2	Age-3	Age-4	Age-5	Age-6	Age-7	Age-8	Age-9	Age-10
2014	0.412	0.451	0.512	0.526	0.469	0.400	0.355	0.332	0.321	0.314
2015	0.426	0.464	0.481	0.420	0.319	0.234	0.182	0.157	0.145	0.138
2016	0.505	0.605	0.648	0.558	0.403	0.272	0.194	0.156	0.139	0.131
2017	0.406	0.430	0.456	0.423	0.345	0.273	0.227	0.205	0.194	0.188
2018	0.526	0.649	0.732	0.684	0.538	0.398	0.313	0.272	0.254	0.244
2019	0.423	0.462	0.511	0.502	0.427	0.348	0.297	0.272	0.261	0.254
2020	0.514	0.627	0.707	0.666	0.531	0.399	0.318	0.280	0.262	0.253
2021	0.405	0.428	0.459	0.438	0.366	0.296	0.251	0.229	0.218	0.212
2022	0.431	0.475	0.508	0.464	0.368	0.281	0.227	0.201	0.189	0.182
2023	0.453	0.519	0.580	0.569	0.478	0.383	0.323	0.294	0.280	0.273

Year	Age-11	Age-12	Age-13	Age-14	Age-15	Age-16	Age-17	Age-18	Age-19	Age-20
2014	0.312	0.311	0.310	0.309	0.309	0.308	0.308	0.307	0.307	0.307
2015	0.136	0.135	0.134	0.133	0.133	0.132	0.132	0.131	0.131	0.131
2016	0.129	0.128	0.127	0.126	0.126	0.125	0.125	0.124	0.124	0.124
2017	0.186	0.185	0.184	0.183	0.183	0.182	0.182	0.181	0.181	0.181
2018	0.242	0.241	0.240	0.239	0.239	0.238	0.238	0.237	0.237	0.237
2019	0.252	0.251	0.250	0.249	0.249	0.248	0.248	0.247	0.247	0.247
2020	0.251	0.250	0.249	0.248	0.248	0.247	0.247	0.246	0.246	0.246
2021	0.210	0.209	0.208	0.207	0.207	0.206	0.206	0.205	0.205	0.205
2022	0.180	0.179	0.178	0.177	0.177	0.176	0.176	0.175	0.175	0.175
2023	0.271	0.270	0.269	0.268	0.268	0.267	0.267	0.266	0.266	0.266

Ages of most red snapper samples (81.7%) were estimated as indicated above via standard otolith-based ageing protocols. Age was estimated for samples that lacked otolith samples utilizing an age-length key (ALK) developed for SEDAR 90. The month-specific ALK was derived from the von Bertalanffy growth model with parameters (SEDAR 2025; L_{inf} = 890.03 mm total length, k = 0.23 y^{-1}, t_0 = -0.41 y, with 66.5). The ALK estimated the probability of being a certain age for fish that are within any distinct 10 mm total length bin in a given month of the year. The ALK can be found at https://github.com/marinegenomicslab/Red-Snapper-CKMR/. To avoid bias caused by the inclusion of otolith data for some but not all individuals the ALK was applied to all individuals.

One approach to calculating the likelihood would have been to sum over different possible birth-year categories for every pair of individuals with each member belonging to a particular length bin and collection month. Because FNR has to be used for CKMR estimation, such bin categories must be further broken down according to the NSL within the pair. This approach was investigated, and it was discovered that doing so would create over 37 million categories of pairs. This amounts to less than a three-fold reduction of the total number of pairs and creates excessive computational demand for calculating the CKMR pseudolikelihood. Instead of this approach, a method of multiple imputation was utilized: each individual has its age (and hence its birth year) imputed by sampling its age from the probabilities of the age-length key. These birth years are then used to place the pairs into categories, with pairs only being retained if the first-born was born in or after 2014, and if the second-born was born in a different (later) year than the first-born, thus ensuring that cross-cohort comparisons are made. In addition, pairs were only considered true HS if they were born four or fewer years apart, to exclude any HA or grandparent-grandchild pairs separated by more than four years of age. This reduced the number of pair categories to a much more manageable number (approximately 8,000). This multiple imputation process was repeated 100 times, with a CKMR population estimate being computed each time. For a final estimate, a Bayesian approach was used with the posterior samples from all 100 age-imputation replicates serving as the sample from the posterior.

The CKMR pseudolikelihood itself relies on P_{HS}, the probability that a given pair of samples is a half-sibling pair, calculated conditionally on the birth years (b_1, b_2) of the two pair members (given they must be in separate year classes to be included in CKMR), the total abundance, N, and the demographic parameters, D, including sample age composition, annual age- and year-specific total survival probabilities, the age-specific fraction of mature fish, and the age-specific relative reproductive output, following Bravington et al. (2016a). This probability is $P_{HS}(b_1, b_2, N, D)$. It is used to calculate the probability that a pair is a half-sibling *and* it is detected as a half-sibling pair, $P^*_{HS}(b_1, b_2, N, D, F)$, where F denotes the genetic detection procedure and is accounted for primarily in the false negative rates, FNR and FNR_{ddRAD}. The probability of detecting an HS pair i is

$$P^*_{HS}(b_1, b_2, N, D, F; \text{HSP}) = P_{HS}(b_1, b_2, N, D)(1 - FNR_i)(1 - FNR_{ddRAD,i}). \quad \text{(equation 3-4)}$$

The probability that a pair is not detected as an HS pair at the GT-seq stage of the analysis is

$$1 - P_{HS}(b_1, b_2, N, D)(1 - \mathrm{FNR}_i). \qquad \text{(equation 3-5)}$$

The above probabilities are combined in a Binomial negative log-likelihood in two parts. First, the contribution of the observed cross-cohort HS pairs after age imputation is calculated as a sum over pairs:

$$NLLHS = -\sum_{HS\ pairs} log\ P^*_{HS}(b_1, b_2, N, D, F; \mathrm{HSP}). \qquad \text{(equation 3-6)}$$

The contribution of pairs that were not detected as HS pairs during the initial GT-seq phase is a sum over the different (roughly 8,000) pair categories (from different NLS and birth years)

$$NLLGT = -\sum_{i \in Categories} n_i\ log(1 - P_{HS}(b_1, b_2, N, D)(1 - \mathrm{FNR}_i)), \qquad \text{(equation 3-7)}$$

where n_i is the number or non-HSP pairs in category i.

A third contribution to the negative log-likelihood would involve the pairs that were candidate HS pairs from the GT-seq genotyping but were found not to be HS pairs upon ddRAD sequencing. The contribution of each such pair differs from those that were not identified at the GT-seq stage by only a factor of $(1 - \mathrm{FNR}_{\mathrm{ddRAD},i})$, which is large (around 0.9). Since the numbers of such pairs (on the order of a few hundred) was so much smaller than the nearly 100 million total pairs, their inclusion is expected to be negligible. Consequently, they were discarded from the likelihood to reduce accounting overhead, and the negative log-likelihood used was *NLLHS* + *NLLGT*.

A few restrictions on the pairwise comparisons were investigated to gain insight into possible population trends and future sampling strategy. The first, "B2>2018," only considered pairs in which the second-born member was born in year 2019 or greater. This ensures the population estimate is affected only by absolute abundance in years after and including 2019. An additional CKMR model was implemented which modeled abundance as a function of year with an initial population size parameter, N_0, the population size at year 2014, and an exponential rate of change parameter, λ. The abundance at time t is given by $N_t = N_0 e^{\lambda t}$.

To assess the sensitivity of the CKMR estimates to the age-composition used as input to the model, three separate experiments were performed. The first experiment, termed the Equilibrium Scenario was set up to provide an estimate using only demographic information. In it, age-specific total survival was assumed constant through time and was obtained as the average of total age-specific annual survival for the years from 2014 to 2023. Computed average survival rates were then used to calculate a single equilibrium age composition which was applied to all years. The remaining two experiments explored the sensitivity of the CKMR estimates to age-composition misspecification resulting from uncertainty around fishing mortality, which is known to be an issue for Atlantic red snapper. In the first of these scenarios, termed "Old Biased" age

composition used in the model was calculated under the assumption that fishing mortality was only 50% of the value used to create the original age composition input. In the second of these two scenarios, "Young Biased," the age composition was obtained under the assumption that fishing mortality was 150% of the value. In both the Old Biased and Young Biased scenarios, the survival vector used as an input to the CKMR model was the non-time-varying one described above.

One assumption of CKMR models is fecundity among individuals is well summarized by the mean values per cohort per year. Within a given year, individuals may experience variance in realized fecundity due to sweepstakes-like recruitment effects. This potential issue is alleviated by only considering cross-cohort siblings in the estimation. However, individuals may have persistent individual differences in fecundity across years, which can confound half-sibling based CKMR estimates (Waples and Feutry 2022). If large more-fecund-than-average individuals in one year also tend to be the large more-fecund-than-average individuals in later years, then this would lead to an increased variance in the number of cross-cohort offspring produced by any individual. This increased variance would drive an increase in the number of cross-cohort half-siblings found in the sample, which, if not accounted for, would bias the abundance estimate downward. The potential sensitivity of the red snapper CKMR model to age-specific variation in size (and hence fecundity) that persists across years was therefore investigated. Simple simulations of the expected number of half-sibling pairs were parameterized using 1) the age composition of our standard model; 2) the assumption that length at each age is normally distributed with a coefficient of variation of 0.13 (a value estimated from length at age data); and, 3) the assumption that rank-order of individuals in terms of size remains the same each year. This final assumption represents a worst-case scenario as to the extent that persistent individual differences could affect a CKMR estimate in that it assumes individual differences are perfectly persistent across years. Average individual length (L_ave) of each individual (in mm) at each age was modeled with the same von Bertalanffy growth equation described above. Individual lengths (L) were assigned from a normal distribution with mean L_ave and sd = L_ave * 0.13. Then, each L was converted to weight (W) in pounds using the relationship $W = 2.2 * a L^b$, with a = 1.65e-8 and b = 2.99, and the individual weights were sorted within age each new year to preserve the rank order of size-at-age between years. Relative fecundity was modeled as proportional to weight. From these simulations, it is possible to deduce that, in the worst-case scenario, HS kinship probabilities would be 15% larger than if there were no persistent individual differences. The results of fitting a model in which a 15% inflation factor is applied to the HS probabilities provides a measure of the greatest degree to which such persistent individual differences in fecundity might change the CKMR estimate.

Lastly, hypothetical FNR scenarios were examined to test potential effects of the FNR on estimates of age-2+ Atlantic red snapper population. In addition to running the CKMR model with the FNR rate estimated during the study, additional model runs were performed with hypothetical posteriors based on an FNR that was twice the estimated rate and one that was half the estimated rate.

Results

Sample Size Estimation

Results of sample size simulations conducted prior to the start of sampling indicated a target annual sample size of 2,500 individuals per year would produce an accurate (±4.5%) red snapper population estimate with CV ≤0.3 for population sizes of 0.5-1.5 x 10^6 individuals. When the fin clip sample size was increased to 5,000 individuals per year, the accuracy of the CKMR estimate was ±4.4% with a CV ≤0.14.

Sample Collection and DNA Sequencing

The target annual sample size was ≥2,500 annual fin clip samples based on results of sample design simulations. That target was greatly exceeded in each study year given the extensive regional cooperation among state and federal agencies, as well as academic partners. Fin clips were sampled from 6,159 individuals in 2021, 6,529 in 2022, and 7,049 in 2023. After filtering the data based on criteria presented above, the GT-seq dataset contained 14,085 individuals genotyped across 195 loci (Table 3-4; Figure 3-4), hence 99,186,570 pairwise comparisons, among years. In total, 11,509 samples had otolith-derived age estimates; 91.4% of samples were ≤7 years old, 11 samples were >age-20 and 1 sample was >age-30 (Figure 3-5). Kinship analysis identified 871 individuals involved in candidate kin pairs that were subsequently prepared for ddRADseq. After filtering, the final dataset contained 844 individuals genotyped at 1,755 haplotyped loci. Across loci, the number of SNPs ranged from 1 to 15, with a total of 11,081 alleles. Mean read depth across all loci was 65. All filtering and analysis scripts, including for ddRAD, can be found at https://github.com/marinegenomicslab/Red-Snapper-CKMR.

In the final round of kin analysis for CKMR, only those pairs that had advanced through the GT-seq stage as candidate HS pairs (not those that were advanced only as possible PO of FS pairs, because calculating the false negative rates for HS pairs originating from those groups was not straightforward) were included. There were 213 such pairs. After filtering for sufficient numbers of ddRAD loci, 188 putative HS pairs remained in the dataset. Of those, 92 pairs satisfied the criteria to be "likely HS pair candidates" as described in the methods. These were the ones used for CKMR estimation. These 92 pairs were composed of separate individuals, except for two pairs, between which a single individual was shared.

The distribution of geographic distances among all individuals sampled in the current study and included in cross-cohort HS pairs was similar to the distribution of distances between any randomly selected 50 individuals (Figure 3-6) and visually there was no obvious clustering of HS pairs geographically (Figure 3-7). Furthermore, the genetic data (Portnoy et al. 2022; Monroe et al. 2025) do not support substructure within the Atlantic. Taken together, this suggests sampling was appropriately executed, and the CKMR population estimate presented only pertains to Atlantic red snapper.

Table 3-4. Atlantic red snapper sample sizes by state, year, and source for fin clips sampled for genetic sequencing in support of close-kin mark-recapture.

2021	Source	NC	SC	GA	FL
	Recreational landings	165	0	37	1244
	Recreational discards	0	0	0	841
	Commercial	43	0	0	134
	Fishery-independent	0	0	0	522
	SERFS	203	93	255	801

2022	Source	NC	SC	GA	FL
	Recreational landings	54	0	10	876
	Recreational discards	0	0	0	743
	Commercial	9	0	6	500
	Fishery-independent	0	0	0	1041
	SERFS	115	83	272	648

2023	Source	NC	SC	GA	FL
	Recreational landings	151	0	112	1201
	Recreational discards	0	0	0	353
	Commercial	33	0	0	567
	Fishery-independent	0	0	0	1439
	SERFS	67	132	180	1137

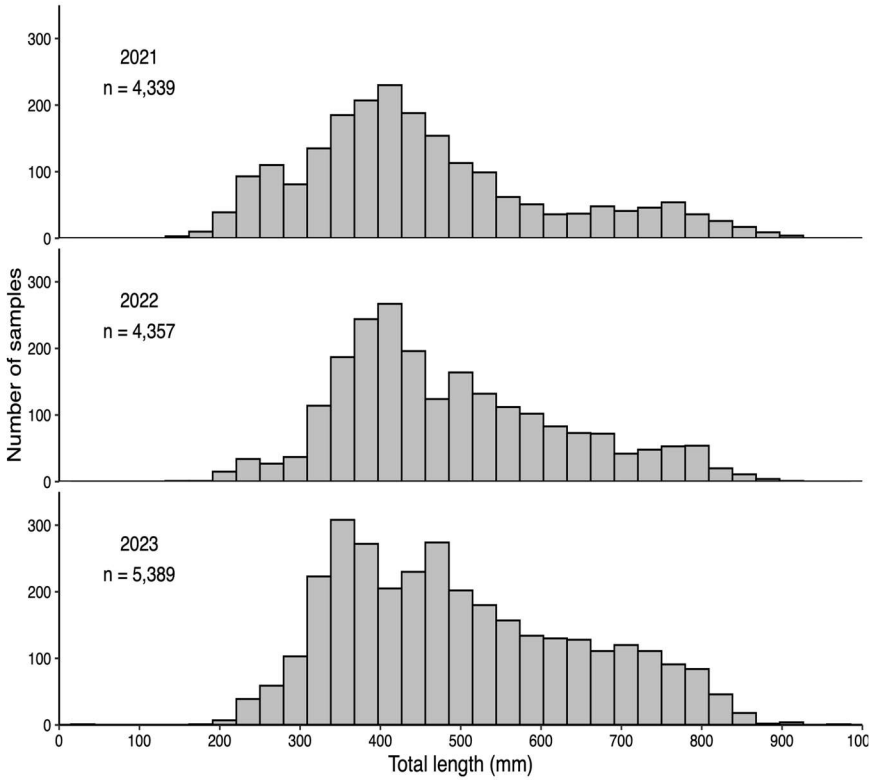

Figure 3-4. Annual total length distributions of Atlantic red snapper for which DNA was extracted from fin clip samples and sequenced with GT-seq to identify potential kinship relationships.

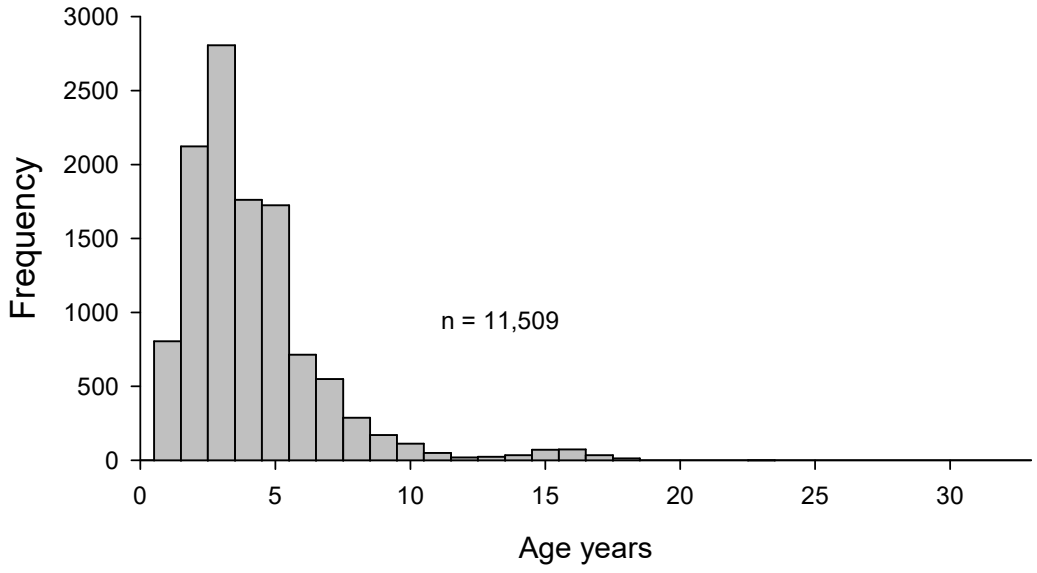

Figure 3-5. Age distribution of genetically sequenced red snapper samples for which otolith-derived age estimation was performed.

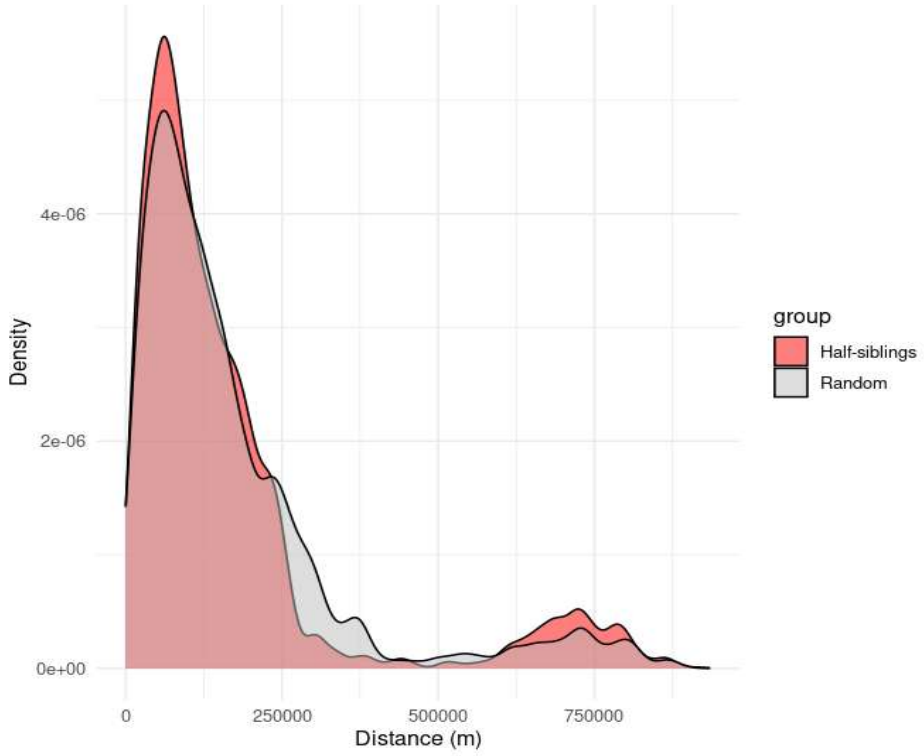

Figure 3-6 Distribution of pairwise geographic distances between all Atlantic red snapper individuals identified in putative half-sibling pairs (red) versus distribution of pairwise geographic distances between sets of the same number of individuals randomly selected 100 times (gray).

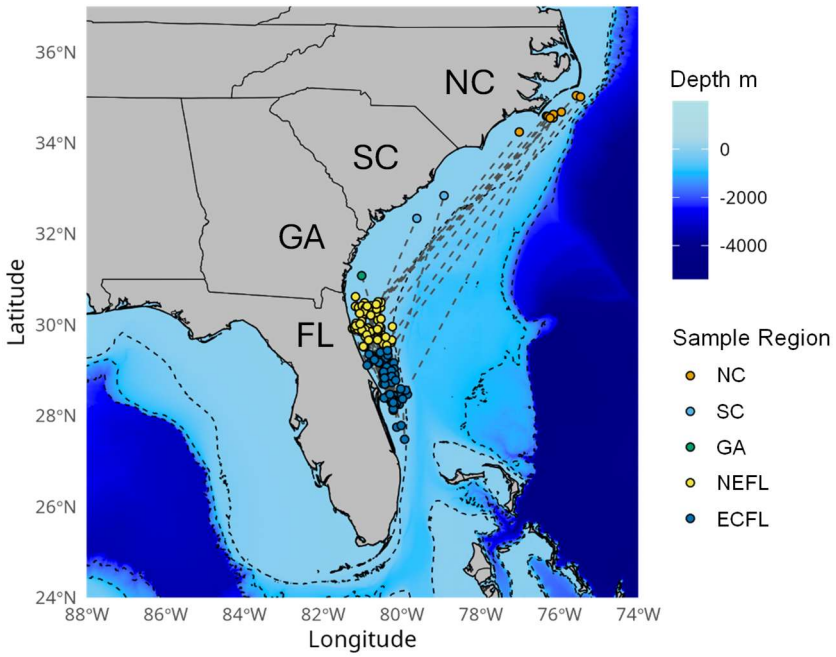

Figure 3-7. Map of Atlantic red snapper putative half-siblings (pairs connected by dashed lines). Colors indicate groupings based on state lines: North Carolina (NC), South Carolina (SC), Georgia (GA), northeastern Florida (NEFL), and east central Florida (ECFL) split arbitrarily at 29.5°N.

The two-stage genotyping strategy deployed here does present large cost-savings relative to using ddRADseq for all individuals, but it does require FPR and FNR for identifying likely kin to be estimated for both sequencing stages. For GT-seq the FPR for HS pairs was set at 10^{-6} and the FNRs corresponding to that FPR depended on the number of NSL in the pair, varying from 0.83 for 100 NSL to 0.44 for 189 NSL (Figure 3-8A). For the ddRADseq data, the FPR from an unrelated individual was very small for all the likely HS pairs. The false negatives in this case come from the filtering that requires $\Lambda_{HS/HAN} > 0$, $\Lambda_{HS/FS} > 0$, and $\Lambda_{HS/PO} > 0$. The FNR_{ddRAD} for these pairs varied from 0.13 with 1,025 ddRAD loci shared to 0.10 with 1,589 ddRAD loci (Figure 3-8B).

The assembled Atlantic red snapper mitochondrial genome was 16,502 bp and the average depth of the reference was 104x. All 37 commonly found genes were present, including 13 protein-coding genes, 22 transfer RNA genes and two ribosomal RNA genes and the noncoding control region. The mitogenome also consisted of 28% adenine, 31% cytosine, 16% guanine and 25% thymine, resulting in a 47% GC.

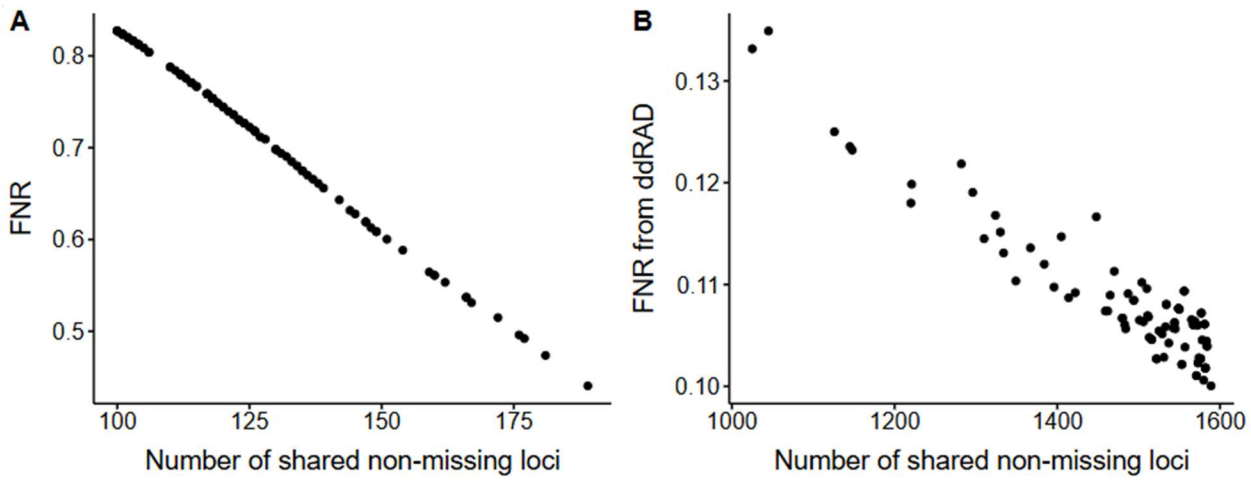

Figure 3-8. The false negative rates (FNRs) of likely kin detection estimated via Monte Carlo simulation as a function of A) the number of shared non missing loci per pair for the GT-seq panel and B) the ddRAD data.

Whole mtDNA genome analysis was performed on 144 individuals, which included 40 potential HSPs (80 individuals) as well as an additional 64 non-related individuals sampled from the Atlantic. Average depth across individuals was 70.3x and ranged from 26.6x to 252.20x, although some contained bases had too little sequencing to make a confident base call thus were coded as missing data. For the final analysis, all sequences were reduced to 16,248 bp, to exclude ~196 bp of the control region where many length variations were observed, which could have been caused by mapping to the tail end of the mitochondrial genome or poor sequencing around the pyrimidine track. The final data contained 104 haplotypes, with H_d = 0.998, π = 0.0020, and p = 32.5.70. Overall, there were 5,356 pairwise comparisons among unrelated individuals, 64 individuals with no kin plus one individual from each kin pair (40), and of those 11 pairs shared a mitochondrial haplotype (0.2%). Within the 40 potential kin pairs, 16 (40%) shared a mother and 245 (60%) shared a father. Using a binomial exact test, this was not significantly different from 1:1 (p = 0.271).

The imputation approach for assigning ages led to some variability across realizations in the number of inferred half-sibling pairs, as well as some variation in the number of non-half-sibling pairs; however, as expected, the variability was considerably smaller for the non-half-sibling pairs, of which there are many orders of magnitude more (Figure 3-9). Across all the realizations, most of the sample pairs had a second-born member born in the year 2020, and the vast majority of half-pairs had second-born members born in years 2019 to 2022. Accordingly, this is the time period over which the data offer the most information about population abundance. The number of half-sibling pairs with a second-born from 2022 appears smaller than expected given the total number of kin pairs (HS pairs + non-HS pairs), which might indicate an increase in abundance in that year.

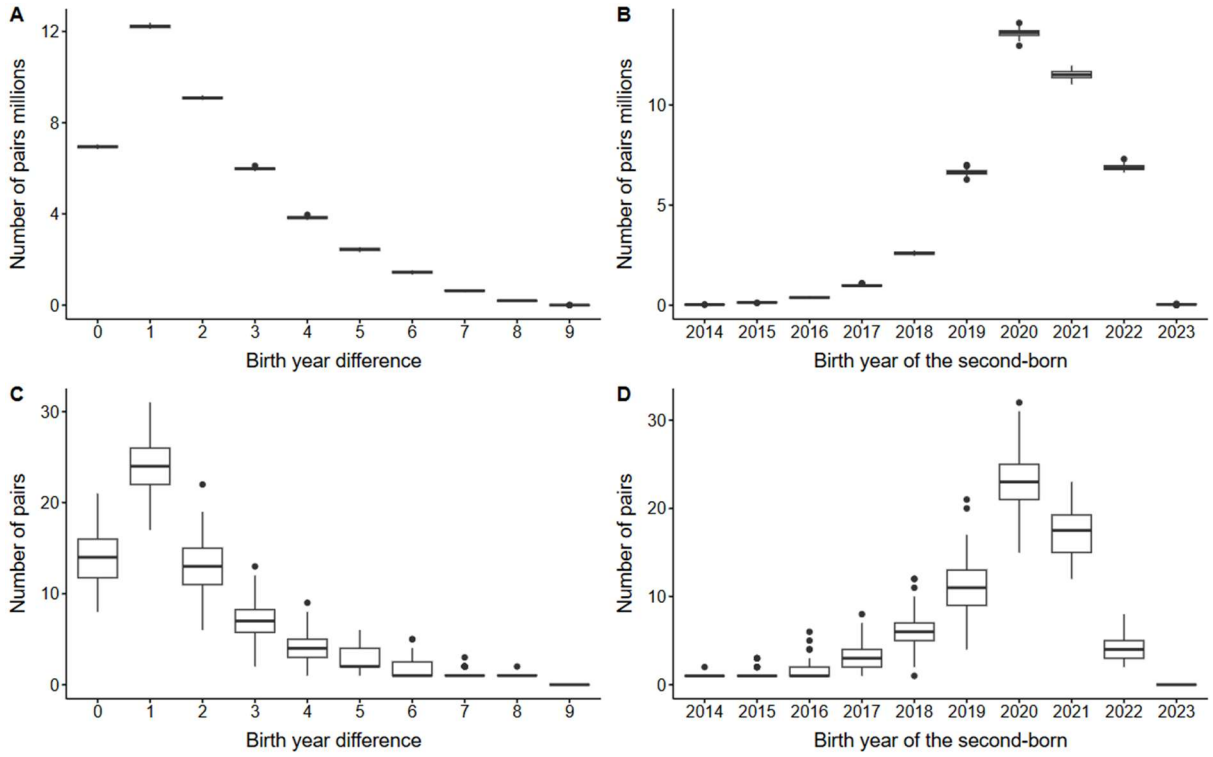

Figure 3-9. The number of non-kin pairs and the number of kin pairs by birth-year difference and by birth year of the second born. Boxplots show the median (dark line) and the upper and lower quartiles (top and bottom of boxes). The upper whisker extends to the largest data point that is no further than 1.5 times the interquartile range (IQR) above the upper quartile and the lower whisker extends to the smallest data point that is no more than 1.5 times the IQR below the lower quartile. Points more than 1.5 times outside the IQR appear as dots. The variability shown is from the 100 realizations of imputed ages of the samples. Top row, (a) and (b) show the number of non-kin pairs, and the bottom row (c) and (d) show the number of inferred half-sibling pairs.

In the first estimation exercise, using all the data from pairs separated by no more than 4 years, 100 imputations were performed of age for each sample. Across those 100 realizations, there were 39 to 56 cross-cohort HS pairs (Figure 3-10A). The maximum likelihood estimates from each of the imputed data sets varied from 1.18M to 1.69M (Figure 3-10B). Merging the MCMC runs from all 100 imputations, the posterior mean estimate of population size was 1,424,434 (maximum a posteriori = 1,338,436; median = 1,395,038), with a posterior CV of 17% and a 90% CI from 1,081,873 to 1,868,904 (Figure 3-10C).

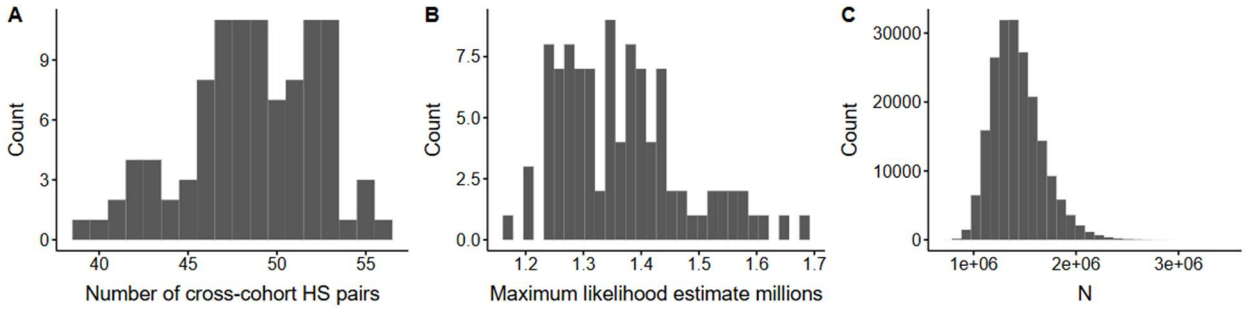

Figure 3-10. Results of CKMR population estimation using all pairs with birth years no more than 4 years apart. A) Number of cross-cohort half-siblings over 100 realizations of imputed ages. B) Distribution of maximum likelihood estimates of population size over 100 realizations. C) Posterior distribution for population size obtained by merging the MCMC samples from 100 realizations.

When restricting the estimation only to pairs separated by no more than 4 years and with no second-born member born before 2019, the estimate is entirely based on population sizes from 2019 and forward. In this case, across the 100 realizations there were between 30 and 47 cross-cohort HS pairs (Figure 3-11A). The maximum likelihood estimates from each of the imputed data sets varied from 1.24M to 1.93M (Figure 3-11B). The posterior mean estimate of population size was 1,522,246 (maximum *a posteriori* = 1,438,284; median = 1,484,011), with a posterior CV of 19% and a 90% CI from 1,124,676 to 2,046,633 (Figure 3-11C).

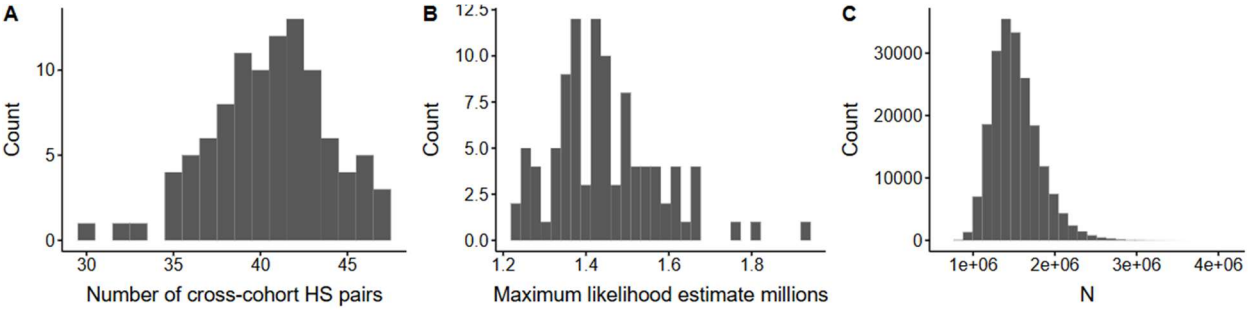

Figure 3-11. Results of CKMR estimation of age-2+ Atlantic red snapper abundance using all pairs with birth years no more than 4 years apart and no second-born members before 2019. (a) Number of cross-cohort half-siblings over 100 realizations of imputed ages. (b) The distribution of maximum likelihood estimates of population size over 100 realizations. (c) The posterior distribution for population size obtained by merging the MCMC samples from 100 realizations.

Applying the CKMR model with an initial population size and a rate of exponential change, the posterior mean and median both showed a trend toward a larger population size over time; however, the 90% and 80% credible intervals around those estimates include scenarios with

population decline as well (Figure 3-12). As is typical of these models, the population size is estimated with narrow credible intervals for the years with most of the data (2019-2021). There is less precision in population estimates for years before or after that range since there are few pairs with second-born members in those years. The posterior mean indicates values similar to those for the constant-population size model (Table 3-5, Figure 3-13).

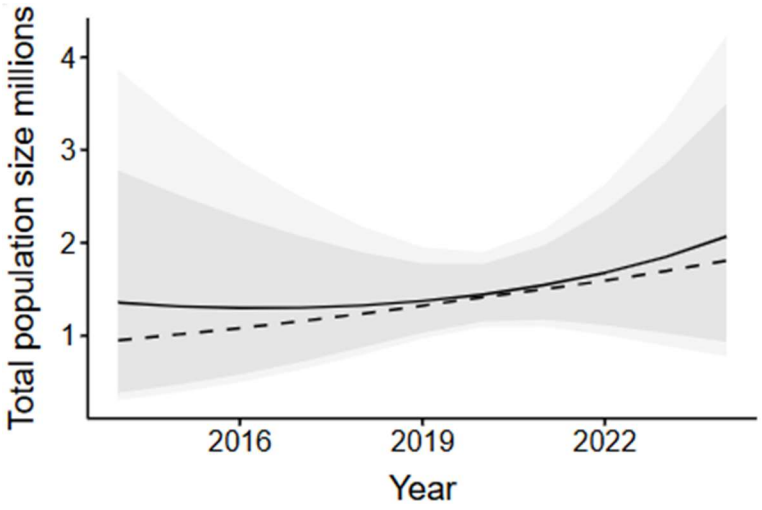

Figure 3-12. Estimated age-2+ Atlantic red snapper population size as a function of year for the CKMR model including population growth or decline. The solid line denotes the posterior mean, the dashed line the posterior median, the dark shaded region the 80% credible interval and the lighter shaded region the 90% credible interval.

Table 3-5. Point estimates, posterior CV, and 90% credible intervals (CI; L = lower, U = upper) for annual estimated age-2+ Atlantic red snapper population size from the CKMR model with exponential population growth/decline. Shown are the years with a sufficient number of half-sibling pairs to estimate population size.

Year	Mean	Max *a posteriori*	Median	Posterior CV	LCI	UCI
2018	1,325,241	1,098,876	1,234,223	0.329	795,999	2,179,853
2019	1,372,580	1,235,717	1,322,613	0.223	968,715	1,953,434
2020	1,444,565	1,359,960	1,414,694	0.172	1,095,837	1,899,379
2021	1,544,455	1,419,144	1,499,618	0.211	1,100,575	2,142,158
2022	1,676,928	1,424,347	1,591,962	0.306	1,009,560	2,630,750

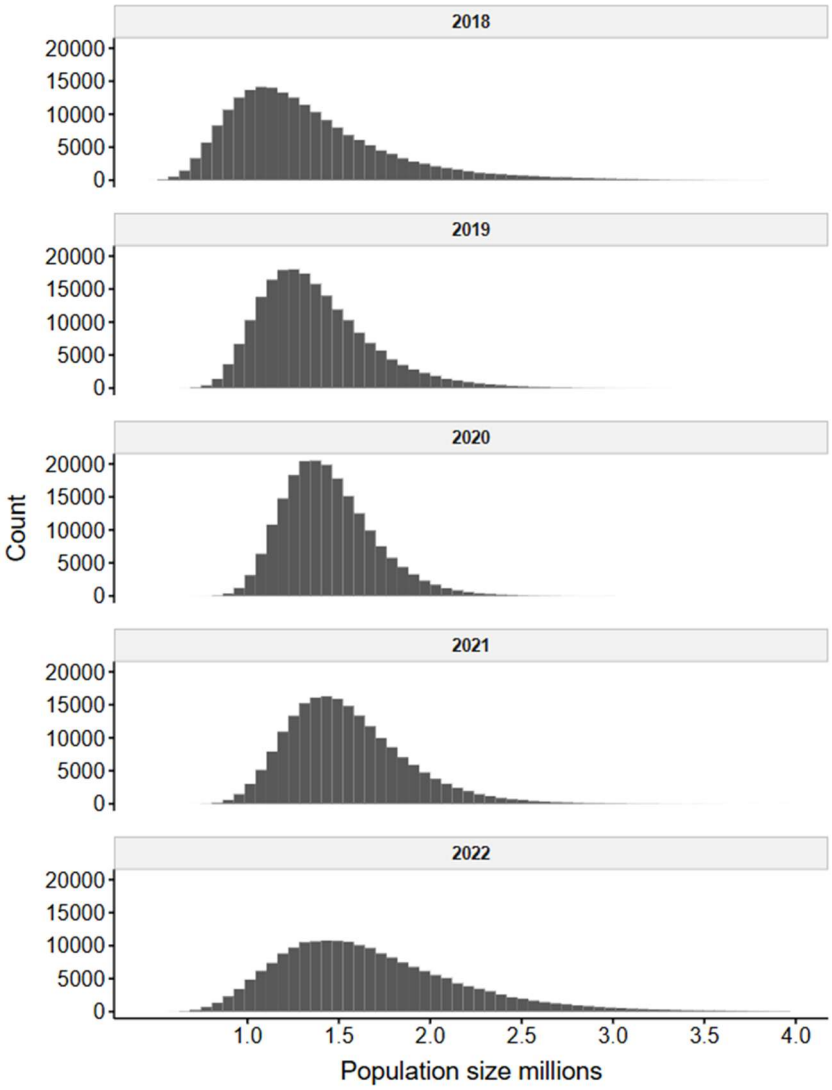

Figure 3-13. Distribution of the posterior Atlantic red snapper age-2+ population size estimates for years 2018 to 2022 in the CKMR model that includes an estimated rate of change of the population size.

Using different values of age-composition and survival rate inputs to the model had only mild effects on the abundance estimates (Figure 3-14). The Equilibrium Scenario produced an estimate for 2019 forward that was very similar to the standard model for 2019 forward, with a posterior mean estimate of population size of 1,448,382 (maximum *a posteriori* = 1,331,410; median = 1,412,131, and a 90% CI from 1,067,777 to 1,951,607. The Biased Old model showed a slight downward bias, with a posterior mean estimate of population size of 1,285,132 (maximum *a posteriori* = 1,216,069; median = 1,252,949, and a 90% CI from 948,719 to 1,731,526 and the Biased Young Model showed a slight upward bias, with a posterior mean estimate of population size of 1,906,170 (maximum *a posteriori* = 1,781,870; median =

1,857,585, and a 90% CI from 1,406,511 to 2,571,715 (Figure 3-14). When each scenario was applied with an initial population size and a rate of exponential change, there were slight changes with bias mirroring what was seen for the single estimates (Figure 3-15)

Figure 3-14: Comparison of posterior distributions for estimates of age-2+ Atlantic red snapper population size using the base model for the study (Standard), a model that uses minimal input from stock assessment (Equilibrium Scenario), fishing mortality at 50% of assessment value (Biased Old) and fishing mortality at 150% of assessment values (Biased Young).

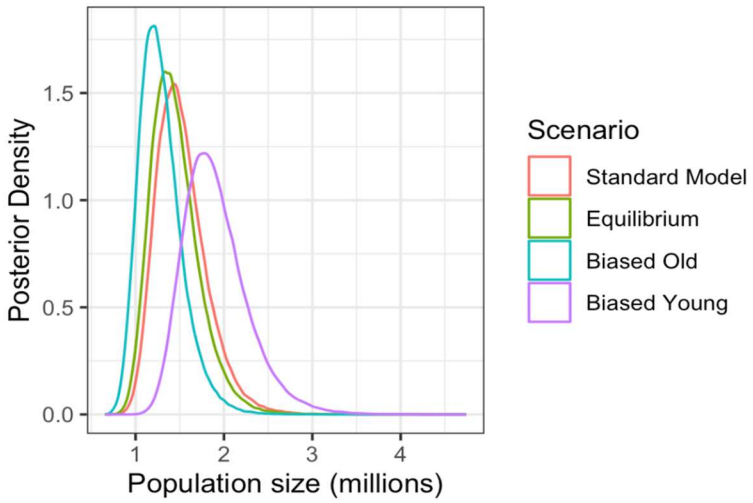

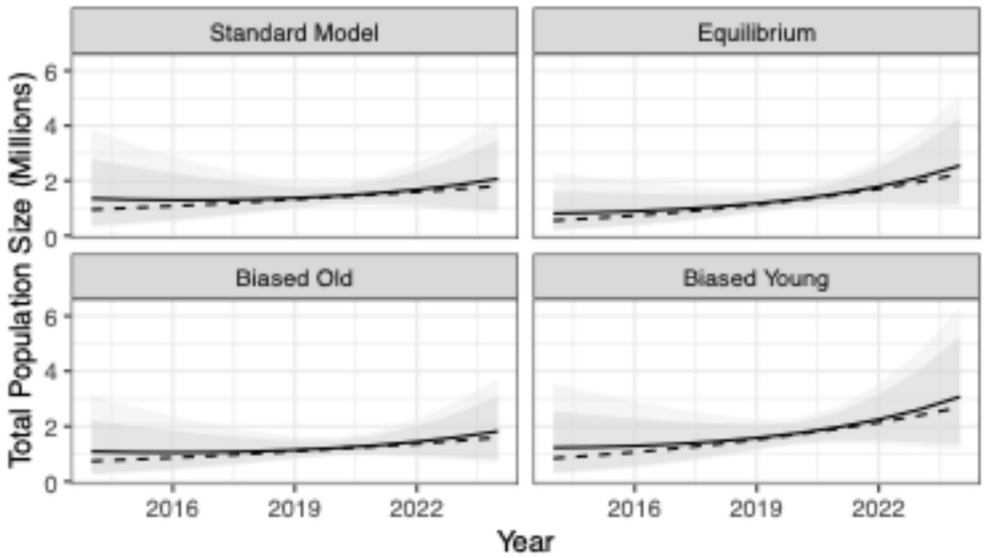

Figure 3-15: Estimated age-2+ Atlantic red snapper population size as a function of year for the base model for the study (Standard), a model that uses minimal input from stock assessment (Equilibrium), fishing mortality at 50% of assessment value (Biased Old) and fishing mortality at 150% of assessment values (Biased Young) allowing for population growth or decline. The solid line denotes the posterior mean, the dashed line the posterior median, the dark shaded region the 80% credible interval and the lighter shaded region the 90% credible interval.

The worst-case scenario of persistent individual differences in lifetime fecundity affected the CKMR population size estimate very little. When incorporating the largest HS probability inflation factor (0.15) that one would expect to see given a length CV within age of 0.13, the posterior mean population size estimate increased from 1.52M to 1.75M with a 90% CI from 1.29M to 2.36M (Fig 3-16).

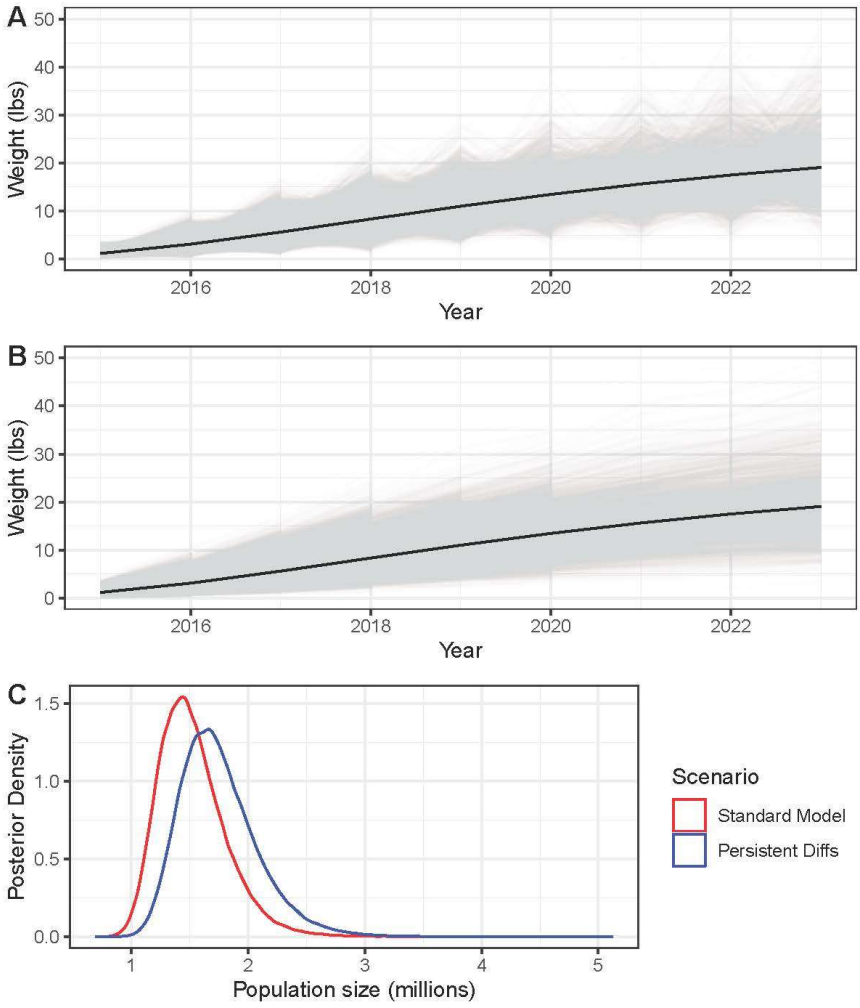

Figure 3-16. Effects of persistent individual fecundity differences. A) Growth and survival trajectories for a simulated red snapper 2014 cohort under the assumption of size-independence between years. This model is implicit in the standard model in that it leads to HS probabilities as calculated in the model, although it shows several unrealistic features (like individuals shrinking between years. B) Simulated trajectories under the "worst-case" scenario in which rank order of size is preserved across years. This scenario is also somewhat unrealistic; it is worst-case in that it leads to the highest inflation of true HS probabilities (of about 15%). C) Comparison of posterior distribution of population size under the standard (base) model (red) versus incorporating the 15% HS probability inflation implied by the worst-case scenario (blue).

Systematic error in estimating the FNR in detecting half-sibling pairs followed expected patterns. In the simulations in which the FNR was set to 2X the rate estimated in the study, then more half-sibling pairs would go undetected than expected, thus overestimating population size (Figure 3-17). Likewise, when the FNR rate was set to 0.5X the rate estimated in the study, the population size estimate would have a negative bias.

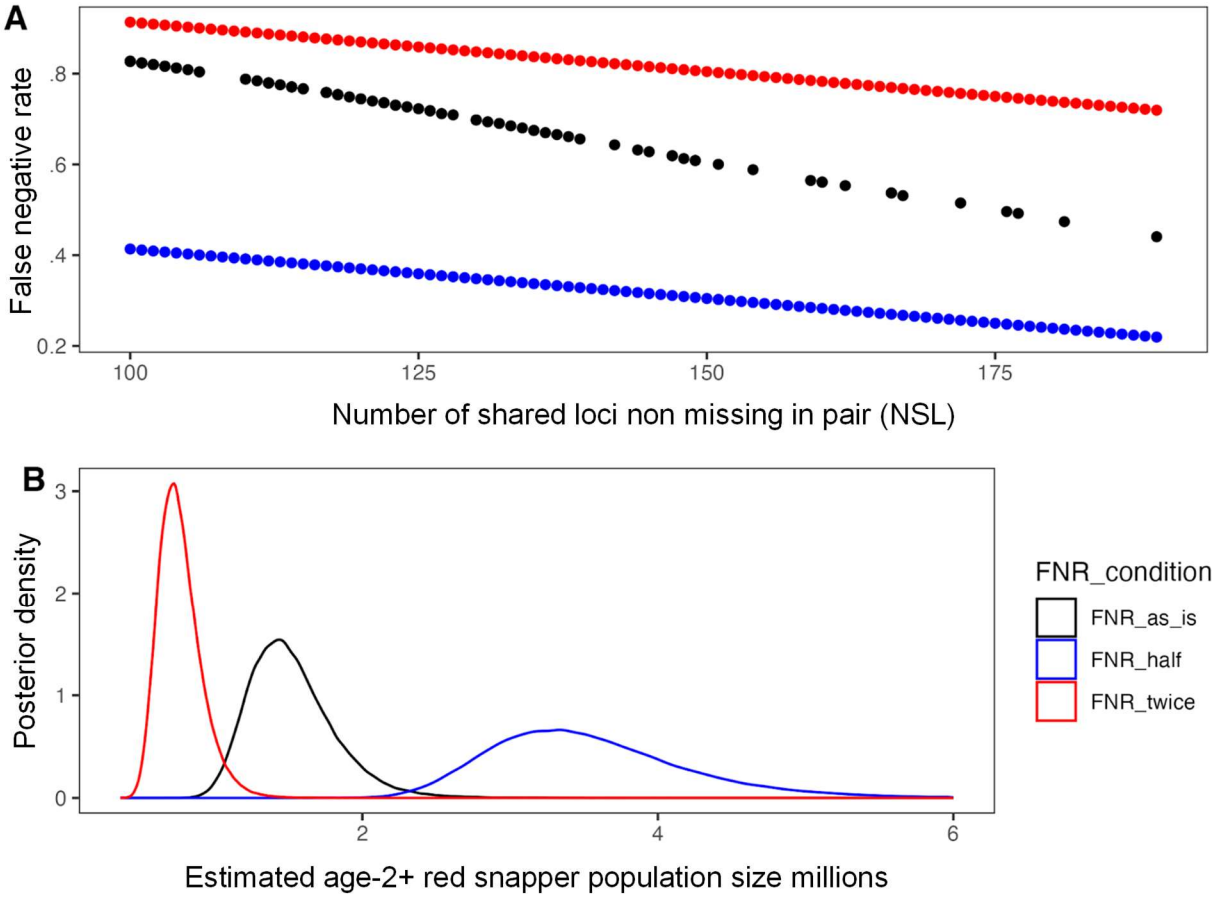

Figure 3-17. A) Illustration of different values of the false negative rate (FNR) of kinship detection as a function of number of shared loci non-missing in a given sample pair. Black dots show the relationship from the observed half-sibling pairs (as-is). Red dots show the FNR 2X scenario, in which FNR values are assumed larger than observed. Blue dots show the FNR 0.5X scenario, in which FNR values are assumed smaller than observed. Because FNR must be between 0 and 1, it is not possible for every value to be 2X or 1/2X in size. B) Posterior densities for estimated population size under different hypothetical FNR assumptions.

Discussion

Atlantic red snapper age-2+ population size was estimated with CKMR for kin relationships identified among 14,085 individuals using a two-stage genotyping approach. Kin data were input into an age-structured, pseudolikelihood CKMR model, incorporating uncertainty for individual ages. All resulting estimates were close to 1.5 million reproductive red snapper (age-2+), had fairly good precision with a CV less than 30%, and the posterior distribution ranged from approximately 1.1 million to 2 million. Because the majority of second born individuals in half-sibling pairs were born between 2019-2022, models which assume constant population size produce an estimate of the equilibrium population size for that time period. While the results provide an important benchmark estimate of population size for assessment of Atlantic red snapper, it is important to carefully assess sources of uncertainty in the estimate.

CKMR models using half-sibling pairs for teleosts require demographic data including the annual age-and year-specific total survival probabilities, the age-specific fraction of mature fish, and the age-specific relative reproductive output (Bravington et al. 2016a). Because little is known about the sensitivity of CKMR analyses to misparameterization of demographic data, a companion simulation study was conducted using red snapper life history (Kehoe et al. 2025c; Appendix XI). The results of that study demonstrate CKMR is fairly robust to errors in demographic data but do highlight two areas of concern. First, for age-structured populations with recruitment variation, CKMR models that inferred equilibrium age structure from the demographic matrices showed poorer performance than models that included an age structure component, with the trend being downward bias. To account for this, age composition data were included (SEDAR 2024) for all age groups in years included in the model. To assess the sensitivity of the reported estimates to the age-composition input, three scenarios were run, one without age structure (Equilibrium), one with relatively older structure (Biased Old) and one with relatively younger (Biased Young). The results for all three scenarios were very consistent with the base model, suggesting that estimates produced here are reasonably robust even in the face of uncertainty about age-structure and/or mortality. Secondly, misparameterization of female fecundity in models that assume nonlinear fecundity with age created a downward bias if the scaling parameter was too low and an upward bias if it was too high. To account for this, female fecundity was treated as proportional to weight, which is consistent with how fecundity was modeled in the SEDAR 90 Data Workshop for Atlantic red snapper (SEDAR 2025). To explore the model's sensitivity to fecundity, the model was run while inflating the half-sibling probabilities by 15%, which was determined through simulation to be a worst-case scenario for the effect of persistent individual differences in size, and hence fecundity. The effect of this change was modest, especially for a worst-case scenario, increasing the estimate from 1.52 million to only 1.75 million.

Another assumption of CKMR is that population size is relatively stable across the time period of interest (Bravington et al. 2016a). This is especially important if there is exponential growth or decline occurring over the time period of the estimate (Swenson et al. 2024). While the actual population size was not evaluated, several fisheries-independent studies have generated

indices of relative abundance for Atlantic red snapper, all of which increase until 2018-2019 at which point they stabilize (Christiansen et al. 2020; Solomon et al. 2025; Vecchio et al. 2025). Therefore, a model was fit in which second-born pair members born prior to 2019 were excluded so the estimate would encompass a period of apparent stability in population size. As a sensitivity analysis, an additional CKMR model with explicit exponential population growth was fit to the data. All approaches yielded similar results.

Sampling bias can also complicate CKMR analysis if population structure exists but is not accounted for or if kin pairs are non-randomly distributed with regard to sampling (Conn et al. 2020). Results of several genetic studies indicate red snapper in the Atlantic are a separate genetic stock from the Gulf (Hollenbeck et al. 2015; Portnoy et al. 2022), including a study run as part of the current project (Monroe et al. 2025, Appendix IV). This conclusion is supported by differences in life history, recruitment, and reproductive data among the basins, as well as tagging data for which no movement between basins was observed (Szedlmayer & Shipp 1994; Patterson III et al. 2001; Addis et al. 2013).

Recent biophysical modeling research estimated non-trivial subsidies of larvae from the eastern Gulf to the Atlantic in a given year (e.g., 5-30%; Karnauskas et al. 2022), which is not congruent with results of genetic studies. One possibility is that unknown aspects of larval or adult behavior were not captured in those biophysical models, creating an overestimate of planktonic transport of larvae from the Gulf to the Atlantic. However, it is also possible that potential connectivity (larval transport) does not equal realized connectivity (larval transport followed by reproduction), and some portion of Atlantic individuals are of Gulf origin but never contribute to the Atlantic gene pool. If the latter possibility were true, then the estimate presented here would be an overestimate, and the magnitude of bias would be dependent on the percentage of sampled individuals that were of Gulf origin. Given significant heterogeneity in allele and genotype distributions among the basins, it should be expected that those percentages are low (and so is associated bias). Nonetheless, future kin-based genomic analyses (e.g., parent-offspring or sibling relationships) that includes samples from the eastern Gulf should provide greater clarity as to whether Gulf-spawned red snapper do indeed settle and survive in the Atlantic.

In CKMR, false positive errors, for example the identification of an unrelated or a half-aunt-niece pair as half-sibling pair, have the potential to bias the abundance estimate. Therefore, it is standard practice to accept some false negatives—failing to identify some half-siblings present in a data set—to avoid committing false positive errors. The chance of false negatives can be accounted for in the CKMR model (as in the present case with the inclusion of the $(1 - FNR_i)$ and $(1 - FNR_{ddRAD,i})$ terms in the likelihood); however, doing so requires that an estimate of the FNR is available. In this study, the FNR was estimated through Monte Carlo simulation of the inheritance of the markers accounting for the physical linkage between them. Because the red snapper genome is not currently a chromosome-level assembly, positions of the markers in a genome matching the karyotype of red snapper were randomly simulated. When a chromosome-

level assembly of the red snapper genome becomes available, the actual genomic positions of markers would be used.

Other applications of CKMR have estimated FNRs from the empirical distribution of observed pairs of putative relationships. Such an approach requires no assumptions on the genomic locations of the markers or recombination rates within the genome. However, with missing data, as encountered in the GT-seq data for Atlantic red snapper, it is unlikely that such an approach would be successful. Systematic error in estimating the FNR has predictable effects, as demonstrated by scenarios in which we doubled or halved the estimated FNR for red snapper. If FNR was underestimated, then more half-sibling pairs would go undetected than expected, thus overestimating population size. Overestimating the FNR would bias the population size estimate downward.

The FNRs are determined by the shape and position of the distribution of log-likelihood ratios in unrelated and related pairs. These are affected by a variety of factors. First and foremost, the distributions are affected by the number of genetic markers and the allele and genotype frequencies at those markers. These two factors were well controlled in this study. Simulations using CKMRsim were done conditioned on the number of shared loci between each pair (NSL), and on patterns of missing data across all pairs with the same NSL. Furthermore, with over 14,000 samples, estimates of allele frequencies in the population are very precise and estimated genotype frequencies conform to the expectation of HWE. This leaves two possible factors that could bias the estimated FNR and subsequent estimates of population size: estimates of genotyping error and possible physical linkage between loci. Given the near-perfect correspondence between the observed and simulated $\Lambda_{PO/U}$ and $\Lambda_{HS/U}$ log-likelihood ratios for unrelated pairs (Figure 3-3), we are confident that the genotyping error model and its parameters are well estimated for this red snapper data set. Nonetheless, to better understand the potential effect of these factors, the magnitude of change in FNR was examined through simulations using CKMRsim in which the true genotyping error rate was set at twice the value or half the value used in the study, to mimic misspecification of the genotyping error rate. The FNR varied by no more than 0.03, which occurred for a genotyping error rate twice the assumed rate. It is very unlikely that the true genotyping error rate is twice the estimated value, because such a departure would have been readily detected in the analysis with *whoa* (Anderson 2021). Consequently, genotyping error misspecification could conceivably be biasing the abundance estimate by only a few percentage points. Finally, lacking a fully assembled genome of red snapper, it was assumed that the amplicon markers were randomly distributed among 24 chromosomes typical of red snapper (Roa-Varón et al. 2025), assuming a genome length of ~1.3 gigabases, and a recombination rate of 1 cM per megabase. If there was less recombination between the amplicon markers, the variance (but not the mean) of the $\Lambda_{HS/U}$ log-likelihood would increase, resulting in increased FNRs < 0.5 and decreased FNRs > 0.5. To assess the sensitivity of FNR to recombination rate assumptions, the markers were condensed into a hypothetical genome of 18 chromosomes with total length of 0.75X the assumed genome length. In this scenario the FNRs changed by less than a few thousandths,

indicating the effect of linkage misspecification on estimates of estimated age-2+ population, in terms of bias, would be negligible.

Individual age data is another important input for CKMR as a means of assigning individuals to cohorts, which is important in the framework applied here for two reasons. First, the pseudolikelihood model uses the difference in birth year between HSPs as an input to estimate population size. While misspecification of ages will impact estimates because of this, the effect size seems to be small (Paul Conn, unpublished simulations). More importantly, only cross-cohort HSPs were considered here, because for bony fish the rate of finding same-cohort pairs is inflated by individual variation in reproductive success within years (Waples and Feutry 2022). Age misspecification could therefore lead to too many or too few cross-cohort HSPs, and biases in that misspecification could lead to an overestimate (too few pairs) or an underestimate (too many pairs). Ages were not provided with many of the samples because they were live discards. To address this uncertainty, ages were imputed probabilistically from an age-length key for all possible cross-cohort siblings, and this imputation was repeated 100 times. The resulting realizations were then used to estimate census size, thus incorporating age uncertainty into variation around the estimate. For ageing uncertainty to create meaningful bias in the estimate, the statistical procedure would have had to produce too many or too few cross-cohort siblings across realizations, a result that seems unlikely unless the age-length key is biased. Epigenetic ageing is currently being applied to these samples to provide consistent, accurate age estimates, at which point CKMR estimation will be repeated, but this is not expected to change the magnitude of the estimate in a particular direction.

Close kin mark-recapture is a promising tool for estimating population size for managed marine species. It has currently been implemented with varying success for a number of species, but in most of these applications the population size was relatively small and the population boundaries relatively well-defined (e.g., lake trout, Marcy-Quay et al. 2025; southern right whale, Førland et al. 2025), making these situations one in which traditional mark-recapture also might be effective. The strength of CKMR is in its application to estimate population size in managed species where population sizes are too large and distributions too great to allow for traditional mark-recapture (Marcy-Quay et al. 2020). Here the technique provided a robust estimate of population size of approximately 1.5 million for an Atlantic red snapper population spread from South Florida to North Carolina, and the scope of such an exercise is well beyond what was involved in most previously published CKMR analyses. The only similar published study, to our knowledge, involves southern bluefin tuna, but that species' life history permitted a sampling design that enhanced the chance of obtaining parent-offspring pairs. A parent-offspring-based approach is simpler, both from a modeling and a computational perspective (Bravington et al. 2016b), and designs incorporating parent-offspring pairs can be more robust to uncertainty in age-composition and in the fecundity-age relationship, as well as to persistent individual differences in size and fecundity (Waples and Feutry 2022). However, designing sampling schemes for such an approach is challenging for Atlantic red snapper or many other bony fishes of management

interest in which it is hard to sample adults and juveniles separately. While we did find likely parent-offspring pairs amongst the snapper genotypes, only a few of them could be confidently distinguished from full-sibling pairs in the absence of direct ageing data. These likely parent-offspring pairs will be revisited with the epigenetic ageing data.

While the present exercise of estimating red snapper abundance by CKMR should be considered a success, there is room for improvement on the current estimate, and the results point at future directions for research. In the near term, epigenetic ageing and a kin-based assessment of genetic connectivity between the Gulf and Atlantic waters off Florida will be conducted to deal with concerns listed above, though the magnitude of the estimate is not expected to change. Improved epigenetic ageing data will also allow parent-offspring pairs in the data that are not otherwise reliably distinguishable from full-siblings to be fully incorporated in the estimation model. The inclusion of such pairs will make the estimate more robust to the form of the fecundity-age relationship (Kehoe et al. 2025c; Appendix XI). Refinements to the reference genome for red snapper will be made, and these will refine the FNR estimates. Continued sampling will provide a time series of data that can be combined with the present data set to detect future changes in abundance.

Chapter 3 Acknowledgements

Funding for this study was principally provided by the South Carolina Sea Grant through the South Atlantic Red Snapper Research Program. We thank Susan Lovelace and Jocelyn Juliano for administering this program and facilitating our study. We would also like to Paul Rudershausen and Jeffrey Merrell at North Carolina State University, Dawn Franco at Georgia Department of Natural Resources, Beverly Sauls, Ellie Corbet, and other members of the Fishery-Dependent Monitoring program at Florida Fish and Wildlife Conservation Commission (FL FWC), and Miaya Taylor, Joseph Tarnecki, Jordan Bajema, and Derek Chamberlin at the University of Florida for organizing fin clip sampling efforts. We thank personnel at South Carolina Department of Natural Resources and Jessica Carroll and FL FWC for ageing samples with otolith thin sections. We also acknowledge members of the Marine Genomics Laboratory who provided logistical support, specifically Elizabeth Dolan and Andrew Fields.

Chapter 3 References

Addis, D.T., W.F. Patterson III, M.A. Dance, and G.W. Ingram Jr. 2013. Implications of reef fish movement from unreported artificial reef sites in the northern Gulf of Mexico. Fisheries Research 147:349–358.

Anderson, E.C. 2021. *whoa*: Evaluation of genotyping error in genotype-by-sequencing data. *R* package version 0.0.2, https://github.com/eriqande/whoa.

Anderson, E.C. 2025a. *CMKRpop*, *R* package, https://github.com/eriqande/CKMRpop.

Anderson, E.C. 2025b. *CKMRsim*, *R* package, https://github.com/eriqande/CKMRsim.

Bacheler, N.M., Z.H. Schobernd, D.J. Berrane, C.M. Schobernd, W.A. Mitchell, B.Z. Teer, K.C. Gregalis, and D.M. Glasgow. 2016. Spatial distribution of reef fish species along the southeast US Atlantic coast inferred from underwater video survey data. PLoS One 11: e0162653.

Bacheler, N.M., W.F. Patterson III, J.H. Tarnecki, K.W. Shertzer, J.S. Buckel, N.J. Hostetter, K. Pacifici, V. Zulian, and W.J. Bubley. 2025. Spatiotemporal dynamics and habitat use of red snapper (*Lutjanus campechanus*) on the southeastern United States Atlantic continental shelf. Fisheries Research 281:107200.

Baetscher, D.S., E.C. Anderson, E.A. Gilver-Horvath, D.P. Malon, E.T. Saarman, M.H. Carr, and J.C. Garza. 2019. Dispersal of a nearshore marine fish connects marine reserves and adjacent fished area along an open coast. Molecular Ecology 28:1611–1623.

Bootsma, M.L., K.M. Gruenthal, G.J. McKinney, L. Simmons, L. Miller, G.G. Sass, and W.A. Larson. 2020. A Gt-seq panel for walleye (*Sander vitreus*) provides important insights for efficient development and implementation of amplicon panels in non-model organisms. Molecular Ecology Resources 20:1706–1722.

Bravington, M.V., H.J. Skaug, and E.C. Anderson. 2016a. Close-kin mark-recapture. Statistical Science 31:259–274.

Bravington, M.V., P.M. Grewe, and C.R. Davies. 2016b. Absolute abundance of southern bluefin tuna estimated by close-kin mark-recapture. Nature Communications. 7:13162.

Brown, S.S., Y.-W. Chen, M. Wang, A. Clipson, E. Ochoa, and M.-Q. Du. 2017. PrimerPooler: automated primer pooling to prepare library for targeted sequencing. Biology Methods and Protocols 2:bpx006.

Camber, C.I. 1955. A survey of the red snapper fishery of the Gulf of Mexico, with special reference to the Campeche Banks. Florida State Board of Conservation Technical Series 12:1–64.

Campbell, N.R., S.A. Harmon, and S.R. Narum. 2015. Genotyping-in-Thousands by sequencing (GT-seq): a cost-effective SNP genotyping method based on custom amplicon sequencing. Molecular Ecology Resources 15:855–867.

Christiansen, H.M., T.S. Switzer, R.B. Brodie, J.J. Solomon, and R. Paperno. 2020. Indices of abundance for red snapper (*Lutjanus campechanus*) from the FWC Fish and Wildlife Research Institute (FWRI) repetitive timed drop survey in the U.S. South Atlantic. SEDAR73-WP06. SEDAR. North Charleston, SC, 23 pp.

Conn, P.B., M.V. Bravington, S. Baylis, and J.M. Ver Hoef. 2020. Robustness of close-kin mark-recapture estimators to dispersal limitation and spatially varying sampling probabilities. Ecology and Evolution 10:5558–5569.

Danecek, P., A. Auton, G. Abecasis, C.A. Albers, E. Banks, M.A. DePristo, R.E. Handsaker, G. Lunter, G.T. Marth, S.T. Sherry, G. McVean, and R. Durbin. 2011. The variant call format and VCFtools. Bioinformatics 27:2156–2158.

Danecek, P., Bonfield, J.K., Liddle, J., Marshall, J., Ohan, V., Pollard, M.O., Whitwham, A., Keane, T., McCarthy, S.A., Davies, R.M., Li, H. 2021. Twelve years of SAMtools and BCFtools. GigaScience 10:giab008.

Delaval, A., V. Bendall, S.J. Hetherington, H.J. Skaug, M. Frost, C.S. Jones, and L.R. Noble. 2023. Evaluating the suitability of close-kin mark-recapture as a demographic modelling tool for a critically endangered elasmobranch population. Evolutionary Applications 16:461–473.

Delomas, T.A., J. Struthers, T. Hebson, and M.R. Campbell. 2023. Development of a microhaplotype panel to inform management of gray wolves. Conservation Genetics Resources 15:49–57.

Edgar, R.C. 2022. Muscle5: High-accuracy alignment ensembles enable unbiased assessments of sequence homology and phylogeny. Nature Communications 13: 6968.

Førland, B., H.J. Skaug, M. Takahashi, and L.A. Pastene. 2025. Close-kin mark-recapture without age information: application to southern right whales. Journal of Agricultural, Biological and Environmental Statistics https://doi.org/10.1007/s13253-025-00689-3

Garrison, E., Marth, G. 2012. Haplotype-based variant detection from short-read sequencing. arXiv:1207.3907.

Hillary, R.M., M.V. Bravington, T.A. Patterson, P. Grewe, R. Bradford, P. Feutry, R. Gunasekera, V. Peddemors, J. Werry, M.P. Francis, C.A.J. Duffy, and B.D. Bruce. 2018. Genetic relatedness reveals total population size of white sharks in eastern Australia and New Zealand. Scientific Reports 8:2661.

Hollenbeck, C.M., D.S. Portnoy, E. Saillant, and J.R. Gold. 2015. Population structure of red snapper (*Lutjanus campechanus*) in U.S. waters of the western Atlantic Ocean and the northeastern Gulf of Mexico. Fisheries Research 172:17–25.

Karnauskas, M., K.W. Shertzer, C.B. Paris, N.A. Farmer, T.S. Switzer, S.K. Lowerre-Barbieri, G.T. Kellison, R. He, and A.C. Vaz. 2022. Source-sink recruitment of red snapper: connectivity between the Gulf of Mexico and Atlantic Ocean. Fisheries Oceanography 31:571–586.

Kehoe, L., K.W. Shertzer, M.V. Lauretta, J.A. Buckel, D.S. Portnoy, W.F. Patterson III, and D.D. Chagaris. 2025b. Estimating reef fish exploitation rates in catch and release fisheries with conventional and genetic tags. Paper in Review; Appendix VII in this report.

Kehoe, L., E.C. Anderson, C.M. Hollenbeck, D.D. Chagaris, K.W. Shertzer, W.F. Patterson III, and D.S. Portnoy. 2025c. Sensitivity of CKMR-derived Atlantic red snapper population estimates to uncertainty in life history parameters. Draft Manuscript, Appendix XI in this report.

Lukacs, P.M, and K.P. Burnham. 2005. Review of capture–recapture methods applicable to noninvasive genetic sampling. Molecular Ecology 14:3909–3919.

Marcy-Quay, B., S.A. Sethi, N.O. Therkildsen, and C.E. Kraft. 2020. Expanding the feasibility of fish and wildlife assessments with close-kin mark–recapture. Ecosphere 11:e03259.

Marcy-Quay B., B. Pientka, and J.E. Marsden. 2025. Evaluation of a recovering lake trout population in Lake Champlain using close-kin mark-recapture and genetic strain assignment. Journal of Great Lakes Research 51:102623.

Meng, G., Li, Y., Yang, C., Liu, S. 2019. MitoZ: a toolkit for animal mitochondrial genome assembly, annotation and visualization, Nucleic Acids Research 47: e63.

Miller, L.M., M.C. Ward, and D.W. Schultz. 2015. Using genetic markers as individual tags: a case study of a mark–recapture estimate of adult muskellunge population size. North American Journal of Fisheries Management 35:210–215.

Monroe, A., C.M. Hollenbeck, C.L. Lanoue, W.F. Patterson III, and D.S. Portnoy. 2025. Genetic population structure of red snapper, *Lutjanus campechanus*, in the U.S. Atlantic and eastern Gulf of America. Draft Manuscript, Appendix IV in this report.

Norrell, A.E., K.L. Jones, and E.A. Saillant. 2020. Development and characterization of genomic resources for a non-model marine teleost, the red snapper (*Lutjanus campechanus*, Lutjanidae): construction of a high-density linkage map, anchoring of genome contigs and comparative genomic analysis. PLoS One 15:e0232402.

O'Leary, S.J., J.B. Puritz, S.C. Willis, C.M. Hollenbeck, and D.S. Portnoy. 2018. These aren't the loci you're looking for: principles of effective SNP filtering for molecular ecologists. Molecular Ecology 27:3193–3206.

Palsbøll, P.J. 1999. Genetic tagging: contemporary molecular ecology. Biological Journal of the Linnean Society 68:3–22.

Palsbøll, P.J., J. Allen, M. Bérube´, P.J. Clapham, T.P. Feddersen, P.S. Hammond, R.R. Hudson, H. Jørgensen, S. Katona, A.H. Larsen. F. Larsen, J. Lien, D.K. Mattila, J. Sigurjónsson, R. Sears, T. Smith, R. Sponer, P. Stevik, and N. Øien. 1997. Genetic tagging of humpback whales. Nature 388:767–769

Patterson III, W.F., J.C. Watterson, R.L. Shipp, and J.H. Cowan Jr. 2001. Movement of tagged red snapper in the northern Gulf of Mexico. Transactions of the American Fisheries Society 130:533–545.

Patterson, T.A., R. Hillary, P. Feutry, R. Gunasakera, J. Marthick, and R.D. Pillans. 2022. Rapid estimation of cryptic adult abundance and breeding dynamics in a critically endangered elasmobranch from close-kin mark recapture. bioRxiv https://doi.org/10.1101/2022.02.24.481858

Portnoy, D.S., A.T. Fields, J.B. Puritz, C.M. Hollenbeck, and W.F. Patterson III. 2022. Genomic analysis of red snapper, *Lutjanus campechanus*, population structure in the U.S. Atlantic and Gulf of Mexico. ICES Journal of Marine Science 17:12–21.

Prystupa, S., G.R. McCracken, R. Perry, and D.E. Ruzzante. 2021. Population abundance in arctic grayling using genetics and close-kin mark-recapture. Ecology and Evolution 11:4763–4773.

Puritz, J.B., C.M. Hollenbeck, and J.R. Gold. 2014. *dDocent:* a RADseq, variant-calling pipeline designed for population genomics of non-model organisms. Peer J 2:e431.

R Core Team, 2024. R: A Language and Environment for Statistical Computing. R Foundation for Statistical Computing, Vienna, Austria. URL https://www.R-project.org/.

Roa-Varón, A., P. Moulos, S. Harter, A. David, A.M. Quattrini, and S. Herrera. 2025. Chromosome-level genome assembly of the vermilion snapper (*Rhomboplites aurorubens*). Scientific Data 12:1281.

Ruzzante, D.E., G.R. McCracken, B. Førland, J. MacMillan, D. Notte, C. Buhariwalla, J.M. Flemming, and H. Skaug. 2019. Validation of close-kin mark–recapture (CKMR) methods for estimating population abundance. Methods in Ecology and Evolution 10:1445–1453.

SEDAR. 2017. SEDAR 41 South Atlantic Red Snapper Assessment Report – Revision 1. SEDAR, North Charleston SC. 805 pp. http://sedarweb.org/sedar-41

SEDAR. 2021. SEDAR 73 South Atlantic Red Snapper Stock Assessment Report. SEDAR, North Charleston, SC. 194 pp. https://sedarweb.org/sedar-73

SEDAR. 2024. Stock Assessment of Red Snapper off the Southeastern United States – Update of SEDAR 73 Assessment. SEFSC, Beaufort, NC. http://sedarweb.org/sedar-73

SEDAR. 2025. SEDAR 90 South Atlantic Red Snapper Data Workshop, North Charleston, SC. https://sedarweb.org/assessments/sedar-90-south-atlantic-red-snapper/

Shertzer, K. W., E.H. Williams, J.K. Craig, E.E. Fitzpatrick, N. Klibansky, and K.I. Siegfried. 2019. Recreational sector is the dominant source of fishing mortality for oceanic fishes in the southeast United States Atlantic Ocean. Fisheries Management and Ecology 26:621–629.

Seutin, G., B.N. White, and P.T. Boag. 1991. Preservation of avian blood and tissue samples for DNA analyses. Canadian Journal of Zoology 69:82–90.

Skaug, H.J. 2001. Allele-sharing methods for estimation of population size. Biometrics 57: 750–756.

Solomon, J.J., H.M. Christiansen, B.B. Russell, J. Lewis, and T.S. Switzer. 2025. Indices of abundance for red snapper (*Lutjanus campechanus*) from the Florida Fish and Wildlife Research Institute (FWRI) repetitive timed drop hooked-gear survey in the U.S. South Atlantic. SEDAR90-DW-23. SEDAR, North Charleston, SC, 19pp.

Szedlmayer, S.T. and R.L. Shipp. 1994. Movement and growth of red snapper, *Lutjanus campechanus*, from an artificial reef area in the northeastern Gulf of Mexico. Bulletin of Marine Science 55:887–896.

Taberlet, P., L.P. Waits, and G. Luikart. 1999. Noninvasive genetic sampling: look before you leap. Trends in Ecology & Evolution 14:323–327.

Taras, B.D., P.B. Conn, M.V. Bravington, A. Kilian, A.R. Lang, A. Bryan, R. Stimmelmayr, and L. Quakenbush. 2024. Estimating demographic parameters for bearded seals, *Erignathus barbatus*, in Alaska using close-kin mark-recapture methods. Evolutionary Applications 17:e70035.

Trenkel, V.M., G. Charrier, P. Lorance, and M.V. Bravington. 2022. Close-kin mark–recapture abundance estimation: practical insights and lessons learned. ICES Journal of Marine Science 79:413–422.

Swenson, J. D., E.N. Brooks, D. Kacev, C. Boyd, M.J. Kinney, B. Marcy-Quay, A. Sévêque, K. A. Feldheim, and L.M. Komoroske. 2024. Accounting for unobserved population dynamics and aging error in close-kin mark-recapture assessments. Ecology and Evolution 14:e10854.

Untergasser, A., I. Cutcutache, T. Koressaar, J. Ye, B.C. Faircloth, M. Remm, and S.G. Rozen. 2012. Primer3—new capabilities and interfaces. Nucleic Acids Research 40:e115.

Vecchio, J., M.W. Finch, and C.M. Willis. 2025. Red snapper fishery-independent index of abundance and age/length composition in US South Atlantic waters based on a chevron video trap survey (2010-2024). SEDAR90-DW-05. SEDAR, North Charleston, SC, 18 pp.

Wacker, S., H.J. Skaug, T. Forseth, O. Solem, E.M. Ulvan, P. Fiske, and S. Karlsson. 2021. Considering sampling bias in close-kin mark-recapture abundance estimates of Atlantic salmon. Ecology and Evolution 11:3917–3932.

Waples, R.S. and P. Feutry. 2022. Close-kin methods to estimate census size and effective population size. Fish and Fisheries 23:273–293.

Willis, S.C., C.M. Hollenbeck, J.B. Puritz, J.R. Gold, and D.S. Portnoy. 2017. Haplotyping RAD loci: an efficient method to filter paralogs and account for physical linkage. Molecular Ecology Resources 17:955–965.

Woods, J.G., D. Paetkau, D. Lewis, B.N. McLellan, M. Proctor, and C. Strobeck. 1999. Genetic tagging of free-ranging black and brown bears. Wildlife Society Bulletin (1973–2006) 27:616–627.

Chapter 4

Summary and Conclusions

William F. Patterson III[1], David S. Portnoy[2], Jeffrey A. Buckel[3], Eric Anderson[4], Nathan M. Bacheler[5], Kyle W. Shertzer[5], and Walter J. Bubley[6]

[1]School of Forest, Fisheries, and Geomatics Sciences, University of Florida, 7922 NW 71st Street, Gainesville, Florida 32653, USA

[2]Marine Genomics Laboratory, Department of Life Sciences, Texas A&M University–Corpus Christi, 6300 Ocean Drive, Corpus Christi, TX 78412, USA

[3]Department of Applied Ecology, Center for Marine Sciences and Technology, North Carolina State University, Morehead City, NC, USA

[4]Southeast Fisheries Science Center, National Marine Fisheries Service, Beaufort, NC 28516, USA

[5]Department of Biology and Department of Fisheries, Wildlife and Conservation Biology, Colorado State University, Fort Collins, CO 80523, USA

[6]Marine Resources Research Unit, South Carolina Department of Natural Resources, Charleston, SC, USA

Summary of Study Results

The primary goal of the South Atlantic Red Snapper Research Program was to produce an independent estimate of age-2+ red snapper population size. Our study team produced two such population estimates, one with a Bayesian hierarchical integrated model (BHIM) and one utilizing close-kin mark-recapture (CKMR). The BHIM approach was proposed because it took advantage of Southeast Reef Fish Survey (SERFS) samples that were already being collected every year. We supplemented SERFS sampling with video sampling with a remotely operated vehicle (ROV) to test whether Atlantic red snapper were found exclusively on or near hardbottom (reef) habitat, or whether they were more widely distributed on the shelf, as Stunz et al. (2021) reported for the western Gulf. In our study, red snapper were found to be associated with hardbottom habitat and rarely observed on open or sandy substrate, unless near a natural reef (Bacheler et al. 2025, Appendix III). That was an important finding because it allowed us to focus on hardbottom habitat to estimate red snapper distribution.

The next component of the BHIM approach was to be able to estimate density from red snapper count data derived from SERFS camera-trap or ROV video samples. We developed two different approaches to accomplish that, with the spatial capture-recapture approach reported by Goldstein et al. (2025, Appendix II) providing Bayesian priors for camera-trap effective sample area (ESA) and ROV catchability that could be incorporated into the BHIM model. Baited cameras are widely used to survey reef fishes because they are relatively easy to deploy and fairly sophisticated underwater cameras can be purchased with minimal investment. However, a central limitation to utilizing this gear to estimate absolute versus relative abundance is the difficulty in converting fish counts into fish density estimates. Density estimates (fish per unit area) are required to scale counts at individual sites to abundance estimates to larger areas, regions, and eventually the entire distribution of a fish population (i.e., fish/area x area = fish abundance). That is precisely what we accomplished with the BHIM approach, which involved the integration of data (fish density, habitat distribution, and depth) across a hierarchy of spatial scales, and ultimately to an estimate of the red snapper population in the 112 x 10^3 km^2 study region of the southeastern U.S. Atlantic (SEUSA) shelf.

The modeling approach we developed advances reef fish science in two important ways. First, we developed and described methods to convert count data into fish density estimates when sampling with stationary cameras. And secondly, we developed the Bayesian model to integrate red snapper density, hardbottom distribution, and depth data across the region to estimate Atlantic red snapper population size. However, in the process we discovered some limitations in the data sources required to scale fish density estimates to a red snapper population estimate for the entire U.S. Atlantic. As pointed out in Chapter 2, despite nearly 2,000 SERFS camera-trap samples being taken in some years, only a small percentage of the available red snapper habitat was surveyed during this study. The SERFS and ROV video samples were randomly distributed on the shelf, so the data should be unbiased, but there is still a substantial amount of variance (imprecision) in the data.

Potential issues with video sample spatial coverage aside, a greater source of uncertainty in our BHIM estimate of Atlantic red snapper population size was the estimated distribution of hardbottom habitat. Two previous studies had compiled available habitat data in an attempt to map hardbottom habitat on the SEUSA shelf (Conley et al. 2017; Steward et al. 2022), and in doing so ranked the reliability of the data sources. In general, we find no fault in the efforts or results from those previous studies. Overall, the habitat distribution estimates from those studies agrees remarkably well with the perception of professional fishermen stakeholders we interviewed to gather information about the distribution of hardbottom habitat and red snapper relative abundance (Rudershausen et al. 2025a, Appendix VIII). However, that agreement was on broad (10s to 100s of km^2) spatial scales and finer resolution habitat data, such as acquired with large-scale sonar mapping, are needed to scale Atlantic red snapper density estimates at individual sample sites to a population estimate across the entire region with greater certainty.

The effect of uncertainty in habitat distribution data on our estimates of red snapper density via the BHIM are obvious. The range in red snapper population size estimates among plausible habitat distribution estimates ranged from 0.79 to nearly 100 million fish. While the estimated hardbottom habitat distribution our team felt was most defensible (see Chapter 2) produced a population estimate of 5.31 million red snapper, the CV of that estimate (0.39) was well above the prescribed precision in the RFP (CV $\leq$ 0.3) and the resultant Bayesian credible intervals ranged from 2.33 to 10.02 million fish (Figure 4-1). Moreover, it is likely some percentage of red snapper counted in video samples was actually age-1 given 20% of the red snapper captured in SERFS trap samples and aged with otoliths in 2021 was estimated to be one year-olds, as was 5% of the trap samples in 2022. This implies our BHIM estimate of red snapper population size is likely biased high, but it is unclear to what extent. Therefore, the BHIM red snapper population estimate likely suffers from bias as well as imprecision.

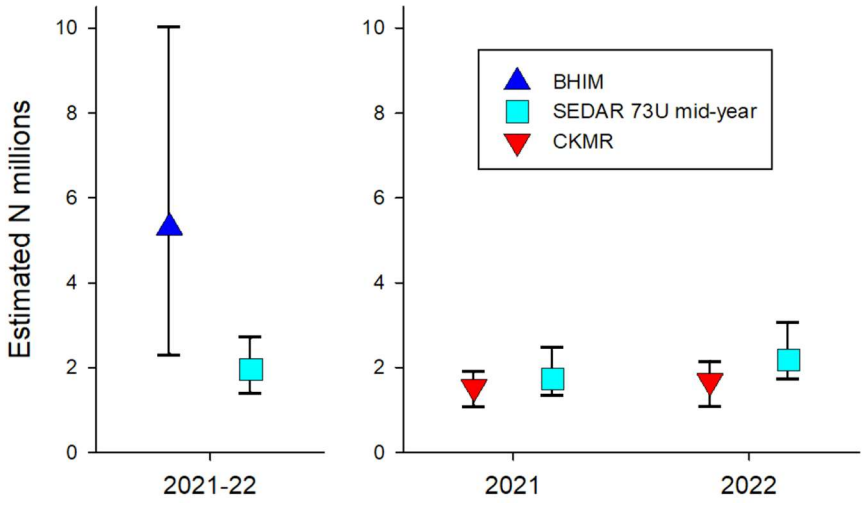

Figure 4-1. Estimates of Atlantic red snapper population size (± 95% credible intervals) in millions of fish produced in this study with a Bayesian hierarchical integrated model (BHIM) utilizing fish count data from video samples and close-kin mark-recapture (CKMR) from kinship analysis versus estimates from the SEDAR 73 update stock assessment (SEDAR 2024).

The second approach our team took to estimate age-2+ population size was CKMR. This is a recently described approach that has only been employed on similarly large scales a few times globally, including for southern bluefin tuna in the Pacific Ocean (Bravington et al. 2016), and Atlantic bluefin tuna more recently (Bravington and Fernández 2024). The sample size simulation work our team did at the proposal phase of this study demonstrated the sampling required to estimate Atlantic red snapper population size with a CV ≤ 0.3 was clearly tractable given state and federal sampling programs in the region. Once the study began, the support we received from state and federal agency partners and administrators was unprecedented in the experience of our diverse study team. We have not attempted to tabulate the value of all the in-kind sampling that went into collecting fin clip samples from nearly 20k red snapper, but we are confident it would be in the millions, and perhaps >$10M.

Our team invested considerable time and effort in the first 18 months of the study to develop the genomics pipelines and bioinformatics methods needed to process the terabytes of genomic data produced during this study. Now established, future CKMR analysis for Atlantic (or Gulf) red snapper would be more efficient and less expensive. Furthermore, we have developed best practices for pursuing CKMR population estimation on large scales (100s of km^2) in U.S. domestic fisheries that may have applications across a range of species.

The CKMR estimates our team produced appear not to suffer from imprecision, nor is it likely they suffer from bias in a particular direction. In Chapter 3, we detailed the various protocols employed to ensure a lack of bias in our CKMR population estimates, as well as ways in which uncertainty in various parameters was incorporated in the Bayesian model's likelihood estimation, as well as carried forward into credible interval or CV estimates. In the end, CKMR estimates of population size were lower than but not statistically different (i.e., overlapping credible intervals) than those produced in the SEDAR 73U stock assessment (Figure 4-1; SEDAR 2021, 2024).

Another similarity between this study and SEDAR 73U, as well as previous Atlantic red snapper stock assessments, is the observed strongly truncated red snapper age distribution. Overall, only 11 of 11,509 otolith-aged samples were aged to be >20 years old, only one was over 30 years old, and 91.4% of samples were estimated to be ≤7 years old. When considering only fishery independent samples collected with hook and line gear (8/0, 11/0, and 15/0 circle hooks) off northeastern Florida, which is the estimated the center of abundance for Atlantic red snapper (Figure 2-5), 94.8% of samples were estimated to be ≤7 years old, and only 4 of 2,990 (0.1%) were estimated to be more than 20 years old. This is notable for a species with a maximum observed longevity of 51 years in the U.S. Atlantic.

One thing important to consider is the SEDAR 73 assessment and its update were computed with recreational landings and discards estimates derived from the federal Marine Recreational Information Program (MRIP). The state of Florida, where the vast majority of Atlantic red snapper fishery removals (landings plus dead discards) are estimated to occur, first deployed its State Reef Fish Survey (SRFS) in 2021 to estimate reef fish landings and discards due to questions about the veracity of MRIP estimates. The SEDAR 90 Data Workshop recommended SRFS data be used to

estimate Florida recreational removals in the forthcoming stock assessment. Over the time period of 2021-2024, estimated stock-wide recreational removals were 46% lower when the Florida removals were estimated with SRFS versus MRIP data (SEDAR 2025). This is important because sensitivity analyses performed as part of SEDAR 73U indicated that decreasing the magnitude of removals by up to 40% had no impact on estimates of fishing mortality (F) relative to the overfishing benchmark ($F_{30\%SPR}$), or spawning stock biomass (SSB) relative to $SSB_{30\%SPR}$ (see SEDAR 2021, Figure 49), but reduced removals did cause the estimated age-2+ red snapper population size to decrease. This is because estimates of mortality are informed by age composition data derived from biological samples, while stock productivity is also informed by the magnitude of estimated removals. For a given mortality level (estimated from age composition data), a larger estimate of removals translates to a larger estimated population size because a larger population would have been required to produce the fish that were removed (as landed catch or dead discards). Therefore, it is possible the Atlantic red snapper population size will be estimated to be lower in the SEDAR 90 assessment than was estimated in SEDAR 73U given the 46% reduction in recent (2021-24) Florida recreational removals when using SRFS versus MRIP data (SEDAR 2025). However, several other population parameters were updated during the SEDAR 90 Data Workshop which may make reconciling differences between our CKMR population estimate and the forthcoming stock assessment more challenging. Our team recommends as close to a continuity run with the SEDAR 73U model parameterization be made during SEDAR 90 but with the lower recreational removals calculated with SRFS data from Florida.

Next Steps and Integration of Study Results

This report includes revisions made following review by Center for Independent Experts (CIE) scientists in January 2026. A second round of peer review will occur by the South Atlantic Fishery Management Council's Scientific and Statistical Committee in April 2026. Following peer review, the intention has always been to incorporate at least CKMR population estimation directly into the Beaufort Assessment Model (BAM) for Atlantic red snapper due to the benefits of freeing the assessment model to fit other parameters, such as natural mortality or fishery selectivity (Punt et al. 2024; Fisch 2025). Toward that end, our team has engaged in a parallel process during the SARSRP project to incorporate the Atlantic red snapper CKMR model into the BAM assessment model. A simulation model developed to test the feasibility of this integration is operational (McLaughlin et al. 2025; Appendix VI). Therefore, the study team is optimistic the integration of CKMR data and population estimation can be accomplished for SEDAR 90. A future goal will be to accomplish the integration of the BHIM framework into the red snapper assessment as well, but that is a lower priority at this stage given the uncertainty in hardbottom habitat distribution, hence BHIM population estimation.

Results of this study demonstrate multiyear tissue sampling can be utilized to track trends in absolute population size with CKMR. The CKMR population estimates for Atlantic red snapper from 2018-2023 indicate an increasing population over that time period, which is consistent with

population trends estimated in recent stock assessments. The study team collected fin clips samples in 2024 and have processed those through the GT-seq stage of genomic analysis. Sampling will occur again in 2026, with an expansion of the multiyear CKMR analysis thereafter. Furthermore, ongoing conventional tagging based on the simulation-informed sample design reported by Kehoe et al. (2025b; Appendix VII) will produce exploitation rate estimates (removals per population size) that can be multiplied by CKMR population estimates to produce independent estimates of the magnitude of recreational discards and perhaps landings. Therefore, the legacy of the investments made in red snapper CKMR sequencing panels, genomics pipelines, and model development should be greater than only population estimation in the future.

Throughout the course of this study our research team has endeavored to be responsible stewards of the taxpayer dollars committed to the SARSRP. We have gone well beyond the originally planned research to test assumptions of our methods, calibrate gear or estimate its effective sample area, or use data opportunistically to model important fishery parameters, such as red snapper release mortality (Rudershausen et al. 2025a, Appendix IX; Zimmermann et al. 2026, Appendix X). Data and analytical products produced during this work have already been incorporated into the SEDAR 90 assessment process, and the parallel process of incorporating CKMR into the assessment model should enable an even greater application of the data and methods developed during this study to be brought to bear for red snapper assessment, management, and conservation. Lastly, the approach and process we have taken for Atlantic red snapper potentially could be a model for other reef fish species in the SEUS, as well as widely distributed species in other regions.

Chapter 4 References

Bacheler, N.M., W.F. Patterson III, J.H. Tarnecki, K.W. Shertzer, J.A. Buckel, N.J. Hostetter, K. Pacifici, V. Zulian, and W.J. Bubley. 2025. Spatiotemporal dynamics and habitat use of red snapper (*Lutjanus campechanus*) on the southeastern United States Atlantic continental shelf. Fisheries Research 281:107200, Appendix III in this report.

Bravington, M.V., P.M. Grewe, and C.R. Davies. 2016. Absolute abundance of southern bluefin tuna estimated by close-kin mark-recapture. Nature Communications. 7:13162.

Bravington, M.V. and C. Fernández. 2024. Model-based sampling design for eastern bluefin tuna close-kin mark-recapture. Collective Volume of Papers of the International Commission for the Conservation of Atlantic tunas 81:SCRS/2024/053:1–32.

Conley, M.F., M.G. Anderson, N. Steinberg, and A. Barnett. 2017. The South Atlantic Bight Marine assessment: species, habitats and ecosystems. The Nature Conservancy, Eastern Conservation Science.

Fisch, N. 2025. Expected improvements in precision when integrating opportunistic close-kin mark-recapture data into fisheries stock assessments. Fisheries Research 281:107222.

Goldstein, B.R., K. Pacifici, J.A. Buckel, N.M. Bacheler, E.M. Schliep, B. Reich, K.W. Shertzer,

J.H. Tarnecki, W.F. Patterson III, and N.J. Hostetter. 2025. An integrated approach to estimating the effective sampling area of baited underwater cameras. Paper in Review, Appendix II in this report.

Kehoe, L., K.W. Shertzer, M.V. Lauretta, J.A. Buckel, D.S. Portnoy, W.F. Patterson III, and D.D. Chagaris. 2025b. Estimating reef fish discard exploitation rates in catch and release fisheries with conventional or genetic tags. Paper in Review; Appendix VII in this report.

McLaughlin, P.S., E.C. Anderson, P.B. Conn, M.D. Damiano, C.M. Hollenbeck, A.A. Monroe, W.F. Patterson III, D.S. Portnoy, K.W. Shertzer, and M.T. Vincent. 2025. Incorporating close-kin mark-recapture data into an integrated stock assessment model for southeast United States Atlantic red snapper (*Lutjanus campechanus*). Draft Manuscript, Appendix VI in this report.

Punt, A.E., R. Thomson, L.R. Little, P. Bessell-Browne, P. Burch, and M. Bravington. 2024. Including close-kin mark-recapture data in statistical catch-at-age stock assessments and management strategies. Fisheries Research 276:107057.

Rudershausen, P.J., B.J. Runde, R.M. Tharp, J.H. Merrell, N.M. Bacheler, W.F. Patterson III, and J.A. Buckel. 2025b. Discard mortality rates of Red Snapper after barotrauma and hook trauma: insights from using acoustic telemetry in the U.S. Atlantic. North American Journal of Fisheries Management 45:270–282, Appendix IX in this report.

Rudershausen, P.J., C.M. Schobernd, N.M. Bacheler, N.J. Hostetter, K. Pacifici, W.F. Patterson III, B.J. Runde, and J.A. Buckel. 2025a. Stakeholder insights corroborate habitat and reef fish abundance on the southeastern U.S. Atlantic continental shelf. In Press in Regional Studies in Marine Science; Appendix VIII in this report.

SEDAR. 2021. SEDAR 73 South Atlantic Red Snapper Stock Assessment Report. SEDAR, North Charleston, SC. 194 pp. https://sedarweb.org/sedar-73.

SEDAR. 2024. Stock Assessment of Red Snapper off the Southeastern United States – Update of SEDAR 73 Assessment. SEFSC, Beaufort, NC. http://sedarweb.org/sedar-73.

SEDAR. 2025. SEDAR 90 South Atlantic Red Snapper Data Workshop, North Charleston, SC. https://sedarweb.org/assessments/sedar-90-south-atlantic-red-snapper/.

Steward, D.N., A.B. Paxton, N.M. Bacheler, C.M. Schobernd, K. Mille, J. Renchen, Z. Harrison, J. Byrum, R. Martore, C. Brinton, K.L. Riley, J.C. Taylor, and G.T. Kellison. 2022. Quantifying spatial extents of artificial versus natural reefs in the seascape. Frontiers in Marine Science 9:980384.

Stunz, G.W., W.F. Patterson III, S.P. Powers, J.H. Cowan, Jr., J.R. Rooker, R.A. Ahrens, K. Boswell, L. Carleton, M. Catalano, J.M. Drymon, J. Hoenig, R. Leaf, V. Lecours, S. Murawski, D. Portnoy, E. Saillant, L.S. Stokes, and R.J.D. Wells. 2021. The Great Red Snapper Count: Estimating the Absolute Abundance of Age-2+ Red Snapper (*Lutjanus campechanus*) in the U.S. Gulf of Mexico. Mississippi-Alabama Sea Grant Consortium, NOAA Sea Grant. 408 pages.

Zimmermann, S., L. Kehoe, M.A. Taylor, J.H. Tarnecki, N.M. Bacheler, Z.A. Siders, and W.F.

Patterson III. 2026. Post-release mortality of red snapper, *Lutjanus campechanus*, in Atlantic waters off northeast Florida estimated with three-dimensional acoustic telemetry. Fisheries Review 291:107703; Appendix X in this report.